NUMERICAL SIMULATION OF THERMAL TRANSPORT IN A HIGH HYDROSTATIC PRESSURE FOOD PROCESSING VESSEL

By

MEENAKSHI KHURANA

A thesis submitted to the

Graduate School-New Brunswick

Rutgers, The State University of New Jersey

in partial fulfillment of the requirements

for the degree of

Master of Science

Graduate Program in Food Science

written under the direction of

Professor Mukund V. Karwe

and approved by

_____

_____

_____

_____

New Brunswick, New Jersey

January 2008

ABSTRACT OF THE THESIS

Numerical Simulation of Thermal Transport in a High Hydrostatic Pressure Food Processing Vessel

MEENAKSHI KHURANA

Thesis Director: Prof. Mukund V. Karwe, Ph.D.

High Hydrostatic Pressure Processing (HHPP) is a novel non-thermal food processing technology for producing safe, high quality food products, with minimum detrimental effects of thermal processing such as loss of original flavor and color. The high pressure range used for processing food products is 100 to 1000 MPa. Clams are high pressure processed in the range of 200-350 MPa and fruit juices between 300-600 MPa. Spores, found mainly in low acid foods, and prions need even higher pressures for inactivation.

When pressure is applied on a food product using liquid medium, adiabatic heat generation occurs due to compression of the pressurizing medium and the food product, which results in increase in their temperatures. This increase in temperature is different for different foods. For example, water heats up by 2-3˚C per 100 MPa increase in pressure. Oils and fats heat more (6-9˚C) due to their higher compressibility, lower thermal conductivity, and lower heat capacity.

In a high pressure process, the heat generated by adiabatic compression is continuously dissipated to the thick metal wall of the vessel during pressurization and pressure hold stages. The heat loss at the wall and the natural convection flow near the vessel wall give rise to non-uniform temperature distribution within the pressurization medium. Therefore, the objective of this research was to carry out numerical simulation of thermal transport in pressurizing medium (water) during HHPP (at room temperature and higher initial temperature) to predict the temperature distribution. Numerical predictions were validated using experimental data. The impact of the response time of the high pressure thermocouple assembly on the measured transient temperature response was taken into account.

Results obtained from the numerical simulation showed that the temperature distribution in the pressurizing medium became non-uniform during the high pressure process and this non-uniformity increased with increasing initial temperatures. Also, increasing the vessel size and inserting an insulating sleeve in the vessel decreased the non-uniformity in temperature.

Non-uniformity in temperature in the pressurizing medium can lead to non-uniform microbial inactivation and is of most relevance when a combination of high pressure and high temperature is used to inactivate spores.

ACKNOWLEDGEMENTS

It is a pleasure to thank the many people who in some way contributed to this thesis.

Foremost, I would like to thank my advisor, Dr. Mukund V. Karwe, who brought me into the world of numerical simulation and shared with me a lot of his expertise and research insight. I am grateful to him for providing me the opportunity to work on this project and for his exceptional guidance, inspiration, support, and cooperation throughout the course of this study. His patience, despite my many, many questions, is greatly appreciated.

I am grateful to Dr. Kit L. Yam, Dr. Paul Takhistov, and Dr. Yogesh Jaluria for kindly agreeing to serve on my thesis committee. Their suggestions and comments are appreciated.

I wish to thank Elmhurst Inc., NY for providing the equipment support. I would also like to acknowledge Dave Petrenka and Frank Caira for their help and support in maintaining the high pressure equipment.

I want to thank the departmental secretaries, Paulette Arico, Karen Ratzan, Karen Conover, Debbie Koch and Miriam Gonzalez for assisting me in many different ways. In addition, I would like to thank Yakov Uchitel for his help and support.

I am indebted to my student colleagues Dilek Kocer, Rohan Tikekar, Shalaka Narwankar, Gabriela Chiappe, José Antonio Maldonado, and Gabriel Mootian for providing a stimulating and fun environment in which to learn and grow.

Finally and most importantly, I cannot end without thanking my family for their enormous love, continued support, and sacrifices for me. To them I dedicate this thesis.

TABLE OF CONTENTS

ABSTRACT OF THE THESIS..... ii

ACKNOWLEDGEMENTS..... iv

TABLE OF CONTENTS..... v

LIST OF FIGURES..... viii

LIST OF TABLES..... xv

NOMENCLATURE..... xvi

1. INTRODUCTION..... 1

1.1. History of Development of Preservation of Foods by HHPP..... 1

1.2. Potential Applications of HHPP..... 2

1.3. Literature Review on Effect of HHPP on Food Products..... 8

1.4. High Pressure Process and Equipment Description..... 9

1.5. Thermal Transport during HHPP..... 12

1.6. Literature Review of Mathematical Modeling of HHPP..... 16

1.7. Experimental Challenges..... 19

1.8. Lead to Hypothesis and Objectives..... 20

1.9. Hypotheses..... 20

1.10. Rationale..... 21

1.11. Objectives..... 21

2. MATERIALS AND METHODS..... 23

2.1. High Pressure Food Processor – Experimental Facility..... 23

2.1.1. High pressure vessel..... 25

2.1.2. Working description of HHPP..... 25

2.1.3. Pressure measurements..... 27

2.1.4. Temperature measurements 27

2.2. Special Experimental Set Up 27

2.2.1. Time constant experiment 28

2.2.2. Initial high temperature experiment 29

3. THEORETICAL CONSIDERATIONS 31

3.1. Strength of Buoyancy Induced Flow (laminar or turbulent flow) 31

3.2. Governing Equations for High Pressure Processing 32

3.2.1. Conservation of mass 32

3.2.2. Conservation of momentum 32

3.2.3. Conservation of energy 33

3.3. Thermodynamics of High Pressure Processing 35

3.3.1. Adiabatic increase in temperature 35

3.3.2. Pressure work or heat generation 39

3.4. Heat Transfer in the Air Gap Between Vessel and Shell 40

3.5. Temperature Correction 41

3.5.1. Correction in experimentally measured temperature due to thermocouple response time 42

3.5.2. Correction in numerically predicted temperature due to addition of water from top 50

4. NUMERICAL SIMULATION 52

4.1. Setting Up the Problem in Fluent 54

5. RESULTS AND DISCUSSIONS 59

5.1. Numerically Predicted Results 59

5.1.1. Conduction heat transfer only 59

5.1.2. Conjugate heat transfer 61

5.1.3. Conduction vs. conjugate heat transfer..... 63

5.1.4. Conjugate heat transfer (laminar vs. turbulent)..... 66

5.1.5. Conjugate heat transfer for high initial temperature..... 68

5.2. Results for Time Constant Experiments..... 73

5.3. Comparison of Numerically Predicted with Experimental Data..... 73

5.3.1. Temperature correction due to water addition from top..... 76

5.4. Effect of Initial Temperature on Transverse and Axial Temperature Distribution..... 80

5.5. Effect of Vessel Size on Temperature Distribution..... 82

5.6. Effect of Insulating Sleeve (Teflon®) on Temperature Distribution..... 83

5.6.1. Numerically predicted results for room temperature (293.15 K)..... 85

5.6.2. Numerically predicted results for high initial temperature (333.15 K)..... 87

5.7. Effect of Changing Properties of Water..... 88

5.7.1. Thermal conductivity..... 91

5.7.2. Thermal conductivity, density and specific heat..... 92

6. CONCLUSIONS..... 98

7. FUTURE WORK..... 100

8. REFERENCES..... 101

LIST OF FIGURES

page no.

Figure 1.1 Typical variation of pressure with time during HHPP. 11

Figure 1.2 Typical pressure and temperature variation with time during HHPP..... 15

Figure 2.1 Rutgers 10 liter high hydrostatic pressure processing facility..... 24

Figure 2.2 Details of Rutgers high hydrostatic pressure processing set up. 24

Figure 2.3 Schematic of Rutgers high hydrostatic pressure processing vessel with dimensions.....26

Figure 2.4 High pressure thermocouple assembly made vertical for measuring the time constant for each thermocouple.....29

Figure 2.5 Experimental set up to heat the steel vessel using a circulating water bath. .. 30

Figure 3.1 Adiabatic compression heating values for water obtained from Food Biotechnology and Food Engineering, TU, Berlin.....38

Figure 3.2 Anticipated response of a thermocouple to ramp input during pressurization, pressure hold and depressurization.....43

Figure 4.1 (a) Dimensions of HHPP vessel. Shaded area represents the radial section for numerical simulation, (b) computational domain used for simulation, Ri = 71 mm, Ro = 223 mm.....53

Figure 4.2 Computational mesh used for numerical simulation. 54

Figure 4.3 Solver window as appearing in Fluent program. 55

Figure 4.4 Residual monitor window as appearing in Fluent to define convergence criteria.....57

Figure 4.5 Iteration window as appearing in the Fluent program. 58

Figure 5.1 Isotherms in water and s.steel wall at T_i = 298.15 K, P = 586 MPa, at the end of (a) pressurization (180 s), (b) hold period (780 s) for conduction heat transfer only.....60

Figure 5.2 Isotherms in water and s.steel wall at T_i = 298.15 K, P = 586 MPa, at the end of (a) pressurization (180 s), (b) hold period (780 s) for conjugate heat transfer when the flow was simulated as laminar flow.....62

Figure 5.3 Streamlines in water T_i = 298.15 K, P = 586 MPa, (a) before pressurization, (b) end of pressurization (180 s), & (c) end of hold period (780 s) for conjugate heat transfer when the flow was simulated as laminar flow.....63

Figure 5.4 Isotherms in water and s.steel vessel at T_i = 298.15 K, P = 586 MPa, at the end of (a) pressurization (180 s), (b) hold period (780 s) for conjugate heat transfer when the flow was simulated as turbulent flow.....64

Figure 5.5 Streamlines in water at T_i = 298.15 K, P = 586 MPa, (a) before pressurization, (b) end of pressurization (180 s), & (c) end of hold period (780 s) for conjugate heat transfer when the flow was simulated as turbulent flow..... 65

Figure 5.6 High pressure computational domain showing horizontal and vertical planes along which temperature variation was plotted. 65

Figure 5.7 Numerically predicted dimensionless temperature variation along the horizontal mid-plane at the end of pressure hold period (780 s) for conduction and conjugate heat transfer.....66

Figure 5.8 Numerically predicted dimensionless temperature variation along the vertical axis at the end of pressure hold period (780 s) for conduction and conjugate heat transfer.....66

Figure 5.9 Numerically predicted dimensionless temperature variation along the horizontal plane at the end of pressure hold period (780 s) for conjugate heat transfer simulated with laminar and turbulent flow. 67

Figure 5.10 Numerically predicted dimensionless temperature variation along the vertical plane at the end of pressure hold period (780 s) for conjugate heat transfer simulated with laminar and turbulent flow. 68

Figure 5.11 Isotherms in water and s.steel vessel at T_i = 288.15 K, P = 586 MPa, (a) before pressurization, (b) end of pressurization, (c) velocity vectors in water, & (d) end of hold period for conjugate heat transfer simulated with turbulent flow 69

Figure 5.12 Isotherms in water and s.steel wall at T_i = 313.15 K, P = 586 MPa, at the end of (a) pressurization (172 s), (b) hold period (772 s) for conjugate heat transfer with turbulent flow 70

Figure 5.13 Streamlines in water at T_i = 313.15 K, P = 586 MPa, (a) before pressurization, (b) end of pressurization (172 s), & (c) end of hold period (772 s) for conjugate heat transfer with turbulent flow 70

Figure 5.14 Isotherms in water and s.steel wall at T_i = 333.15 K, P = 586 MPa, at the end of (a) pressurization (180 s), (b) hold period (780 s) for conjugate heat transfer simulated for turbulent flow 71

Figure 5.15 Streamlines in water at T_i = 333.15 K, P = 586 MPa, (a) before pressurization, (b) end of pressurization (180 s), & (c) end of hold period (780 s) for conjugate heat transfer with turbulent flow 71

Figure 5.16 Isotherms in water and s.steel wall at T_i = 353.15 K, P = 586 MPa, at the end of (a) pressurization (180 s), (b) hold period (780 s) for conjugate heat transfer with turbulent flow.....72

Figure 5.17 Streamlines in water at T_i = 353.15 K, P = 586 MPa, (a) before pressurization, (b) end of pressurization (180 s), & (c) end of hold period (780 s) for conjugate heat transfer with turbulent flow.....72

Figure 5.18 Comparison of corrected experimental and numerically predicted time-temperature variations at T_i = 298.15 K, P = 586 MPa, for the thermocouple located (a) near top of the vessel, (b) in between, & (c) near bottom of the vessel in water..... 74

Figure 5.19 Comparison of corrected experimental and numerically predicted time-temperature variations at T_i = 288.15 K, P = 586 MPa, for the thermocouple located (a) near top of the vessel, (b) in between, and (c) near bottom of the vessel in water..... 75

Figure 5.20 Comparison of corrected experimental and numerically predicted time-temperature variation at T_i = 313.15 K, P = 586 MPa, for the thermocouple located (a) near the top of the vessel, (b) in between, & (c) near bottom of the vessel in water..... 77

Figure 5.21 Comparison of corrected experimental and numerically predicted time-temperature variations at T_i = 333.15 K, P = 586 MPa, for the thermocouple located (a) near top of the vessel, (b) in between, & (c) near bottom of the vessel in water..... 78

Figure 5.22 Comparison of corrected experimental and corrected numerical prediction time-temperature variation at T_i = 313.15 K, P = 586 MPa, for the thermocouple located (a) near top of the vessel, (b) in between, & (c) near bottom of the vessel in water.....79

Figure 5.23 Comparison of corrected experimental and corrected numerical prediction time-temperature variation at T_i = 333.15 K, P = 586 MPa, for the thermcouple located (a) near top of the vessel, (b) in between, & (c) near bottom of the vessel in water.....80

Figure 5.24 Numerically predicted dimensionless temperature profile along the vertical axis, at different values of T_i..... 82

Figure 5.25 Numerically predicted dimensionless temperature profile along the radial distance in water at the horizontal mid-plane, at different values of T_i..... 82

Figure 5.26 Numerically predicted dimensionless temperature variation along the horizontal mid-plane for vessels with different inner radii at the end of..... 84

Figure 5.27 Isotherms in water and s.steel wall at T_i = 293.15 K, P = 586 MPa, at the end of pressurization (180 s) (a) without Teflon® sleeve, (b) with Teflon® sleeve 0.635 cm thick.....86

Figure 5.28 Isotherms in water and s.steel wall at T_i = 293.15 K, P = 586 MPa, at the end of hold period (780 s) (a) without Teflon® sleeve, (b) with Teflon® sleeve 0.635 cm thick.....86

Figure 5.29 Isotherms in water and s.steel wall at T_i = 333.15 K, P = 586 MPa, for Teflon insulating sleeve of different thickness at the end of pressurization.....88

Figure 5.30 Isotherms in water and s.steel wall at T_i = 333.15 K, P = 586 MPa for Teflon insulating sleeve of different thickness at the end of hold period (780 s).....89

Figure 5.31 Streamlines in water at T_i = 333.15 K, P = 586 MPa, for Teflon insulation of different thickness at the end of hold period (780 s).....89

Figure 5.32 Numerically predicted dimensionless temperature profile for with and without insulation along the radial distance in water at the horizontal mid-plane at the end of hold time (780 s).....90

Figure 5.33 Numerically predicted dimensionless temperature profile for with and without insulation along the axial distance in water at the vertical plane at the end of hold time (780 s).....90

Figure 5.34 Isotherms in water and s.steel wall at T_i = 333.15 K, P = 586 MPa, at the end of (a) pressurization (180 s), (b) hold period (780 s) when thermal conductivity was pressure and temperature dependent.....94

Figure 5.35 Isotherms in water and s.steel wall at T_i = 333.15 K, P = 586 MPa, at the end of (a) pressurization (180 s), (b) hold period (780 s) when thermal conductivity was only temperature dependent.....94

Figure 5.36 Streamlines in water at T_i = 333.15 K, P = 586 MPa, (a) before pressurization, (b) end of pressurization (180 s), & (c) end of hold period (780 s) when thermal conductivity was pressure and temperature dependent.95

Figure 5.37 Streamlines in water at T_i = 333.15 K, P = 586 MPa, (a) before pressurization, (b) end of pressurization (180 s), & (c) end of hold period (780 s) when thermal conductivity was only temperature dependent.....95

Figure 5.38 Isotherms in water and s.steel wall at T_i = 333.15 K, P = 586 MPa, at the end of (a) pressurization (180 s), (b) hold period (780 s) when pressure-temperature dependent thermophysical properties were used.....96

Figure 5.39 Isotherms in water and s.steel wall at T_i = 333.15 K, P = 586 MPa, at the end of (a) pressurization (180 s), (b) hold period (780 s) when thermophysical properties were only temperature dependent. 96

Figure 5.40 Streamlines in water at T_i = 333.15 K, P = 586 MPa, (a) before pressurization, (b) end of pressurization (180 s), & (c) end of hold period (780 s) when pressure-temperature dependent thermophysical properties were used.....97

Figure 5.41 Streamlines in water at T_i = 333.15 K, P = 586 MPa, (a) before pressurization, (b) end of pressurization (180 s), & (c) end of hold period (780 s) when thermophysical properties used were only temperature dependent. 97

LIST OF TABLES

page no.

Table 1.1 Adiabatic compression heating values for certain food substances obtained from various sources. 14

Table 3.1 Theoretically calculated adiabatic compression heating values of water at different initial emperatures.....37

Table 3.2 Adiabatic compression heating values for water extracted from Figure 3.1.....38

Table 3.3 Adiabatic compression heating values of water obtained from NIST-IAPSW standard database plots. 39

Table 5.1 Difference (in K) between the maximum (near the top) and the minimum (near the bottom) temperature in water. 81

NOMENCLATURE

A	area (m^2)
C_P	specific heat (J/ [kg K])
C_{Pa}	specific heat of water at T_a (J/[kg K])
C_{Pf}	specific heat of water at T_f (J/[kg K])
C_{Pi}	specific heat of water at T_i (J/[kg K])
D	diameter of the cylinder (m)
$\vec{F}$	driving force for natural convection
Gr_x	Grashof number with x as characteristic dimension (= $g\beta\Delta Tx^3/\nu^2$)
Gr_L	Grashof number with length L as characteristic dimension
g	acceleration due to gravity (m/s^2)
g_z	acceleration due to gravity along negative z direction (m/s^2)
h	heat transfer coefficient (W/m^2 K)
k	thermal conductivity (W/m K)
L	length of the cylinder (m)
m_a	mass of water added (kg)
m_f	final mass of water (kg)
m_i	initial mass of water (kg)
m_t	mass of thermocouple
P	pressure (Pa)
Pr	Prandtl number, dimensionless (= $\mu C_P/k$)
Q	heat source term (W/m^3)
r	radial coordinate (m)

Ra_x	Rayleigh number, dimensionless (Gr_x. Pr)
Ri	inner radius of the vessel (m)
Ro	outer radius of the vessel (m)
s	specific entropy (J/[kg K])
t	time (s)
t_{cum}	pressure come up time (s)
t_{hold}	pressure hold time including t_{cum} (s)
T	temperature (K)
T_a	temperature of water added (K)
T_{cum}	temperature of water at the end of pressurization at t_{cum} (K)
T'	temperature read by thermocouple during pressurization (K)
T″	temperature read by thermocouple during hold period (K)
T_f	final temperature of water (K)
T_f	film temperature (K)
T_{hold}	temperature of water at the end of hold time at t_{hold} (K)
T_i	initial temperature of water (K)
T_{ip}	initial temperature of thermocouple probe (K)
T_{max}	maximum temperature (K)
T_s	surface temperature (temperature of the wall) (K)
T_w	temperature of water in which thermocouple is immersed
T_∞	fluid temperature far from surface of object or ambient temperature (K)
T_∞	temperature of constant water bath (K)
x	characteristic length (m)

∇	operator in axisymmetric cylindrical coordinates
z	axial coordinate
V	velocity vector (m/s)

GREEK SYMBOLS

α	thermal diffusivity of water [k/ ρ C_P] (m^2/s)
α_s	thermal diffusivity of steel (m^2/s)
β	coefficient of thermal expansion (K^{-1})
ε_m	momentum eddy viscosity (m^2/s)
ε_t	turbulent thermal diffusivity (m^2/s)
ρ	density of water (kg/m^3)
ρ_a	density of ambient medium (kg/m^3)
ρ_o	density at T_o (kg/m^3)
μ	absolute viscosity (Pa s)
φ_v	viscous dissipation
ν	kinematic viscosity (m^2/s)
υ	specific volume (m^3/kg)
τ	time constant of the thermocouple (s)

1. INTRODUCTION

High hydrostatic pressure processing (HHPP or HPP) is a novel, non-thermal technology used in the food industry to improve quality and safety of food products, and to extend the shelf life of products. During HHPP, foods (solids or liquids, packaged or unpackaged) may be subjected to pressures up to 1000 MPa (145,000 psi). To get an idea of how high is this high pressure, one has to imagine pressure under a dime if three big elephants (weighing 4-5 tons each) are made to stand on it! Although the proof of concept of HHPP was demonstrated more than hundred years ago, its utility and successful applications have been demonstrated only in last couple of decades.

1.1. History of Development of Preservation of Foods by HHPP

HHPP was first demonstrated as a possible food preservation process in 1899 by Hite (Hoover et al., 1989; Knorr, 1999). He showed that high pressure treatment can delay the souring of milk at ambient temperatures (Knorr, 2003). Bridgman (1914) observed coagulation of egg white with high pressure treatment. The technology did not attract wide recognition in this period due to non-availability of suitable high pressure equipment (Rastogi et al., 2007) but re-surfaced in food industry as an emerging technology in the late 1980s. Between 1982-1988 Professors Farkas, Hoover and Knorr at University of Delaware attempted to repeat Hite's work using a cold isostatic press and showed that pressures of 350 MPa (50,000 psi) can inactivate a wide range of pathogenic and spoilage microbes (Farkas, 2005). During the same period, studies were undertaken in Japan on preservation of foods by high pressure. In 1992, the first commercialized high pressure processed products in the world (high acid products including apple, strawberry, and pineapple jams) were marketed in Japan (Hayashi, 2002). Since then, high pressure

processing has also been applied to fruit preserves, rice cakes, raw squid, grape juice, and mandarin orange juice in Japan (Hayakawa et al., 1996; Rastogi et al., 2007). High pressure processed foods are in the market in Japan since 1992 (Suzuki, 2002), and in Europe and USA since 1996 (Knorr, 1999; Knorr et al., 2002). In US, the impetus for high pressure technology came from US Army research center in Natick, MA, to obtain better quality MREs (Meal Ready to Eat) for the troops. In 1993, they initiated a study to preserve foods using high pressure. They teamed up with professors at University of Delaware and Oregon State University to study the effect of pressure on microbes and to demonstrate pressure preservation of food products. Work over the next two years resulted in the successful preservation of spaghetti with meat sauce, Spanish rice, yogurt with peaches and a fruit mix. Samples were shown to be microbiologically stable for up to 120 days at room temperature. The first commercial high pressure product in US was Avo Classic Guacamole (a heat sensitive product) with extended refrigerated shelf life manufactured by Avomex Inc., Keller, TX. Other, commercially available high pressure processed products in Europe and the US include orange juice, milk, and oysters.

1.2. Potential Applications of HHPP

Initial emphasis of high pressure treatment was directed mostly towards food preservation by destruction of microorganisms, with the aim of extending shelf life of the food product while achieving minimum impact on product quality. With subsequent research, its potential for physical modification of structure and function of food and food constituents as well as the possibility for development of new processes such as pressure assisted freezing, thawing, frying and rehydration etc. were recognized (Rastogi et al., 2007). Other influences of pressure on food materials include protein denaturation or

modification, enzyme activation or inactivation, changes in enzyme substrate interactions and changes in the properties of polymer carbohydrates and fats (Butz and Tauscher, 2002).

The two basic principles that govern the effect of high pressure processing on foods are Pascal's isostatic principle and Le Chatelier's principle (Venugopal, 2006). According to Pascal's principle high pressure acts uniformly and instantly throughout mass of a food. The physico-chemical changes occurring during HHPP follow the Le Chatelier's principle, which states that any reaction, conformational change, or phase transition that is accompanied by a decrease in volume will be favored at high pressures, while reactions involving an increase in volume will be inhibited (Lopez-Malo et al., 2000).

The application of high pressure processing has considerable potential as an alternative to conventional thermal treatment in terms of instantaneous pressure transmission, i.e., time for pressurization treatment is independent of size and shape of food product (hence a large batch does not need longer processing time than a smaller batch), reduced process times, retention of freshness, texture, flavor, and color (Butz et al., 1997). Therefore, HHPP offers a unique way to produce new, safe, high quality products, with minimum detrimental effects that are associated with thermal processing such as loss of original flavor and color.

Some of the potential applications of high pressure processing are discussed in detail in the next few sections.

Quality Retention and Enhancement

In general, chemical reactions associated with reduction in volume are favored during HHPP. However, high pressure does not affect the covalent bonds in foods (Knorr, 1999). Therefore, the retention of color, nutrients and taste in high pressure processed foods is better compared to thermally processed foods. Butz et al. (2002a) showed no major changes in nutritional values and in antioxidant activity of tomato and carrot after HHPP. Butz et al. (2002b) found that chlorophyll was stable at 75˚C and 600 MPa for long treatment times (10-40 min) and that vitamin C was stable after high pressure processing. Butz and Tauscher (2002) found that under pressure aspartame decayed to its non-sweet components faster in milk but in acidic medium like juices or carbonated drinks it was insensitive to pressure. They also showed that during HHPP of carrot puree, carotenoids were well protected since they are buried in lipophilic environments, which implies that the food matrix offers protection against loss of quality (Butz and Tauscher, 2002). In another study done on orange juice sensory panel could not perceive difference between pressure treated and unpressurized juice (Knorr, 2001). In addition, control juice showed signs of fermentation after 2 weeks at 6˚C and became organoleptically unacceptable, pressure treated juice remained free from fermentation for 5 weeks.

Modification of Structure and Function of Foods

High pressure has a great potential for modification of structure and function of food and food constituents such as protein denaturation and starch gelatinization (Knorr, 1999). Enzymes are a special group of proteins which have been shown to activate under lower pressures (100-200 MPa) while higher pressures generally induce enzyme inactivation

(Knorr, 1999). Protein denaturation with pressure is affected by pH, presence of salt, substrate concentration, and subunit structure of enzyme (Hoover et al., 1989). Process parameters like pressure, time, and temperature affect restructuring of proteins, which may lead to high value products (Messens et al., 1997). Molina and Ledward (2003) studied the gelation of soy proteins and found that pressurizing the proteins before heat treatment or pressure treatment alone gave different results from heating alone. The spectrum of pressure denatured protein has more features of native protein than spectrum of temperature denatured protein (Knorr, 2001). Aqueous starch dispersions could be gelatinized at room temperature under high pressure (Solt and Autio, 1998). They further found that pressure induced gels of waxy maize and potato starch were stronger than heat induced gels. Thus, combination of heat and high pressure can offer novel textures and novel products.

Microbial Inactivation

Pressure induced inactivation mechanism of microorganisms is a complex phenomenon, which includes protein denaturation, phase change, morphological changes, and membrane effects. Studies involving the mechanism of cell lysis show that pressure affects microorganisms in different ways. High pressure can cause an inactivation in membrane transport systems that results in sublethal injury or it can affect metabolic activity and damage the cell membrane (Hartmann & Delgado, 2003). Intracellular gas vacuoles can collapse at pressures of 0.6 MPa (Hoover et al., 1989). Some microorganisms, such as *Listeria monocytogenes,* show higher inactivation rates at low temperature high pressure treatments (Knorr, 1999). High pressures up to 600 MPa can inactivate vegetative cells and enzymes without heat, but not bacterial spores (Hayakawa

et al., 1996). Spores are resistant to high pressures even up to 800 MPa partly because of the low water content in the spore coat compared to vegetative cells (Hayakawa et al., 1996). However, high pressure processing can be used with heat to inactivate spores of *Bacillus stearothermophilus* at 90˚C for 30 min at 150 MPa to bring about 2 log reduction from an original count of 10^6, and of *B. subtilus* at 70˚C and 150 MPa (Knorr, 1999; Balasubramanian and Balasubramaniam, 2003). Knorr (1999) stated that metabolite production of some microorganisms can be increased with high pressure and inactivation of some microorganisms is not correlated with temperature or pressure interaction. This will create unique opportunities for selective inactivation of some microorganisms in a mixture (Knorr, 1999).

Inactivation of hepatitis A virus (HAV) and feline calicivirus, a Norovirus surrogate, by high hydrostatic pressure has been shown by Kingsley et al., (2002). They found 7 log reduction after processing at 450 MPa for 5 minutes for HAV and at 275 MPa for 5 minutes for feline calicivirus. The NIH recently conducted a study using HHPP (690-1200 MPa) to inactivate infectious prions responsible for bovine spongiform encephalopathy (BSE) (Schauwecker, 2004; Brown et al., 2003). These experiments were carried out at elevated temperatures (121-137˚C) suggesting that combination of high temperature and high pressure is needed for the inactivation of BSE prions.

Sudden Decompression

The time to increase the pressure from ambient to 1000 MPa may be 3-4 minutes but releasing pressure takes only a few seconds (Hayakawa et al., 1996). Sudden release of pressure has been found to be sometimes more effective than pressure alone (Hayakawa

et al., 1996). Fast release of pressure or decompression causes more damage to spores than increasing the exposure time at high pressure.

Pressure Assisted Processes

(a) Freezing and Thawing

HHPP offers a possibility for new process options like high pressure assisted freezing and thawing, and pressure shift freezing and thawing (Knorr, 1999). Pressure assisted process is the normal freezing or thawing occurring under a constant pressure while pressure shift freezing or thawing is achieved during sudden pressure release (depressurization). Decrease in melting and freezing point of water with pressure to a minimum of –22˚C at 207.5 MPa (Denys et al., 1997; Cheftel et al., 2000; Le Bail et al., 2002a&b) leads to rapid ice nucleation resulting in small and uniform ice crystals during pressure release and causes less structural damage to the food compared to conventional slow freezing. It was found that pressure shift freezing (140 MPa, -14˚C) resulted in smaller and more uniform ice crystals compared to air blast freezing (Chevalier et al., 2002). In general, conventionally thawing occurs more slowly than freezing, further damaging the food. Pressure induced thawing reduces the loss of water holding capacity and improves color and flavor preservation in fruits (Rastogi et al., 2007). Also, high pressure treatment has been shown to reduce the thawing time of frozen meat to one-third of time necessary at atmospheric pressure and also reduce drip loss (Chourot et al., 1997; Denys et al., 1997; Le Bail et al., 2002).

(b) Dehydration and Rehydration

Dehydration process like osmotic dehydration is a slow process. Application of high pressure causes permeabilization of cell structure thus allowing enhanced mass transfer.

It has been shown that after pressure treatment of 600 MPa for 15 min drying rate of potatoes was increased significantly (Rastogi et al., 2007). Similarly, enhanced water removal and solid gain was observed during osmotic dehydration of pineapple (Rastogi et al., 2007). Most dehydrated foods are rehydrated before consumption. Loss of solids during rehydration is a major problem associated with dehydrated foods. Increased water uptake during soaking of glutinous rice was found after a pressure treatment of up to 600 MPa (Rastogi et al., 2007).

1.3. Literature Review of HHPP of Food Products

As discussed in the previous section, in addition to food preservation, HHPP can result in products with novel structure and texture, or increased functionality of certain ingredients providing the possibility for development of new food products (Rastogi et al., 2007).

HHPP has been shown to be used for improving shelf life of yogurt and defrosting frozen seafood (Hayakawa et al., 1996). It has also been shown to improve rennet or acid coagulation of whey proteins and increases cheese yield (Trujillo et al., 2000). HHPP can be used to design or improve existing products like cream caramel with fresher taste and more juiciness (Ponce et al., 1998). HHP treatment may increase mass transfer and juice yield, and enhance drying (Knorr, 2003). HHPP can result in improved release of metabolites from plants and reduced fat uptake of French fries (Knorr, 1999). A reduction of 40 % in oil uptake during frying was observed, when thermally blanched frozen potatoes were replaced by high pressure blanched potatoes (Rastogi et al., 2007). Sanchez-Moreno et al. (2003b) have found that carotenoid and vitamin A in orange juice could be extracted better with increasing pressure from 100 to 400 MPa.

Although the effect of high pressure on foods up to 1000 MPa (145,000 psi) has been investigated, but equipment design limitations restrict the commercial applications up to 690 MPa (100,000 psi).

1.4. High Pressure Process and Equipment Description

High pressure food processing is typically carried out as a batch process where foods, solids or liquids are subjected to pressures between 50 and 1000 MPa. High pressure equipment with pressures up to 800 MPa and temperatures in the range of 5˚C to 90˚C for process times up to 30 min or longer are currently available to the food industry (Henry and Chapman, 2002). The two types of high pressure equipments available for the food industry are: conventional batch systems and semi-continuous systems. In batch systems, both solid and liquid food products can be treated whereas only low viscous pumpable liquid foods can be treated in semi-continuous systems. For high pressure to be effective the food substances must contain water or oil and not have internal air pockets. Food substances containing entrapped air such as strawberries or marshmallows would be crushed under high pressure and dry solids do not have sufficient moisture to make high pressure processing effective for microbial destruction.

Currently, available semi-continuous systems use a pressure vessel containing a free piston to compress liquid foods. In the US, Avure Technologies (Kent, WA) manufactures semi-continuous systems for processing clear liquids such as juices. A low pressure food pump is used to fill the vessel. When filled, the input port is closed and high pressure process water is introduced behind the free piston to compress the food. After certain pressure hold, the system is decompressed by releasing the pressure on the high pressure process water. The liquid after treatment is discharged from the pressure

vessel into a sterile hold tank. Then the treated liquid food can be filled aseptically into pre-sterilized containers.

During a batch high pressure process the food products are generally vacuum packed in a flexible pouch or a container and loaded in the vessel, the vessel is then filled with a pressure transmitting medium. Water is frequently used as a pressure transmitting fluid in the food industry from its mechanical safety and economic point of view (Makita, 1992). The high pressure process is then accomplished in three phases, compression (pressurization) phase where pressure is increased from ambient to the desired high pressure as shown in **Figure 1.1**. High pressure does not destroy food because pressure is applied isostatically, i.e., equally from all the directions which provides a uniform effect.

Also, during pressurization phase the work done for compression gets converted into heat and increases the temperature of the pressurizing medium. The thermal effects associated with high pressure process are discussed in detail in next section. The pressurization phase is followed by a pressure holding phase where the pressure is held constant at the elevated pressure level for several minutes. Finally, the pressure is reduced to ambient during depressurization phase. The product is then taken out for further treatment or packaging.

High pressure can be generated in the system by three ways: direct compression, indirect compression, and heating of pressure transmitting medium. In direct compression a piston with a large end and a small end is used. The large end of the piston is connected to a low pressure pump and small end is used to reduce the volume of the pressure

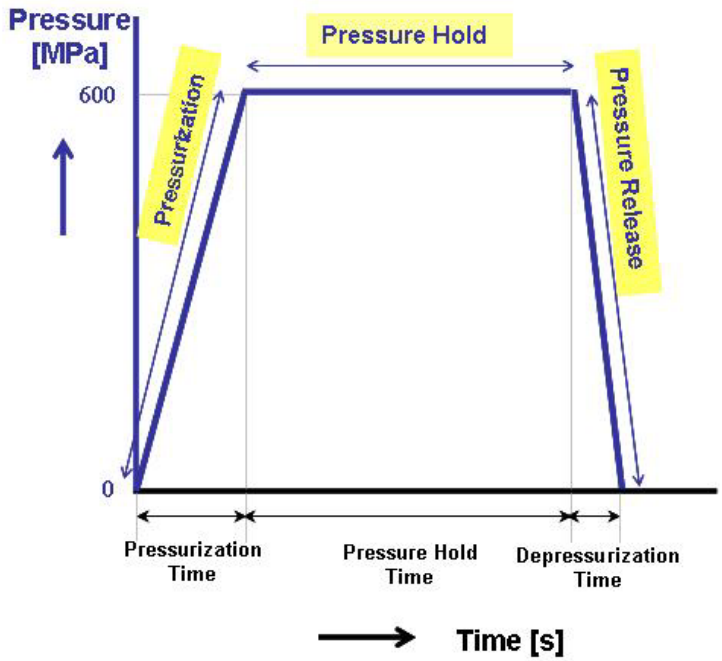

Figure 1.1 Typical variation of pressure with time during HHPP.

transmitting medium by the action of hydraulic pressure applied over large end of piston. Indirect compression uses a high pressure intensifier to pump the pressurizing medium from a reservoir directly into a closed and deaerated vessel to reach a given pressure (Venugopal, 2006). This system also uses a piston to increase the pressure, as in direct compression, but the displacement of the piston is achieved by pumping water with an intensifier (high pressure pump) into the vessel. The third pressurization method which is not used in food industry so far, involves the heating of the pressure transmitting medium inside the vessel to cause expansion by increase in temperature (Venugopal, 2006).

Typical batch high pressure equipment consists of a cylindrical steel vessel with high tensile strength, two end closures, a means for restraining end closures (a closing yoke to cope with high axial forces), direct or indirect pressure pumps for pressure generation, and necessary pressure and temperature controls (Henry and Chapman, 2002). The cylindrical steel vessel used can be a monobloc cylinder with several advantages such as

simple construction, high precision in strength calculations and low production costs but they can be used only for smaller size vessels. They are not suitable for large size vessels due to problems like reduction in strength. Very high fluid pressures produce high forces and thus need thick walled cylinders. In monobloc cylinders, the hoop stress at outside of the wall thickness is appreciably less than that at the inside surface, hence, wall material is not used to the fullest strength (Fryer and Harvey, 1997). One method to mitigate this has been through residual stresses imposed by multilayered cylinder (compression fitted) and wire winding of cylinder. In multi layered cylinder two or more cylinders are shrinkage fitted (compression fitted) which give rise to high compressive residual stresses within the inner cylinder due to compression fitting and increase the fatigue strength, thus assuring safety even when fatigue failure occurs within the cylinder. Wire winding of cylinders also results in compressive residual stresses within the wall of the cylinder and thus high tensile stresses do not arise when wire wound cylinders are subjected to internal pressures, giving them higher strength (Koizumi and Nishihara, 2001). It also provides 'leak before break' failure mode to for large cross-section vessels and thus ensures safety.

1.5. Thermal Transport During HHPP

Although, HHPP is termed as a non-thermal process, thermodynamics dictates that all compressible substances undergo increase/decrease in temperature during processes of compression/expansion. Most of the food substances including water are incompressible at lower pressures but at high pressures they undergo substantial compression. For example, water which is a polar substance gets compressed by 15% at 600 MPa (Venugopal, 2006) whereas hexane (non-polar) is compressed by 25% at 600 MPa. When high pressure is applied to a food substance, the molecules of the food get compressed,

i.e., their intermolecular distance decreases and heat is generated due to work done against the intermolecular forces. The heat so generated is known as adiabatic heat of compression which results in an increase in temperature of the food. This rise in temperature is reversed upon depressurization as the heat is absorbed. Temperature increase in ˚C per 100 MPa increase in pressure is generally known as the compression heating value of a substance. The compression heating value for foods during high pressure process depend on factors such as process pressure, compressibility, initial temperature, composition of food, and their thermodynamic properties like viscosity, thermal conductivity and specific heat (Rasanayagam et al., 2003). **Table 1.1** shows adiabatic compression heating values for different food substances. Dependence of compression heating value of a food on process pressure is expected as for water this value changes with increase in pressure (Barbosa-Canovas and Rodriguez, 2005).

As seen from **Table 1.1** the compression heating values for foods range from 2-40˚C. For water this value is 2-3˚C whereas for oils and fats it is 6-9˚C due to their higher compressibility, lower thermal conductivity and lower heat capacity. Compression heating value of lipids (~20˚C) is independent of length of hydrocarbon chain but higher degree of unsaturation of hydrocarbon chain lowers the compression heating value (~14˚C) for lipids (Knorr, 2001). For solvents such as hexane this value could be as high as 40˚C. It has also been shown that the compression heating value of water increases with increasing initial temperature while compression heating value of oil is not significantly affected by initial temperature (Rasanayagam et al., 2003). In food industry, water is most commonly used as a pressure transmitting medium because of its safety, low cost, and comparable compression heating value to most foods like juices.

Table 1.1 Adiabatic compression heating values for certain food substances obtained from various sources.

Substance at 25˚C	Temperature change per 100 MPa (˚C)
Water	~ 3.0
Orange Juice	~ 3.0
2% Fat Milk	~ 3.0
Tomato Salsa	~ 3.0
Salmon	~ 3.2
Chicken Fat	~ 4.5
Beef Fat	~ 6.3
Olive Oil	~ 6.0 to 8.7
Soy Oil	~ 6.2 to 9.0
Hexane	~ 40.0

Also, if the pressure transmitting fluid has high compression heating value like oils, the inactivation data could include unintended thermal effects (Ting et al., 2002).

The heat generated due to adiabatic compression heating of the pressurizing medium results in temperature difference between the food sample, pressurizing medium and the vessel wall, and is continuously dissipated through the thick metal walls of the vessel by heat conduction. This happens during pressurization and also during pressure hold time when there is no heat generation. Therefore, upon depressurization, the temperature drops below the initial temperature as shown in **Figure 1.2.**

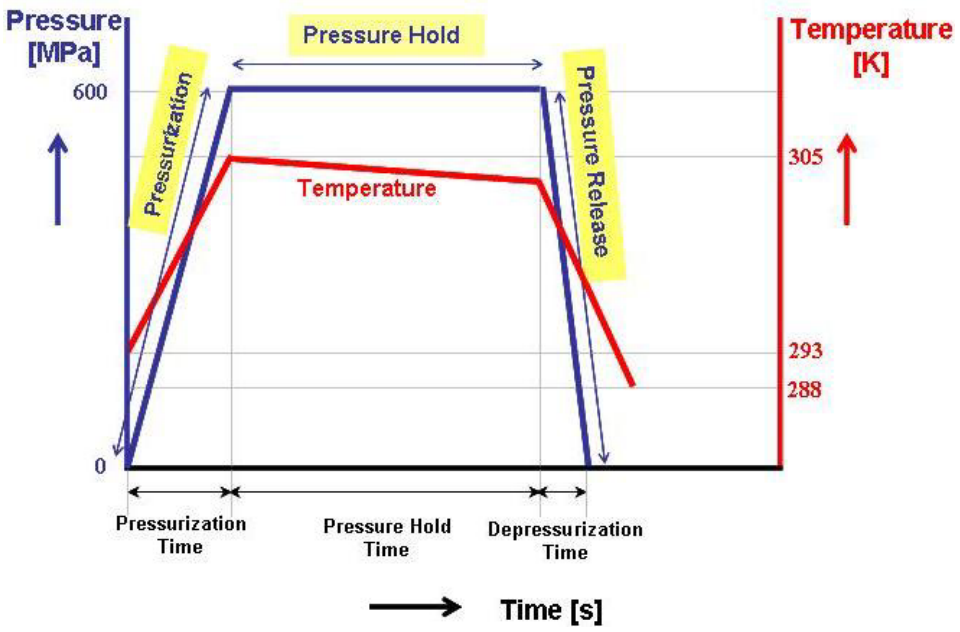

Figure 1.2 Typical pressure and temperature variation with time during HHPP.

The heat loss at the wall gives rise to non-uniform temperature distribution with the fluid at the center of vessel being warmer than the fluid near the wall. Also, free convection sets in near the vessel wall affecting the temperature distribution. Makita (1992) observed that, although temperature of high pressure medium at the wall of the vessel decreases quickly due to high thermal conductivity of the vessel metal, the central high pressure medium reaches a maximum temperature that equals the sum of initial temperature of medium and increase in temperature due to compression heating. In addition, during indirect pressurization, additional liquid has to be pumped into the vessel through an external source which can be at a temperature different from existing temperature of the liquid in the vessel further affecting the temperature distribution.

When high pressure treatment is applied to microorganisms that can be inactivated by application of high pressure alone, temperature distribution in the vessel is of no practical relevance. Therefore, at lower initial temperatures, i.e., room temperature, temperature

non-uniformity in the process does not pose any threat to the safety of the product. However, bacterial spores can either survive pressures above 1000 MPa at ambient temperatures (Balasubramanian and Balasubramaniam, 2003). However, only moderate pressures (~600 MPa) are needed at moderate temperatures (> 70˚C) if a combined pressure-temperature treatment (Ghani and Farid, 2007) is used. In that case, non-uniform temperature distribution during the process can cause non-uniform inactivation of the spores that are resistant to lower pressures but are susceptible to high pressure and high temperature combination treatment. Thus, it becomes necessary to understand the temperature distribution established in the vessel due to conjugate (conduction and convection) heat transfer to design process control strategies in order to achieve high degree of process uniformity.

As foods undergo minimal nutrient destruction at temperatures below 100˚C (373.15 K), HHPP can be applied at moderate temperatures to a number of food products, especially those contaminated with spores, which are usually sterilized thermally at a temperature near 121˚C (394.15 K). Ghani and Farid (2007) stated that adiabatic heating caused by fluid compression at high pressure can cause significant temperature distribution throughout the treated food. By taking into account the non-uniform temperature distribution during the process, it can be assured that the objective of the process has been accomplished everywhere within the food product (Denys et al., 2000).

1.6. Literature Review of Mathematical Modeling of HHPP

Mathematical modeling studies facilitate understanding of the thermal transport of a system better but they should be supported with experimental data (Pehl et al., 2002). Modeling of hydrodynamic and thermal changes during HHPP has been attempted by

several researchers (Hartmann, 2002; Hartmann et al., 2003; Pehl et al., 2000; Otero et al., 2002a, 2002b, 2002c). These researchers followed a deterministic approach based on governing equations for the high pressure process for their numerical models. One of the main difficulties when modeling heat transfer in high pressure process is lack of appropriate thermophysical properties of different food materials under pressure.

Pehl and Delgado (1999, 2002) and Pehl, Werner, and Delgado (2002) were the first to examine the dynamic effects of fluid convection and heat transfer in high pressure process. For this study they used a high pressure optical cell of 2 ml volumetric capacity. They developed high pressure digital particle image thermography and high pressure digital particle image velocimetry which allow determination of time scales for hydrodynamic and thermal compensation of liquids under high pressures up to 800 MPa (Hartmann et al., 2003). These experimental analyses were confirmed by the numerical investigations of Hartmann (2002) and Hartmann and Delgado (2002a) and were found to be in good agreement.

Hartmann and Delgado (2002b) investigated the effect of convective heat transfer during high pressure on enzyme inactivation using finite volume numerical scheme. They investigated the effect of geometrical scale of the vessel and medium viscosity on the thermal non-uniformity during high-pressure treatment. In their model they used viscosity as a function of temperature and pressure. They found that larger vessel size increased the inactivation rate due to higher average temperature, which is caused by less heat loss at the walls (Hartmann and Delgado, 2002b; Hartmann et al., 2003; Hartmann and Delgado, 2003).

Hartmann et al. (2003) studied the effect of convective and diffusive transport on inactivation of *Escherichia coli* in packed food (milk) under high pressure. They used a finite volume numerical approach and included temperature conduction equation for package in the model. Also, in their model they used density, heat capacity and viscosity of water (medium) as a function of temperature and pressure. They found that non-uniformities of more than one log cycle can be observed depending on the package material parameters, on the position and arrangement of the packages in the vessel. For packed liquid food systems with lower thermal conductivity package, induced natural convection may lead to non-uniformities, depending on the viscosity of the packed food. In absence of these thermal non-uniformities, the inactivation would be higher and processing time could be reduced for larger scale vessels (Hartmann et al., 2003; Hartmann and Delgado, 2003).

Hartmann and Delgado (2004) have numerically simulated the mechanical effects of the compression of a yeast cell under high hydrostatic pressure, using a finite element method. They found that the deformation of cell under pressure deviated strongly from the isotropic volume reduction.

Denys et al. (1998 and 2000) modeled conductive heat transfer during HHPP using a finite difference numerical approach. They considered an overall heat transfer coefficient model to account for heat transfer between pressurizing medium and vessel wall. Pressure dependent thermal conductivity and thermal expansion coefficient of the product were determined experimentally and incorporated in the numerical scheme. They showed numerically that with pressure cycling, 8 cycles each of 30s compression time and 2 min holding time at 500 MPa pressure, higher inactivation rate for *Bacilus subtilus* α-amylase

were achieved compared to one step application at same pressure and same total process time. This was associated to the temperature increase during compression. They also observed that the maximum temperature reached during the cycling process is lower than when same pressure was established in one step. On the other hand, higher heterogeneity in terms of temperature was observed with cycling (Denys et al., 2000).

Improvements are needed for the contribution of the convection heat transfer in the high-pressure fluid (Denys et al., 1997). Several researchers (Pehl et al., 2002; Hartmann and Delgado, 2002a, 2002b) have indicated that more viscous foods give more thermal heterogeneity. 50% sucrose solution gave 6 times larger temperature gradient compared to water under the same conditions (Pehl et al., 2002). Therefore, viscosity of food under pressure should be a known parameter and thermofluiddynamical processes need to be investigated.

1.7. Experimental Challenges

Some of the challenges associated with the research in this area are lack of techniques to measure and visualize temperature, pressure, and velocity in the vessel while under high pressure. This results in a limitation to accurately validate the numerical simulation results. Thermocouples installed inside the high pressure chamber are currently used to validate the temperature history at particular points in the vessel and a pressure transducer is used to measure the inline pressure. Using a 2 mL high pressure cell Pehl et al. (2000) have shown that they can use thermochromic liquid crystals for temperature visualization under high pressure. However, more experimental research is needed to develop methods that can aid in better visualization of temperature, pressure, and velocity in a commercial size vessel during the high pressure process.

1.8. Lead to Hypotheses and Objectives

As pointed out earlier, the work done on the fluid during pressurization results in increased internal energy of the system which causes temperature to increase. This increase in temperature and the heat loss at the vessel wall cause variation in density within the fluid and a flow can be induced due to buoyancy force. The induced flow along with the heat loss to the vessel wall can lead to non-uniform temperature distributions within the fluid. Also, addition of water to the vessel during pressurization to compensate for compression will affect the flow field and the temperature distribution.

Ideally, a thermocouple should respond faithfully to fluctuating temperatures it is supposed to measure regardless of the time rate of change of temperature but in practice this is seldom the case (Beckwith et al., 1982). When a thermocouple is subjected to a rapid temperature change, it will take some time to respond. If response time is slow as compared to the rate of change of temperature being measured, the thermocouple will not be able to faithfully represent the dynamic response to temperature change. Therefore, it is important to know the dynamic response of the high pressure thermocouple assembly.

1.9. Hypotheses

The hypotheses for this research were as follows:

1. The temperature distribution inside a HHPP vessel becomes non-uniform during the process and this non-uniformity in temperature arises because of adiabatic compression heating and concomitant heat loss to the thick wall of the vessel.

2. In a large scale vessel there is a lag in the temperature measurement due to the thick metal sleeve surrounding the thermocouple wires.

3. Changing the curved surface area/volume ratio of a pressure chamber will result in substantially different temperature distribution.

4. Adding an insulating sleeve will reduce the temperature non-uniformity.

1.10. Rationale

In high pressure processes it is extremely important to know the temperature distribution in the vessel when a combination of temperature and pressure is needed for inactivation of certain bacterial spores. Non-uniform temperature in the vessel can lead to non-uniform inactivation. Also, determining accurate temperature distribution in a high pressure vessel will help to differentiate the effect of temperature and pressure and generate understanding of the synergy between pressure and temperature on inactivation kinetics of enzymes, nutritional and flavor compounds, and microorganisms.

To evaluate the process performance and its effectiveness, it is important to know the effect of initial temperature, and properties of food material, pressurizing medium and vessel, on the temperature distribution during high pressure processing. Modeling heat transfer in high-pressure food processes can be used as an effective tool to ensure that the treatment is uniform.

1.11. Objectives

The overall objective of this research was to study the temperature distribution in a commercial high pressure food processing vessel during a typical high pressure process.

The specific objectives of the project were as follows:

1. To numerically simulate the temperature distribution inside a large commercial size high pressure food processing vessel and to study the temperature non-uniformity arising in the pressurizing medium (water).

2. To validate the numerical simulation results with experimental data at selected initial temperatures taking into account the lag between the true temperature and the temperature measured by the high pressure thermocouple assembly.

3. To investigate the effect of vessel size on the temperature distribution in the pressurizing medium.

4. To investigate the effect of an insulating sleeve on the temperature non-uniformity in the medium.

2. MATERIALS AND METHODS

The research methodology included both experimental and numerical approaches. The precise control of parameters like ambient temperature and initial temperature of fluid during experiments was difficult, therefore, the experiments were performed first and the initial experimental conditions were then used as an input to the numerical simulation program for prediction of temperature distribution inside the vessel. The experiments were carried out with water as the test fluid.

2.1. High Pressure Food Processor – Experimental Facility

High hydrostatic pressure processing unit used for experimental investigations was put together using equipment manufactured by Elmhurst, Inc., Albany, NY and is shown in **Figure 2.1**. The unit comprised of a 10 liter high pressure vessel with an external heating tank and a 20 HP intensifier pump to build a maximum pressure of 690 MPa (100,000 psi) in 3 min or less. The equipment was rated for a temperature range of 5˚C to 90˚C and was capable of pressure hold times of up to 60 min. It also had pressure cycling capability. The detailed setup of the unit is shown in **Figure 2.2**, which shows the processing vessel, the pump, the yoke and the control panel. The processing vessel is a tilt vessel assembly for easy loading and unloading of samples. An intensifier pump was used to raise the pressure in the vessel with filtered tap water. The function of the yoke is to restrain the end closures and cope with high axial forces. A PLC control panel was used to control, display, and maintain the process pressure and time during the process along with start up and emergency shut down procedures. It was also used for controlling real time record of pressure and temperature.

Figure 2.1 Rutgers 10 liter high hydrostatic pressure processing facility.

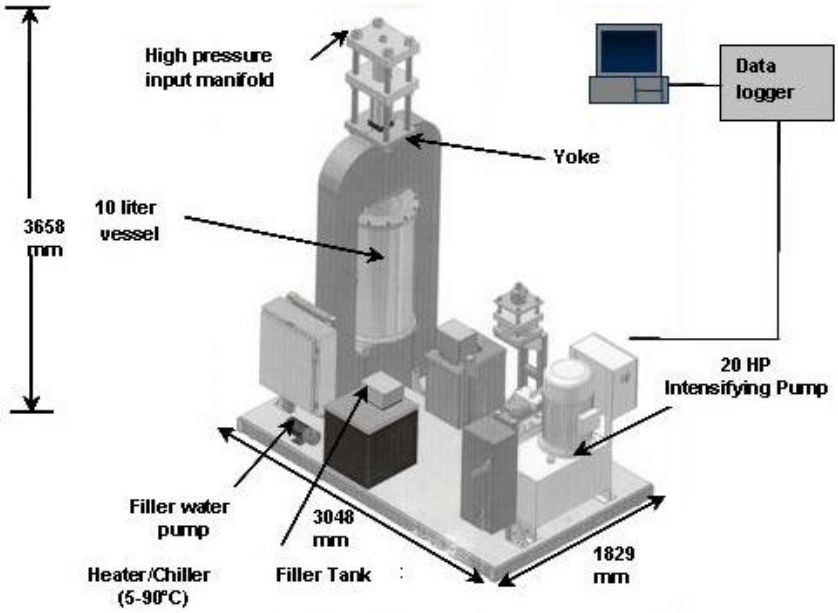

Figure 2.2 Details of Rutgers high hydrostatic pressure processing set up.

2.1.1. High pressure vessel

The high hydrostatic pressure processing unit comprised of a stainless steel cylindrical vessel. The overall length of the cylinder was 1090 mm and the external diameter was 445 mm. The pressure cavity in the cylinder had a diameter of 142 mm and length of 823 mm, surrounded by thick s.steel wall as shown in **Figure 2.3**. The vessel had an outer shell with air gap of 2.38 mm between solid steel wall and the shell as shown schematically in **Figure 2.3**. It also shows the high top and bottom closures. The purpose of these closures is to provide an ideal seal while the vessel is pressurized. In present study the vessel bottom closure was fixed whereas, the top closure was removable for loading and unloading. In both the bottom and top closures sealing is accomplished by a combination of o-ring and separate metal and polymer back up rings. The o-ring is always made of a softer material (an elastomer) and deforms under pressure filling and sealing any irregularities on the connecting surfaces. The metal and polymer back up rings are designed to expand and contract as pressure increases or decreases, thus continuously confining the o-ring in place with no clearance. Also, for the given vessel the water input to the vessel during pressurization was through the top closure. The steel sleeves shown in **Figure 2.3**, were the part of the top closure assembly that fitted into pressure cavity.

2.1.2. Working description of HHPP

The high pressure vessel remained in horizontal position when not in use. In general, food was loaded into the pressure cavity in this position, top closure inserted and then the vessel was made vertical and filled with water. But in the present study pressure

transmitting medium, water itself was used as the test fluid, therefore, the top closure was inserted and the tilt vessel assembly allowed filling of water into the pressure cavity through an opening in the top closure. Vessel filled with water was made vertical. Using the PLC panel the desired final pressure (586 MPa) and hold time (10 min) were set. The vessel was pressurized using an intensifier (20 HP high pressure pump). Water was automatically pumped into the vessel from the top closure until the set pressure was achieved. Pressure in the vessel was held constant for defined period of time (10 min). At the end of hold time, the vessel was depressurized.

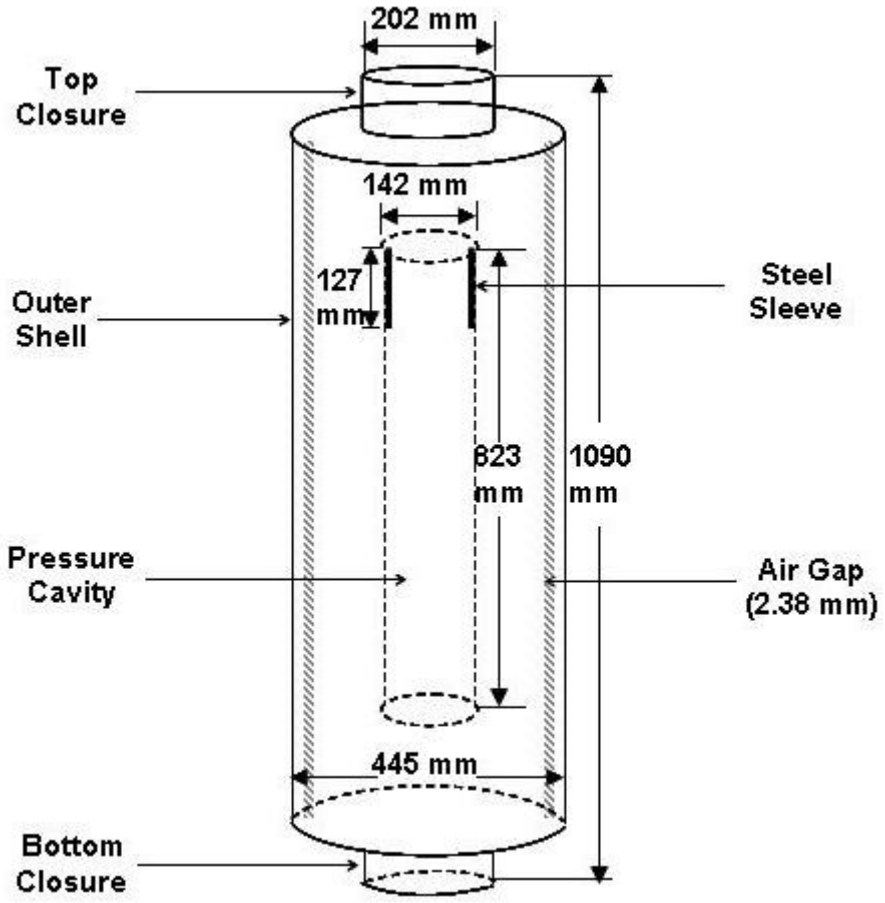

Figure 2.3 Schematic of Rutgers high hydrostatic pressure processing vessel with dimensions.

2.1.3. Pressure measurements

The pressure in the system during the process was measured using a transducer which measured the line pressure and it was assumed that it was the same pressure as the pressure in the vessel. Pressure data as a function of time was recorded at a frequency of 4 Hz, over the entire period of pressurization, pressure hold and depressurization by a data acquisition system from National Instruments (LabVIEW^{TM} 7 Express), Austin, TX.

2.1.4. Temperature measurements

The pressure vessel came equipped with three thermocouple probes that were threaded to the inside of the top closure. These thermocouples facilitated measurement of temperature of water in the vessel during the high pressure process. The probes were type K (Ni-Cr/Ni-Al) thermocouples (ungrounded) in high pressure tubing (inner diameter 2.1 mm). The temperature range for type K thermocouple is -200˚C to 1200˚C. Often type K thermocouples are used in high pressure vessel because their calibration is not sensitive to pressure. The tips of the thermocouples were located at three different depths (203 mm, 318 mm and 546 mm from the top of the pressure cavity) and 10 mm away from the wall. Temperature data as a function of time for all three thermocouples were recorded at a frequency of 4 Hz over the entire period of pressurization, pressure hold and depressurization by a data acquisition system from National Instruments (LabVIEW^{TM} 7 Express).

2.2. Special Experimental Set Up

A special experimental setup was used for performing the experiments at higher initial temperature and to calculate the time constant of the thermocouples.

2.2.1. Time constant experiment

The dynamic response of a high pressure thermocouple assembly is a function of the design of the thermocouple. In our case the delay in the response was due to the high pressure tubing surrounding the thermocouples. The time constant values for the three thermocouples were determined in a specially designed experiment and the values were used as an input in the equations (3-48) and (3-69) to find the true temperature as discussed in section 3.5.1.

The response of a thermocouple to step change in temperature is given by

$$\frac{[T_\infty - T]}{[T_\infty - T_{ip}]} = e^{(-t/\tau)} \quad \text{.....} \quad (2\text{-}1)$$

where, T_∞ is the temperature of constant water bath, T is the temperature of thermocouple probe, T_{ip} is the initial temperature of thermocouple probe, t is the time, and τ represents the time constant of the thermocouple.

To experimentally obtain the value of the time constant τ for each thermocouple, the high pressure thermocouple assembly was taken out of the high pressure vessel and made vertical by hanging it using a support system as shown in **Figure 2.4**. In three different experiments the thermocouples were immersed in constant water baths (ice point bath, boiling water bath and a fixed temperature bath at 50˚C (323.15 K)) and the time-temperature data were recorded using LabVIEW^{TM} 7 Express. Each experiment was repeated a minimum of three times. The time constant τ value for each thermocouple was obtained by plotting natural logarithm of left hand side term of equation (2-1) as a function of time and fitting a straight line to this data. The negative reciprocal of the

slope of the best fit line is the time constant τ. The analysis of variance (ANOVA) was performed to estimate the significance of the effect of high pressure thermocouple tube length and heating medium temperature on the time constant value.

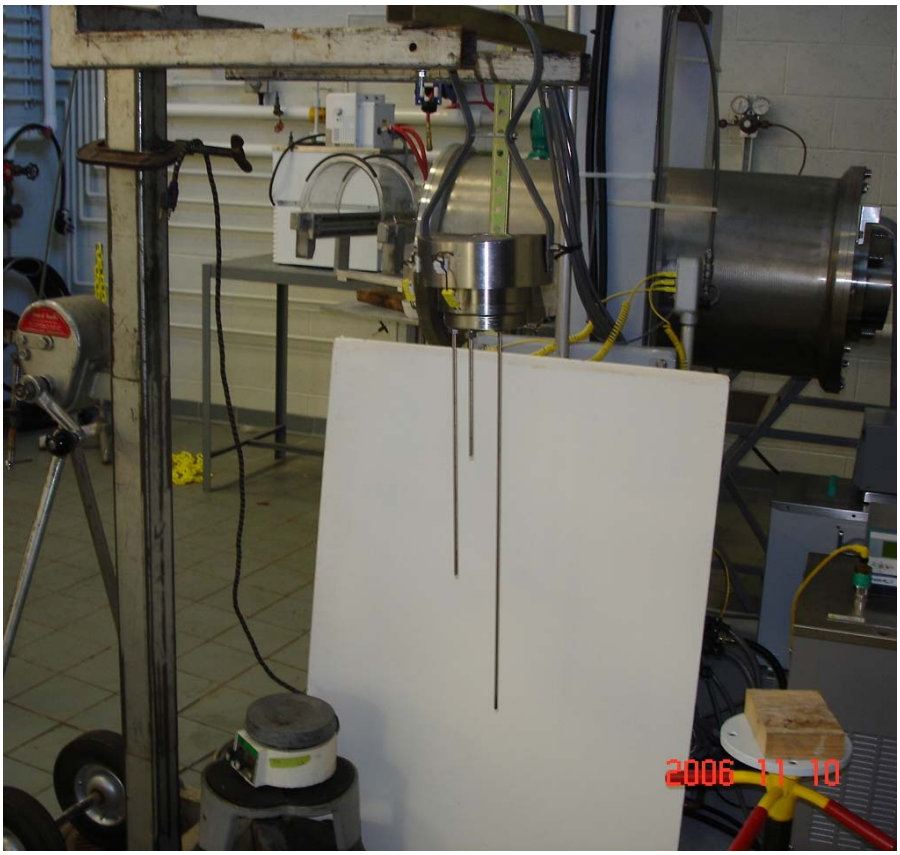

Figure 2.4 High pressure thermocouple assembly made vertical for measuring the time constant for each thermocouple.

2.2.2. Initial high temperature

For experiments at initial temperatures higher than ambient temperature the steel mass was heated to the desired initial temperature prior to experimental run because if water at higher temperature was filled in the vessel with surrounding steel mass at lower ambient temperature, the water rapidly lost heat to the giant steel vessel and its temperature dropped rapidly. Therefore, an external water bath was used to circulate hot water in the

vessel to pre-heat the vessel steel mass overnight and equilibrate it at the desired temperature before starting the experiments as shown in **Figure 2.5**. In addition, a 13 liter external water tank was used to pre-heat the water to the desired temperature for filling it in the pre-heated 10 liter vessel just before the experiment.

Figure 2.5 Experimental set up to heat the steel vessel using a circulating water bath.

3. THEORETICAL CONSIDERATIONS

3.1. Strength of Buoyancy Induced Flow (laminar or turbulent flow)

In order to develop an appropriate mathematical model and to carry out numerical simulation, it was necessary to know whether the natural convection induced flow within the vessel was laminar or turbulent. Since no correlations are available in the literature for natural convection flow on the inner surface of a vertical cylinder, the inner cylinder surface was approximated as a vertical flat plate for the purpose of choosing the laminar or turbulent flow model. This approximation was based on the correlation that for isothermal surfaces a vertical cylinder may be treated as a vertical flat plate (Holman, 1981) if

$$\frac{D}{L} \geq \frac{35}{Gr_L^{\frac{1}{4}}} \qquad \text{..... (3-1)}$$

where, D is the diameter of the cylinder, L is the length of the cylinder, Gr_L is the Grashof number with length as the characteristic dimension. The Grashof number is a dimensionless number used in free convection systems and defined as the ratio of buoyant forces to viscous forces (Singh and Heldman, 2001).

$$Gr_L = \frac{L^3 g\beta(T_s - T_\infty)}{\nu^2} \qquad \text{..... (3-2)}$$

In the above relation, g is the acceleration due to gravity, L is the characteristic length, β is the thermal expansion coefficient, T_s is the surface temperature (temperature of the wall), T_∞ is the fluid temperature far from surface of the object, and ν is the kinematic viscosity.

It was assumed that equation (3-1) was applicable for flow on the inner surface and it was found to be valid in our case. According to Singh and Heldman, (2001), for a flat plate in vertical orientation transition to turbulent occurs around Gr equals 10^9. In our case, this value was of the order of 10^9 at room temperature and 10^{11} at higher initial temperatures. Therefore, the flow was assumed to be turbulent in the mathematical model and in the numerical simulation.

3.2. Governing Equations For High Pressure Processing

The physical domain for the problem under consideration is shown in **Figure 3.1(a)**. However, since the problem can be considered as axisymmetric, only a radial slice of the physical domain as shown in **Figure 3.1(b)** was used to obtain the overall solution.

3.2.1. Conservation of mass

Continuity equation is a general mass balance that holds in all problems with no net generation of mass and with no mass transfer (Brodkey and Hershey, 2003).

$$\frac{\partial \rho}{\partial t} + \nabla \cdot \left(\rho \overline{V}\right) = 0 \qquad \text{……..... (3-3)}$$

In above equation, t is time, ρ is density, ∇ is operator in axisymmetric cylindrical coordinates, and V represents velocity vector. Since density of fluid (water) was assumed to be constant, the equation of continuity for fluid got simplified to

$$\nabla \cdot (\overline{V}) = 0 \qquad \text{..... (3-4)}$$

3.2.2. Conservation of momentum

The Navier-Stokes equation for constant fluid properties (density and viscosity) and turbulent flow is given by

$$\frac{D\overline{V}}{Dt} = \frac{\partial \overline{V}}{\partial t} + \overline{V} \cdot \nabla \overline{V} = \vec{F} + (\nu + \varepsilon_m)\nabla^2 \overline{V} - \frac{1}{\rho}\nabla \overline{P} \quad \text{..... (3-5)}$$

In the above equation, P is pressure,ν is kinematic viscosity, ε_m is the momentum eddy viscosity, $\vec{F}$ represents the driving force for natural convection and bar on the quantities represents the time-averaged values for turbulent flow.

The driving buoyancy force for the vertical flow arises due to the difference between the body force and the force due to hydrostatic pressure gradient in ambient medium given by $g(\rho_a - \rho)$ (Jaluria, 1980), where ρ_a represents density of ambient medium. Although density of fluid was assumed to be constant but in momentum equation, Boussinesq approximation was applied as density difference causes natural convection flow to occur. Gao, Mei, & Chen (2003) stated that in Boussinesq approximation, variations in fluid density are ignored, except insofar as they give rise to a gravitational force, therefore the force term is given by equation (3-6). This approximation is accurate as long as changes in the density are small.

$$g(\rho_a - \rho) \cong -\rho\beta(T - T_a) \quad \text{....……..... (3-6)}$$

Therefore, final governing equation for momentum transfer in turbulent flow with Boussinesq approximation is given by

$$\frac{D\overline{V}}{Dt} = \frac{\partial \overline{V}}{\partial t} + \overline{V} \cdot \nabla \overline{V} = \underbrace{\hat{g}_z \beta(\overline{T} - T_i)}_{\text{only in z direction}} + (\nu + \varepsilon_m)\nabla^2 \overline{V} - \frac{1}{\rho}\nabla \overline{P} \quad \text{.....……..... (3-7)}$$

Where, g_z represents acceleration due to gravity along negative z direction, β is coefficient of thermal expansion, and T_i is the initial temperature of water.

3.2.3. Conservation of energy

The energy conservation equation for constant fluid properties in turbulent flow is given by

$$\frac{D\overline{T}}{Dt} = \frac{\partial \overline{T}}{\partial t} + V \cdot \nabla \overline{T} = \nabla \cdot (\alpha + \varepsilon_t)\nabla T + \frac{Q}{\rho C_P} + \beta \overline{T} \frac{D\overline{P}}{Dt} + \frac{\mu}{\rho C_P} \varphi_v \quad \text{..... (3-8)}$$

In the above equation, α is thermal diffusivity, ε_t is the turbulent thermal diffusivity, Q is the source term (heat of chemical reaction or other volumetric heat sources), φ_v is viscous dissipation (thermal energy dissipated by viscous heating), C_P is heat capacity, and μ is dynamic viscosity. The terms on the right hand side of equation (3-8) represent conduction of heat, heat source, pressure work, and viscous dissipation, respectively. The second term was zero as there was no source term. If we expand the third (pressure work) term we get,

$$\beta \overline{T} \frac{D\overline{P}}{Dt} = \beta \overline{T} \left[\frac{\partial \overline{P}}{\partial t} + \overline{V}.\nabla \overline{P} \right] \quad \text{..... (3-9)}$$

$$= \beta \overline{T} \left[\frac{\partial \overline{P}}{\partial t} + \overline{V}_x \frac{\partial \overline{P}}{\partial x} + \overline{V}_y \frac{\partial \overline{P}}{\partial y} + \overline{V}_z \frac{\partial \overline{P}}{\partial z} \right] \text{..... (3-10)}$$

Since there is no significant pressure variation within the fluid (water), ($\partial \overline{P} / \partial x$), ($\partial \overline{P} / \partial y$), and ($\partial \overline{P} / \partial z$) were taken as zero. Therefore, the pressure work term became

$$\beta \overline{T} \frac{D\overline{P}}{Dt} = \beta \overline{T} \frac{\partial \overline{P}}{\partial t} \quad \text{..... (3-11)}$$

The fourth term on the right hand side of equation (3-8) which represents viscous dissipation was neglected due to low velocity gradients and low viscosity of water.

Therefore, the governing equation for conservation of energy in turbulent flow is given by

$$\frac{D\overline{T}}{Dt} = \frac{\partial \overline{T}}{\partial t} + \overline{V} \cdot \nabla \overline{T} = \nabla \cdot (\alpha + \varepsilon_t) \nabla \overline{T} + \beta \overline{T} \frac{\partial \overline{P}}{\partial t} \quad \text{.....(3-12)}$$

The energy conservation equation for solid region (vessel steel wall) with constant physical properties is given by

$$\frac{1}{\alpha_s} \frac{\partial T}{\partial t} = \nabla^2 T \quad \text{.....(3-13)}$$

3.3. Thermodynamics of High Pressure Processing

3.3.1. Adiabatic increase in temperature

As discussed in section 1.5, work done during pressurization/depressurization causes increase/decrease in temperature in both food and pressurizing medium. During modeling, this temperature variation produced by pressure change can be derived by assuming high pressure vessel to be a closed system and the process to be adiabatic, i.e., no heat is transferred through the boundaries. The increase in temperature can be estimated by a thermodynamic equation which can be derived from total derivative of the entropy of the pressurized system

$$ds = \left(\frac{\partial s}{\partial T}\right)_P dT + \left(\frac{\partial s}{\partial P}\right)_T dP \quad \text{.....(3-14)}$$

where, s is the specific entropy. Assuming a reversible process, the entropy change would be zero,

$$\therefore \quad \left(\frac{\partial s}{\partial T}\right)_P dT + \left(\frac{\partial s}{\partial P}\right)_T dP = 0 \quad \text{.....(3-15)}$$

From Maxwell's relations, we know that

$$\left(\frac{\partial s}{\partial P}\right)_T = -\left(\frac{\partial \upsilon}{\partial T}\right)_P \quad \text{.....(3-16)}$$

Substituting equation (3-16) in Equation (3-15), we get

$$\left(\frac{\partial s}{\partial T}\right)_P dT - \left(\frac{\partial \upsilon}{\partial T}\right)_P dP = 0 \quad \text{..... (3-17)}$$

Also, from Abbott and Van Ness (1972) we know,

Isobaric heat capacity is defined as $C_P = \left(\frac{\partial s}{\partial T}\right)_P T$ ..... (3-18)

and coefficient of thermal expansion is defined as $\beta = \frac{1}{V}\left(\frac{\partial \upsilon}{\partial T}\right)_P$ ..... (3-19)

Substituting equation (3-18) and (3-19) in equation (3-17), we get

$$\frac{C_P}{T} dT - \beta \upsilon dP = 0 \quad \text{..... (3-20)}$$

Rearranging equation (3-20), we obtain

$$\frac{dT}{dP} = \frac{T \upsilon \beta}{C_P} \quad \text{..... (3-21)}$$

In the above equation, υ represents the specific volume. It can be seen from the equation (3-21) that dT/dP depends on physical quantities which are function of composition of the sample and further these physical properties also depend on temperature and pressure (Makita, 1992). This makes the calculation of dT/dP complicated. In the present work these values were assumed to be constant, i.e., were considered to be only a function of initial temperature of water.

(a) Theoretical Compression Heating Values of Water

The compression heating values for water at different initial temperatures were calculated using equation (28), and are given in **Table 3.1**. The values of β, ρ, and C_P for water at different initial temperatures were taken from Singh and Heldman, (2003). The main

constraint during theoretical calculations of increase in temperature with pressure is the specific volume under pressure, which should not be taken as constant under these conditions (Rasanayagam et al., 2003). It was observed that theoretical values show a discrepancy from values found in literature.

Table 3.1 Theoretically calculated adiabatic compression heating values of water at different initial temperatures.

T (˚C)	T (K)	β (K^{-1})	ρ (kg/m^3)	Cp (J/kg K)	dT/dP (˚C/100 MPa)
10	283.15	0.000095	999.7	4195	0.64
20	293.15	0.00021	998.2	4182	1.47
25	298.15	0.00028	997.1	4180	2.00
30	303.15	0.0003	995.7	4176	2.18
40	313.15	0.00039	992.2	4175	2.95
60	333.15	0.00053	983.2	4181	4.29

(b) Compression Heating Values for Water Obtained from Literature

The compression heating values for water were available in literature from different sources. Hendrickx and Knorr (2001) stated that for water at an initial temperature of 25˚C the increase in temperature is given as 2˚C /100 MPa whereas it was found to be 3˚C/100 MPa at 25˚C by Rasanayagam et al. (2003). Also, they gave the compression heating value for water at 60˚C as 4˚C/100 MPa.

The compression heating values as calculated from **Figure 3.1** (Food Biotechnology and Food Process Engineering, TU, Berlin) are given in **Table 3.2**.

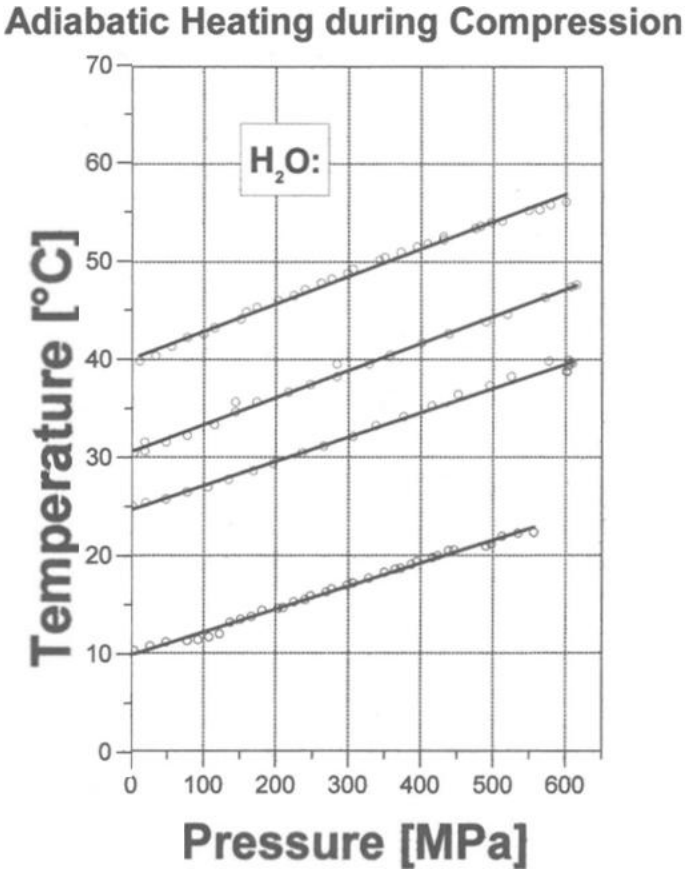

Figure 3.1 Adiabatic compression heating values for water obtained from Food Biotechnology and Food Engineering, TU, Berlin.

Table 3.2 Adiabatic compression heating values for water extracted from Figure 3.1.

T (˚C)	T (K)	dT/dP (˚C /100 MPa)
10	283.15	2.32
20	298.15	2.5
30	303.15	2.8
40	313.15	2.8

The compression heating values of water dT/dP at different initial temperature are also available from NIST-IAPSW standard reference database version 10 section 2.2 as given

by Barbosa-Canovas and Rodriguez (2005). These are shown in Table 4. It shows that dT/dP values are also a function of pressure.

Table 3.3 Adiabatic compression heating values of water obtained from NIST-IAPSW standard database plots.

		dT/dP (˚C/100 MPa)					
Initial Temperature (˚C)	**Initial Temperature (K)**	**0.1-100 MPa**	**100-200 MPa**	**200-300 MPa**	**300-400 MPa**	**400-500 MPa**	**500-600 MPa**
20	293.15	1.5	2.5	2.8	3	3.15	3.15
30	303.15	2.2	2.8	3.15	3.3	3.3	3.3
40	313.15	2.8	3.2	3.4	3.4	3.4	3.4
60	333.15	4.2	4.1	4	3.8	3.8	3.8
80	353.15	5.6	5.2	4.8	4.6	4.4	4.2

Thus, a variation was found between dT/dP values obtained from different sources in the literature. For the purpose of this research compression heating values obtained from NIST –IAPSW database were used since it includes both the effect of initial temperature and increase in pressure on compression heating values.

3.3.2. Pressure work or heat generation

The pressure work term in equation (3-12) was modified to take into account temperature increase during pressurization. From equation (3-12),

$$\text{Pressure Work} = \beta T \frac{dP}{dt} \quad \text{..... (3-22)}$$

Rearranging equation (3-21) we get

$$\beta T = \frac{C_P}{\upsilon}\frac{dT}{dP} \qquad \text{..... (3-23)}$$

Substituting value of βT from equation (3-23) into equation (3-22), we obtain,

$$\text{Pressure Work} = \frac{C_P}{\upsilon}\frac{dT}{dP}\frac{dP}{dt} \qquad \text{..... (3-24)}$$

$$\therefore \quad \text{Pressure Work} = \rho C_P \frac{dT}{dP}\frac{dP}{dt} \qquad \text{..... (3-25)}$$

where, ρ is the density of water and C_P is the heat capacity.

The values of density and heat capacity were taken from Singh and Heldman (2003) at initial temperature of water. The dT/dP values for water at different initial temperature were used as given in **Table 3.3**. The values of dT/dP were calculated from the experimental data. Pressure work term so calculated was fed to the numerical simulation program as source term. To calculate pressure work term for 80˚C (353.15 K), dT/dP values were assumed to be constant as we could not carry out the experiments for initial temperature more than 60˚C (333.15 K) due to the experimental set up limitations.

3.4. Heat Transfer in the Air Gap Between Vessel and Shell

In order to determine whether there would be flow in the air gap between the main vessel and the shell, we need to calculate Rayleigh number. Rayleigh number is dimensionless number, defined as a product of Grashof number and Prandtl number. For free/natural convection near a vertical wall, Rayleigh number is given by

$$Ra_x = Gr_x \cdot Pr = \frac{x^3 g\beta}{\nu^2}(T_s - T_\infty) \cdot Pr \qquad \text{....……..... (3-26)}$$

where, Ra_x is the Rayleigh number, Gr_x is the Grashof number, Pr is the Prandtl number, and x is the characteristic length. The above fluid properties needed to calculate Gr_x and Pr were evaluated at the film temperature, which is defined as

$$T_f = \frac{T_s + T_\infty}{2} \quad \text{..... (3-27)}$$

Gebhart et al. (1988) stated that for vertical rectangular closures their is a little increase in the heat transfer over that due to conduction alone for Ra < 1000 if L/d is large, where L is the length and d is the width of the rectangular enclosure.

For room temperature 15˚C (288.15 K), the properties were evaluated at T_f = 288.15 K from Singh and Heldman (2003). Thickness of the air gap (0.00238 m) was taken as the characteristic length. It was assumed that temperature difference between air surface and shell was 1 K. The value of Ra_x obtained was 1.41. Even if we assume the temperature difference to be of the order of 100 K, the conclusion would remain unchanged because the Rayleigh number will be smaller than the 1000, therefore, conduction heat transfer would dominate in the air gap. Hence, air was treated as a solid continuum in numerical simulation.

3.5. Temperature Correction

The experimental verification of non-uniformity in temperature and the record of temperature history are obtained from the transient temperature that is measured by the thermocouples. The correction in measured temperature was included for two reasons. Firstly, to account for the finite lag that exists between the actual temperature and the measured temperature due to the mass of the thermocouple assembly which consists of high pressure metal tubing surrounding the thermocouple wires. This correction is

applied to the experimentally measure temperatures. And second, to include change in temperature of water due to addition of water during pressurization. This correction is applied to the numerically predicted temperatures.

3.5.1. Correction in experimentally measured temperature due to thermocouple response time

In a high pressure vessel, the temperature increases linearly as pressure is increased during the pressurization stage. During the pressure hold period, the temperature decreases, albeit slowly, but almost linearly, Therefore, we need to include the response of the thermocouples to linearly increasing and decreasing temperature input during pressurization and pressure hold time.

Thermocouple response to ramp input

The dynamic response of a thermocouple to ramp input (linear temperature increase with time) can be modeled as a first-order system. A simplified heat transfer analysis was used to derive the response of a thermocouple to ramp input. The unsteady state energy equation (lumped) for a thermocouple subjected to heat transfer is

$$m_t C_P \frac{dT}{dt} = hA(T_w(t) - T) \qquad \text{..... (3-28)}$$

In the above equation, m_t is mass of thermocouple, h is the heat transfer coefficient, $T_w(t)$ is the temperature of water in which thermocouple is immersed as a function of time, and A is the surface area. **Figure 3.2** shows, schematically the response of a thermocouple to ramp input.

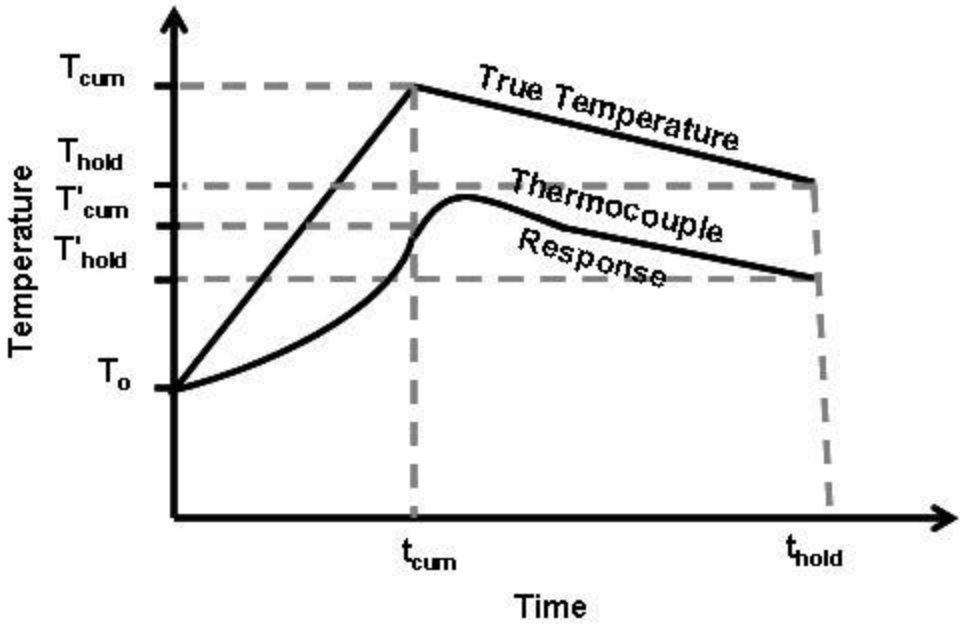

Figure 3.2 Anticipated response of a thermocouple to ramp input during pressurization, pressure hold and depressurization.

The thermocouple response to ramp input can be obtained analytically as follows:

(a) For $0 \le t \le t_{cum}$ [during pressurization]

Assuming linear temperature increase of water from **Figure 3.2**, we can write

$$\frac{(T_w - T_o)}{(T_{cum} - T_o)} = \frac{(t - 0)}{(t_{cum} - 0)} \quad \text{..... (3-29)}$$

$$T_w = T_o + \frac{(T_{cum} - T_o)}{t_{cum}} t \quad \text{..... (3-30)}$$

Defining T' as the temperature as read by the thermocouple during pressurization, we get

$$mC_P \frac{dT'}{dt} = hA\left[\left(T_o + \frac{(T_{cum} - T_o)}{t_{cum}} t\right) - T'\right] \quad \text{..... (3-31)}$$

$$mC_P \frac{dT'}{dt} = hAT_o + hA\frac{(T_{cum} - T_o)}{t_{cum}} t - hAT' \quad \text{..... (3-32)}$$

Dividing both sides of the equation (3-32) by mC_P, we get

$$\frac{dT'}{dt}+\frac{hA}{mC_P}\left(T'-T_o\right)=\frac{hA}{mC_P}\left(\frac{T_{cum}-T_o}{t_{cum}}\right)t \quad \text{..... (3-33)}$$

Let $\left(T'-T_o\right)=\theta'$ ..... (3-34)

$$\therefore \frac{dT'}{dt}=\frac{d\theta'}{dt} \quad \text{..... (3-35)}$$

Using equation (3-35), equation (3-33) becomes

$$\frac{d\theta'}{dt}+\frac{hA}{mC_P}\theta'=\frac{hA}{mC_P}\left(\frac{T_{cum}-T_o}{t_{cum}}\right)t \quad \text{..... (3-36)}$$

Equation (3-36) is of the form Leibnitz Linear Equation (Grewal, 1995), i.e.,

$$\frac{dy}{dx}+Py=S(x)$$

We define Integrating Factor (I.F.) = $e^{\int\frac{hA}{mC_P}dt}$

$$= e^{\left(\frac{hA}{mC_P}\right)t}$$

Now, we know that $\frac{mC_P}{hA}=\tau=$ time constant of thermocouple ..... (3-37)

$$\therefore \quad \theta' e^{\frac{t}{\tau}}=\frac{1}{\tau}\left(\frac{T_{cum}-T_o}{t_{cum}}\right)\int e^{\frac{t}{\tau}}tdt \quad \text{..... (3-38)}$$

$$\therefore \quad \theta' e^{\frac{t}{\tau}}=\frac{1}{\tau}\left(\frac{T_{cum}-T_o}{t_{cum}}\right)\left[t\int e^{\frac{t}{\tau}}dt-\int\left(\frac{dt}{dt}\int e^{\frac{t}{\tau}}dt\right)dt\right] \quad \text{..... (3-39)}$$

$$\therefore \quad \theta' e^{\frac{t}{\tau}}=\frac{1}{\tau}\left(\frac{T_{cum}-T_o}{t_{cum}}\right)\left[\tau te^{\frac{t}{\tau}}-\tau^2 e^{\frac{t}{\tau}}\right]+c \quad \text{..... (3-40)}$$

$$\therefore \quad \theta' e^{\frac{t}{\tau}}=\left(\frac{T_{cum}-T_o}{t_{cum}}\right)\left[te^{\frac{t}{\tau}}-\tau e^{\frac{t}{\tau}}\right]+c \quad \text{..... (3-41)}$$

$$\therefore \quad \theta' = \left(\frac{T_{cum} - T_o}{t_{cum}}\right)\left[t - \tau\right] + ce^{-t/\tau} \qquad \text{..... (3-42)}$$

Replacing $\theta' = \left(T' - T_o\right)$ in equation (3-42), we get

$$T' - T_o = \left(\frac{T_{cum} - T_o}{t_{cum}}\right)\left[t - \tau\right] + ce^{-t/\tau} \qquad \text{..... (3-43)}$$

$$\therefore \quad T' = T_o + \left(\frac{T_{cum} - T_o}{t_{cum}}\right)\left[t - \tau\right] + ce^{-t/\tau} \qquad \text{..... (3-44)}$$

At t = 0; T' = T_o, we get

$$T_o = T_o + \left(\frac{T_{cum} - T_o}{t_{cum}}\right)\left[0 - \tau\right] + ce^{-\frac{0}{\tau}} \qquad \text{..... (3-45)}$$

$$\therefore c = \tau\left(\frac{T_{cum} - T_o}{t_{cum}}\right) \qquad \text{..... (3-46)}$$

Substituting expression for 'c' in equation (3-44), we get

$$T' = T_o + \left(\frac{T_{cum} - T_o}{t_{cum}}\right)\left[t - \tau\right] + \left[\tau\left(\frac{T_{cum} - T_o}{t_{cum}}\right)e^{-t/\tau}\right] \qquad \text{..... (3-47)}$$

$$\therefore \quad T' = T_o + \tau\left(\frac{T_{cum} - T_o}{t_{cum}}\right)\left[\frac{t}{\tau} - 1 + e^{-t/\tau}\right] \qquad \text{..... (3-48)}$$

Thus the response of a thermocouple to a ramp input or linearly increasing temperature i.e. during pressurization is given by equation (3-48).

(b) For $t_{cum} \le t \le t_{hold}$ [during pressure hold]

Assuming that temperature decreases linearly with time during pressure hold as shown in **Figure 3.2**, we can write

$$\frac{\left(T_w - T_{cum}\right)}{\left(T_{hold} - T_{cum}\right)} = \frac{\left(t - t_{cum}\right)}{\left(t_{hold} - t_{cum}\right)} \qquad \text{..... (3-49)}$$

$\therefore$ Temperature of water T_w varies with time t as follows

$$T_w = T_{cum} + \left(\frac{T_{hold} - T_{cum}}{t_{hold} - t_{cum}} \right) [t - t_{cum}] \quad \text{..... (3-50)}$$

Defining T″ as the temperature read by the thermocouple during the pressure hold phase, we can write

$$mC_P \frac{dT''}{dt} = hA \left[\left(\frac{T_{hold} - T_{cum}}{t_{hold} - t_{cum}} \right) (t - t_{cum}) + T_{cum} - T'' \right] \quad \text{..... (3-51)}$$

Let $t - t_{cum} = t''$ ..... (3-52)

$\therefore$ $dt = dt''$ ..... (3-53)

$$mC_P \frac{dT''}{dt''} = hA \left[\left(\frac{T_{hold} - T_{cum}}{t_{hold} - t_{cum}} \right) t'' + T_{cum} - T'' \right] \quad \text{..... (3-54)}$$

Divide both sides of equation (3-54) by mC_P, we get

$$\frac{dT''}{dt''} + \frac{hA}{mC_P} (T'' - T_{cum}) = \frac{hA}{mC_P} \left(\frac{T_{hold} - T_{cum}}{t_{hold} - t_{cum}} \right) t'' \quad \text{..... (3-55)}$$

Let $T'' - T_{cum} = \theta''$ ..... (3-56)

$$\therefore \quad \frac{dT''}{dt''} = \frac{d\theta''}{dt''} \quad \text{..... (3-57)}$$

Substituting the expression from equation (3-57) in equation (3-55), we get

$$\frac{d\theta''}{dt''} + \frac{hA}{mC_P} \theta'' = \frac{hA}{mC_P} \left(\frac{T_{hold} - T_{cum}}{t_{hold} - t_{cum}} \right) t'' \quad \text{..... (3-58)}$$

Following the method described earlier to solve Leibnitz Linear Equation and using

Integrating Factor (I.F) = $e^{\int \frac{hA}{mC_P} dt''}$

$$= e^{\left(\frac{hA}{mC_P} \right) t''} = e^{\frac{t''}{\tau}}$$

we can write,

$$\theta'' e^{\frac{t''}{\tau}} = \frac{1}{\tau}\left(\frac{T_{hold} - T_{cum}}{t_{hold} - t_{cum}}\right)\int e^{\frac{t''}{\tau}} t''dt'' \quad \text{..... (3-59)}$$

$$\theta'' e^{\frac{t''}{\tau}} = \frac{1}{\tau}\left(\frac{T_{hold} - T_{cum}}{t_{hold} - t_{cum}}\right)\left[t''\int e^{\frac{t''}{\tau}} dt'' - \int\left(\frac{dt''}{dt''}\int e^{\frac{t''}{\tau}} dt''\right)dt''\right] \quad \text{..... (3-60)}$$

$$\theta'' e^{\frac{t''}{\tau}} = \frac{1}{\tau}\left(\frac{T_{hold} - T_{cum}}{t_{hold} - t_{cum}}\right)\left[\tau t'' e^{\frac{t''}{\tau}} - \tau^2 e^{\frac{t''}{\tau}}\right] + c \quad \text{..... (3-61)}$$

$$\theta'' e^{\frac{t''}{\tau}} = \left(\frac{T_{hold} - T_{cum}}{t_{hold} - t_{cum}}\right)\left[t'' e^{\frac{t''}{\tau}} - \tau e^{\frac{t''}{\tau}}\right] + c \quad \text{..... (3-62)}$$

$$\theta'' = \left(\frac{T_{hold} - T_{cum}}{t_{hold} - t_{cum}}\right)\left[t'' - \tau\right] + ce^{-t''/\tau} \quad \text{..... (3-63)}$$

Replacing $\theta'' = \left(T'' - T_{cum}\right)$ in equation (3-63), we get

$$T'' - T_{cum} = \left(\frac{T_{hold} - T_{cum}}{t_{hold} - t_{cum}}\right)\left[t'' - \tau\right] + ce^{-t''/\tau} \quad \text{..... (3-64)}$$

$$T'' = T_{cum} + \left(\frac{T_{hold} - T_{cum}}{t_{hold} - t_{cum}}\right)\left[t'' - \tau\right] + ce^{-t''/\tau} \quad \text{..... (3-65)}$$

At $t = t_{cum}$; $T'' = T'_{cum}$

$\therefore$ At $t'' = 0$; $T'' = T'_{cum}$

$$T'_{cum} = T_{cum} + \left(\frac{T_{hold} - T_{cum}}{t_{hold} - t_{cum}}\right)\left[0 - \tau\right] + ce^{-0/\tau}$$

$$c = T'_{cum} - T_{cum} + \tau\left(\frac{T_{hold} - T_{cum}}{t_{hold} - t_{cum}}\right) \quad \text{..... (3-66)}$$

Substituting expression for 'c' in equation (3-65), we get

$$T'' = T_{cum} + \left(\frac{T_{hold} - T_{cum}}{t_{hold} - t_{cum}}\right)\left[t'' - \tau\right] + \left[T'_{cum} - T_{cum} + \tau\left(\frac{T_{hold} - T_{cum}}{t_{hold} - t_{cum}}\right)\right]e^{-t''/\tau} \quad \text{..... (3-67)}$$

Replace $t'' = t - t_{cum}$ ..... (3-68)

$$T'' = T_{cum} + \left(\frac{T_{hold} - T_{cum}}{t_{hold} - t_{cum}}\right)\left[t - t_{cum} - \tau\right] + \left[T'_{cum} - T_{cum} + \tau\left(\frac{T_{hold} - T_{cum}}{t_{hold} - t_{cum}}\right)\right]e^{-(t - t_{cum})/\tau} \quad \text{..... (3-69)}$$

Thus response of a thermocouple during pressure hold is given by equation (3-69), where T'_{cum} is the temperature as read by the thermocouple at end of pressurization.

Equations (3-48) and (3-69) can be used to predict the response of a thermocouple having time constant, τ during pressurization and pressure hold respectively, given the actual variation of temperature that the thermocouple is measuring. In our case, we had the thermocouple response data i.e., variation of T' and T″ with t. Using the above equations in inverse, i.e., replacing T_{cum} by T_w and t_{cum} by t, respectively, in equation (3-48) and T_{hold} by T_w and t_{hold} by t, respectively, in equation (3-69), a program in EXCEL was written to predict the actual variation of temperature T_w with time t, which was called as the corrected experimental temperature variation.

Inverse analysis to find true variation of temperature of water as a function of time

Given T' and T″ from actual experimental data, we can calculate "true" variation of water temperature as a function of time by rearranging equations (3-48) and (3-49).

(a) For $0 \le t \le t_{cum}$ [during pressurization]

From equation (3-48), we know that

$$T' = T_o + \tau\left(\frac{T_{cum} - T_o}{t_{cum}}\right)\left[\frac{t}{\tau} - 1 + e^{-t/\tau}\right] \quad \text{..... (3-70)}$$

Since slope of above equation $\left(\frac{T_{cum} - T_o}{t_{cum}}\right)$ was assumed to be constant for all points during pressurization, we can replace it by $\left(\frac{T_w - T_o}{t}\right)$, where T_w is the true temperature corresponding to T' at time t.

$$\therefore T_w - T_o = \frac{(T' - T_o)t}{\tau\left[\frac{t}{\tau} - 1 + e^{-t/\tau}\right]} \quad \text{..... (3-71)}$$

$$\therefore T_w = T_o + \frac{(T' - T_o)t}{\tau\left[\frac{t}{\tau} - 1 + e^{-t/\tau}\right]} \quad \text{..... (3-72)}$$

Equation (3-72) was used to predict the corrected or "true" variation of water temperature with time't' during pressurization.

(b) For $t_{cum} \le t \le t_{hold}$ [during pressure hold]

From equation (3-69), we know that

$$T'' = T_{cum} + \left(\frac{T_{hold} - T_{cum}}{t_{hold} - t_{cum}}\right)\left[t - t_{cum} - \tau\right] + \left[T'_{cum} - T_{cum} + \tau\left(\frac{T_{hold} - T_{cum}}{t_{hold} - t_{cum}}\right)\right]e^{-(t-t_{cum})/\tau} \text{ .... (3-73)}$$

$$T'' - T_{cum} - T'_{cum}e^{-(t-t_{cum})/\tau} + Te^{-(t-t_{cum})/\tau} = \left(\frac{T_{hold} - T_{cum}}{t_{hold} - t_{cum}}\right)\left[t - t_{cum} + \tau e^{-(t-t_{cum})/\tau} - \tau\right] \text{.... (3-74)}$$

Since slope of above equation $\left(\frac{T_{hold} - T_{cum}}{t_{hold} - t_{cum}}\right)$ is assumed to be constant for all points during pressure hold, we can replace it by $\left(\frac{T_w - T_{cum}}{t - t_{cum}}\right)$, where T_w is true temperature corresponding to T″ at time T.

$$T'' - T_{cum} - T'_{cum}e^{-(t-t_{cum})/\tau} + T_{cum}e^{-(t-t_{cum})/\tau} = \left(\frac{T_w - T_{cum}}{t - t_{cum}}\right)\left[t - t_{cum} + \tau e^{-(t-t_{cum})/\tau} - \tau\right] \text{... (3-75)}$$

$$T'' + T_{cum}\left(e^{-(t-t_{cum})/\tau} - 1\right) - T'_{cum}e^{-(t-t_{cum})/\tau} = \left(\frac{T_w - T_{cum}}{t - t_{cum}}\right)\left[t - t_{cum} + \tau e^{-(t-t_{cum})/\tau} - \tau\right] \quad \text{..... (3-76)}$$

$$T_w = T_{cum} + (t - t_{cum})\left[\frac{T'' + T_{cum}\left(e^{-(t-t_{cum})/\tau} - 1\right) - T'_{cum}e^{-(t-t_{cum})/\tau}}{t - t_{cum} + \tau e^{-(t-t_{cum})/\tau} - \tau}\right] \quad \text{..... (3-77)}$$

The corrected experimental temperature during pressure hold was predicted by equation (3-77).

3.5.2. Correction in numerically predicted temperature due to addition of water from top

Water is pumped into the vessel during pressurization to compensate for the reduction in volume of the compressed water in the vessel. The added water is usually at room temperature and can affect the temperature distribution in the vessel when temperature of water inside the vessel is different from the temperature of water that is added by the pump. To estimate the effect of water addition from top of the vessel on the temperature change of water in the vessel, a simple enthalpy balance was performed and the correction was applied to numerically predicted temperature values. Enthalpy balance of water in the vessel gives

$$m_i C_{P_i} T_i + m_a C_{P_a} T_a = m_f C_{P_f} T_f \quad \text{..... (3-78)}$$

Where, T_i is the initial temperature of water, m_i is the initial mass of water in the vessel, C_{Pi} is the specific heat of water at T_i, T_a is the temperature of water added, m_a is the mass of water added, C_{Pa} is the specific heat of water at T_a , T_f is the final temperature of water, m_f is the final mass of water, and C_{Pf} is the specific heat of water at T_f.

Assuming C_P at T_i, T_a, and T_f to be constant (if variation in temperature is not substantial), we get

$$m_i T_i + m_a T_a = m_f T_f \quad \text{..... (3-79)}$$

$$\therefore T_f = \frac{m_i T_i + m_a T_a}{(m_i + m_a)} \quad \text{..... (3-80)}$$

$$\therefore T_i - T_f = T_i - \frac{m_i T_i + m_a T_a}{(m_i + m_a)} \quad \text{..... (3-81)}$$

Rearranging equation (3-81), we get

$$T_i - T_f = \frac{m_i T_i + m_a T_i - m_i T_i - m_a T_a}{m_i + m_a} \quad \text{..... (3-82)}$$

$$T_i - T_f = \frac{m_a (T_i - T_a)}{m_i + m_a} \quad \text{..... (3-83)}$$

Usually at 600 MPa, $\frac{m_a}{m_i} \approx 0.15$ for water.

$$\therefore \frac{m_a}{m_i + m_a} \approx \frac{1}{0.15 + 1} = \frac{1}{1.15} \quad \text{..... (3-84)}$$

$\therefore T_i - T_f \approx \frac{1}{1.15}(T_i - T_a)$ was assumed at 586 MPa ..... (3-85)

Using equation (3-85), the correction ($T_i - T_f$) in numerically predicted temperature at 40˚C was found to be 2˚C and at 60˚C, it was found to be 5˚C.

4. NUMERICAL SIMULATION

Numerical simulation of heat transfer and fluid flow was carried out for high pressure assembly (water in the pressure cavity and the vessel wall) used in the experimental investigation using finite volume based commercial computational fluid dynamics (CFD) software FLUENT® (Version 6.2.16, Fluent Inc., Lebanon, NH). The governing equations of conservation of mass, momentum, and energy as described in section 3.1 were numerically solved for computational domain shown in **Figure 4.1** to predict velocity and temperature fields within the pressurizing medium (water) and the energy (conduction) equation (3-13) was solved for the vessel wall. The high pressure vessel due to its axial symmetry was modeled as a 2-d axisymmetric cylinder and numerical simulations were carried out in a radial slice of the cylinder. The details of the radial geometry are shown in **Figure 4.1(b)**. The centerline of the axisymmetric geometry was defined as the axis boundary.

In order to use numerical simulation program Fluent® to solve the governing equations the computational domain was discretized into small control volumes. The discretized domain called the computational mesh was generated using commercial mesh generating software Gambit (Version 2.3.30, FLUENT Inc., Lebanon, NH). As a starting point, the computational domain was discretized using a structured uniform quadrilateral face mesh as shown in **Figure 4.2**. Initially, the mesh was coarse (2568 nodes) but while carrying out the numerical solution using FLUENT® the computational mesh was adapted repeatedly based on the developing velocity gradients in the water column during the process until a grid independent solution was obtained. The final grid had 16393 nodes.

To evaluate the effect of an insulating sleeve, three new geometries were generated with 3.175 mm, 6.35 mm and 1.2 mm thick sleeve respectively, on the inner surface of the metal cylinder. The geometry with 6.35 mm thick insulation had 4125 nodes initially, and 19531 nodes after adaptation. Properties of Teflon® were used for the insulating sleeve.

For the purpose of validation of the numerical program, three thermocouple points were marked in the computational domain located at exactly the same position as in the experimental setup, as shown in **Figure 4.2**.

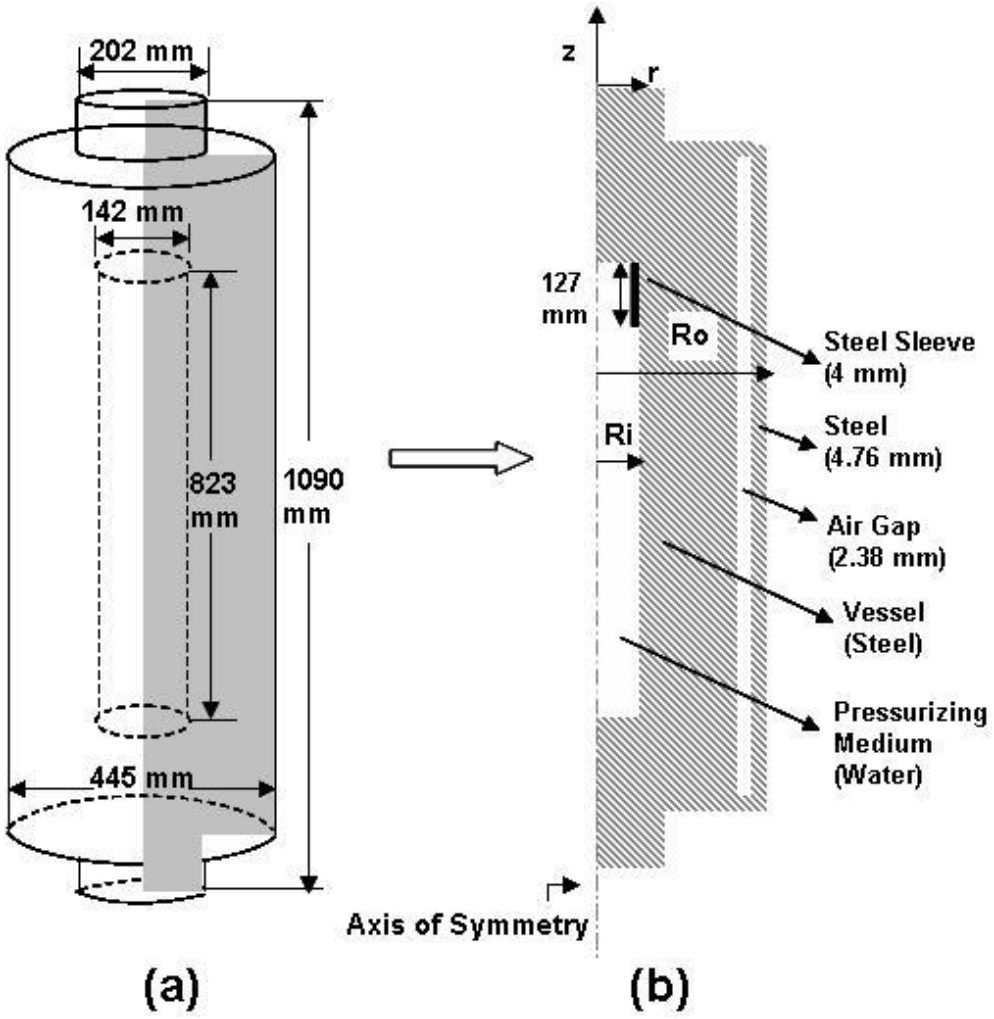

Figure 4.1 (a) Dimensions of HHPP vessel. Shaded area represents the radial section for numerical simulation, (b) computational domain used for simulation, Ri = 71 mm, Ro = 223 mm.

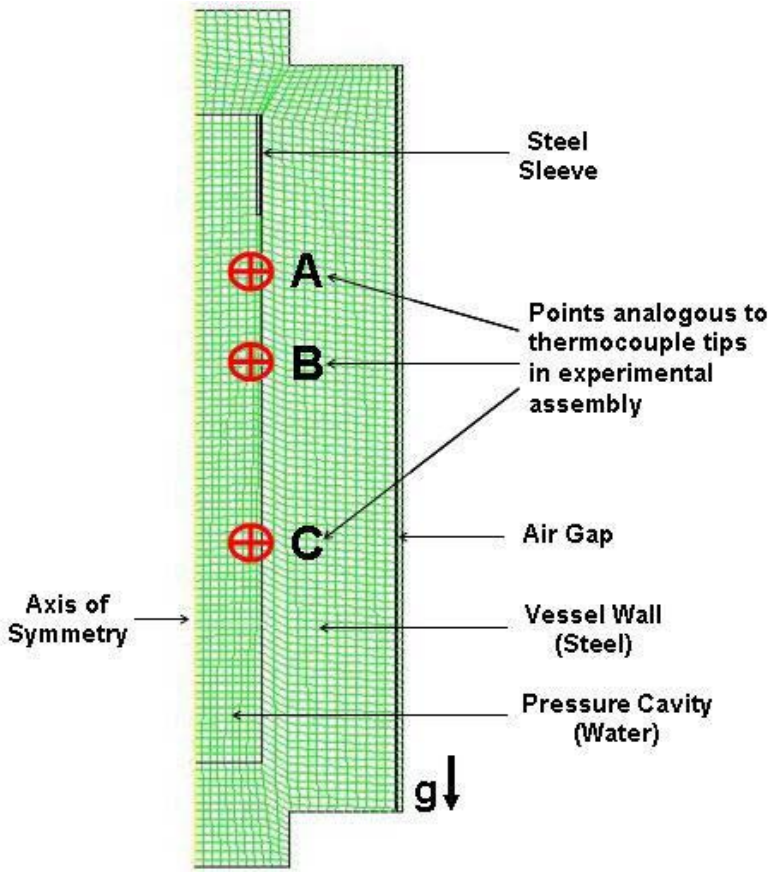

Figure 4.2 Computational mesh used for numerical simulation.

4.1. Setting Up the Problem in Fluent

The computational mesh/grid geometry generated in Gambit was imported into Fluent program. Grid check was done to check domain extents, volume statistics and face area statistics. Since the grid geometry was created in centimeters, grid scaling was used to convert it to SI units (meters) as required by Fluent. For the numerical simulation, unsteady implicit solver as shown in **Figure 4.3** was used to solve for thermal and velocity fields.

Since we were dealing with a thermal transport problem, energy equation was turned on. The next step was to define the physical properties of steel, water and air.

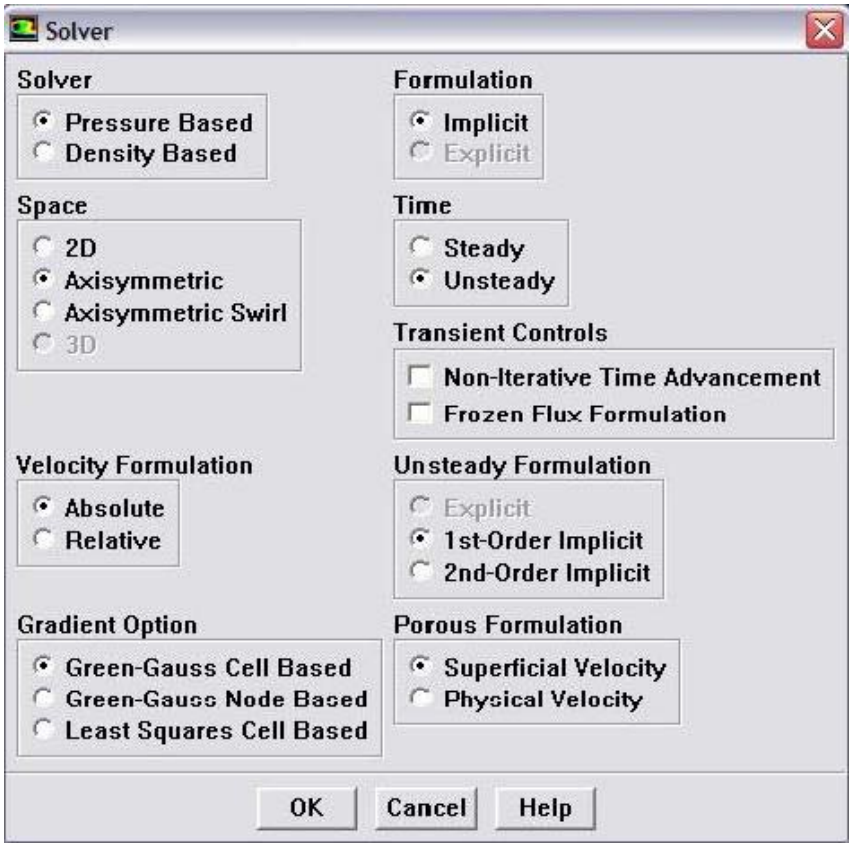

Figure 4.3 Solver window as appearing in Fluent program.

The current study was carried out based on assumption that no significant changes in density, specific heat, thermal conductivity, viscosity and thermal expansion coefficient of water occurred while under pressure. These considerations could be included in the future research. Therefore, physical properties of steel, air, and water at different initial temperatures were given as an input to the numerical program. The properties were obtained from Singh and Heldman (2003).

Natural convection flow in water was modeled by employing the Boussinesq approximation. Therefore, water density was treated as a constant value in all solved equations, except for buoyancy term in momentum equation (refer to section 3.2.2 for details).

Subsequently, boundary conditions for the domain were defined. The axis boundary condition was defined on the centerline of the axisymmetric geometry. A coupled thermal boundary condition was defined between the water column and the steel vessel, i.e., both the continuum domains (solid steel and water as fluid) were coupled by the common edge. Also, for insulation model coupled boundary condition was defined between water and Telon, and Teflon and solid steel interfaces. On the outside surface of the vessel, thermal convection boundary condition for walls was used with heat transfer coefficient of 10 W/m^2K on the vertical side and bottom walls, and 5 W/m^2K on the top wall. The approximate values of h on the outer surface were calculated using the relations provided by Churchill and Chu as given in the textbook by Holman (1981), although it was found that the results were not sensitive to small variation in value of h.

Another question in the numerical simulation was whether the flow within the vessel was laminar or turbulent. The inner cylinder surface was approximated as a vertical flat plate for the purpose of selecting the laminar or turbulent flow model, for details refer to section 3.1. In the numerical simulation model, turbulence was included using the standard k-ε model (Jaluria & Torrance, 1986) to describe the turbulence.

To indicate the convergence of the solution, convergence criteria were defined for residuals such as energy, continuity, k and ε. A convergence criteria of 10^{-6} was defined for all the residuals, as shown is **Figure 4.4**.

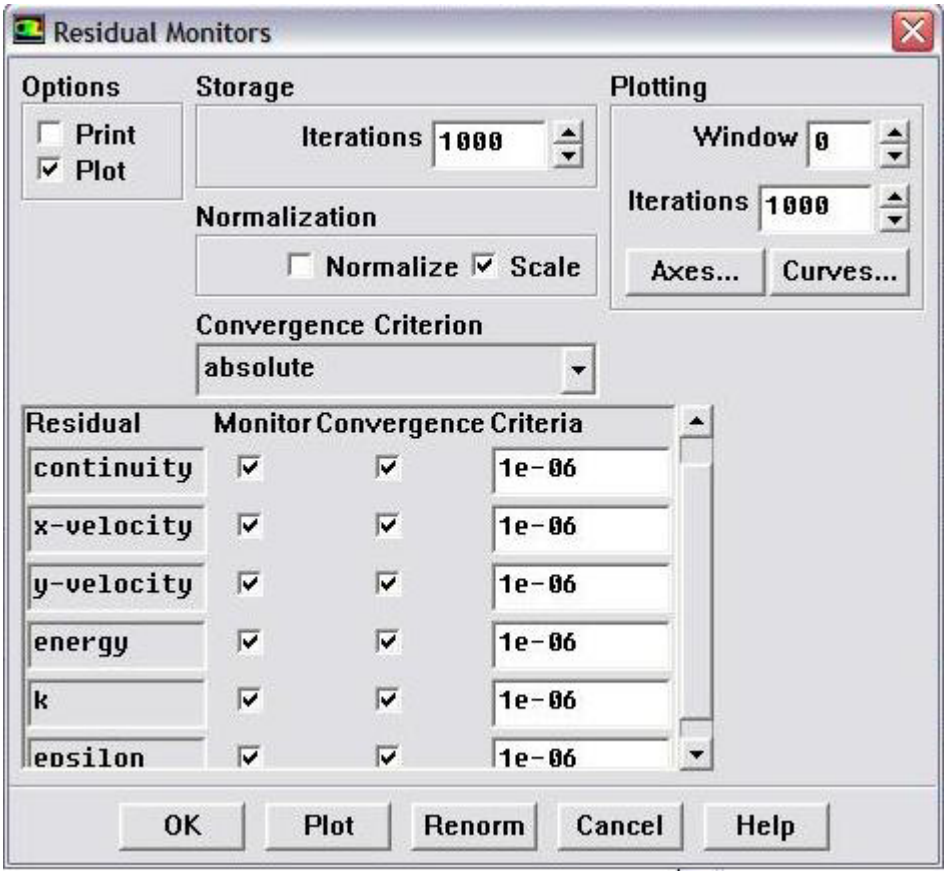

Figure 4.4 Residual monitor window as appearing in Fluent to define convergence criteria.

The model was initialized at the given initial temperature of water and vessel steel mass and iterated. A time step size of 0.1 s was used as shown in **Figure 4.5**. Number of time steps were defined based on needs of the individual case.

Computational time needed to run one simulation was approximately 36 hrs on a desktop computer with Intel® Pentium® 4 processor and 2 GB RAM.

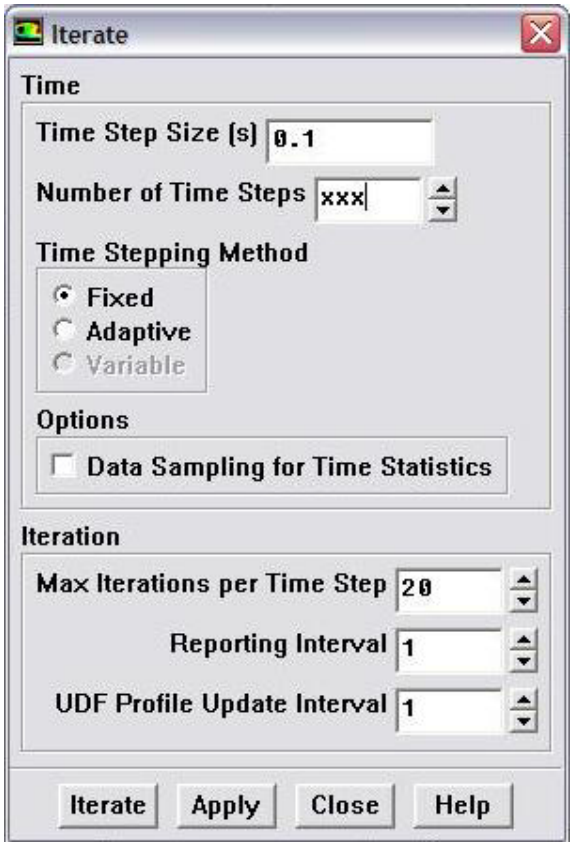

Figure 4.5 Iteration window as appearing in the Fluent program.

5. RESULTS AND DISCUSSION

5.1. Numerically Predicted Results

Although compression heating occurs uniformly throughout the pressurizing medium (water) and causes the temperature of the medium to increase, a temperature gradient is established between the medium and the colder vessel wall which causes heat transfer to occur from water to thick vessel wall. The resulting density differences give rise to convection currents within the pressurizing medium. To emphasize the importance of including convection in the model, the temperature distribution was predicted for the case when there is no convection, i.e., only conduction heat transfer and compared with conjugate (conduction and convection) heat transfer case.

5.1.1. Conduction heat transfer only

The numerical simulation was carried out to predict the temperature distribution in water and vessel wall when conduction was the primary mechanism of heat transfer. For this case gravity in the model was turned off. Therefore, heat loss from water occurred only at the walls due to temperature difference between water and thick steel wall. The initial temperature of water and thick steel wall of vessel was 298.15 K. The temperature of 298.15 K was chosen because while carrying out experimental run the ambient temperature, temperature of steel mass and water were at this temperature. To compare the numerically predicted results with experimental data numerical simulation was carried out with initial temperature of 298.15 K. The pressure work term was included in the model as a source term in water boundary condition to pressurize the vessel to 586 MPa. The pressure work was calculated from equation (3-25) in terms of pressure,

compression time (i.e. time required for pressure build up) and dT/dP value interpolated at 298.15 K from **Table 3.3**.

Figure 5.1 shows the isotherms obtained from the numerical simulation. As shown in **Figure 5.1(a)** the temperature of water increased from an initial value of 298.15 K to 315 K at the end of pressurization due to adiabatic compression heating. The difference in temperature between the water and the vessel wall resulted in conduction heat loss to the wall which gave rise to temperature gradients in water near the wall as shown in **Figure 5.1(b)**. The temperature of the water near the wall dropped to 306 K at the end of the hold time. Therefore, it was observed that conduction process gives rise to temperature gradients in water both in radial and axial directions.

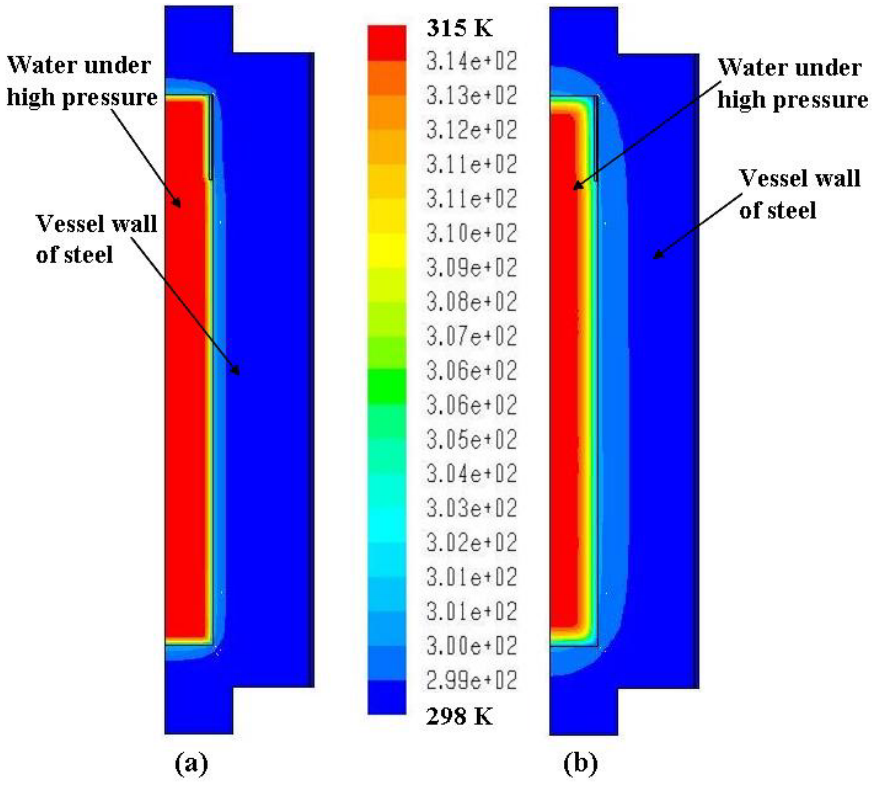

Figure 5.1 Isotherms in water and s.steel wall at T_i = 298.15 K, P = 586 MPa, at the end of (a) pressurization (180 s), (b) hold period (780 s) for conduction heat transfer only.

5.1.2. Conjugate heat transfer

For conjugate heat transfer i.e., when convection in water was simulated along with conduction in the vessel wall the Grashoff no. (Gr) at room temperature (298.15 K) was found to be in the transition flow region, therefore, the temperature data was predicted for both laminar and turbulent flow, and compared with the experimental data. In order to include convection heat transfer in the model, the gravity in the model was turned on and Boussinesq approximation was used for the density of water. The initial temperature of water and thick steel wall of vessel was 298.15 K. The vessel was pressurized to 586 MPa, i.e., in the model the pressure work term was included as a source term in water boundary condition. The pressure work term used in the model was same as in conduction only case.

For flow modeled as laminar flow, **Figure 5.2** shows the isotherms obtained at the end of pressurization (180 s) and end of hold time (780 s). The temperature of water increased from an initial value of 298.15 K to maximum of 315 K at the end of pressurization as a result of adiabatic heat generation in water as shown in **Figure 5.2(a)**. At the same time we can see that initially uniform temperature became non-uniform at the end of the pressurization due to combined effect of adiabatic heat generation in water and cooling at the walls. It was found that the temperature non-uniformity became worse during the hold period and remained so as the maximum temperature in the vessel dropped to 309 K at the end of hold period as shown in **Figure 5.2(b)**. The temperature gradients arising from the bottom of the vessel indicated convection currents in water. Also, **Figure 5.3** shows the corresponding streamlines in water at the end of pressurization and end of hold

period. Irregular flow pattern indicated that the flow has not yet developed completely and perhaps laminar model was not suitable.

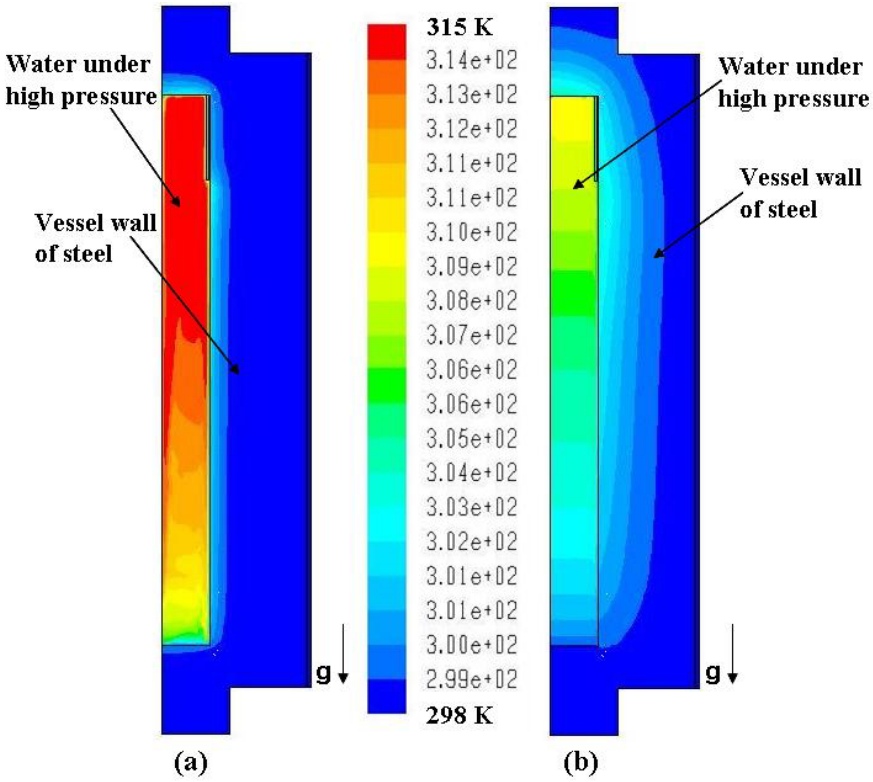

Figure 5.2 Isotherms in water and s.steel wall at T_i = 298.15 K, P = 586 MPa, at the end of (a) pressurization (180 s), (b) hold period (780 s) for conjugate heat transfer when the flow was simulated as laminar flow.

For the flow modeled as turbulent flow using k-ε model, **Figure 5.4(a)** shows the isotherms in water and the s.steel vessel wall at the end of pressurization when pressure was increased from 0.1 to 586 MPa in 180 s, when the initial temperature of the vessel and water was 298.15 K. **Figure 5.4(b)** shows the isotherms at the end of hold time when the pressure was maintained at 586 MPa for 600 s. Here we can see that at the end of pressurization the maximum temperature in the vessel reached 315 K and there is some non-uniformity arising from the bottom of the vessel. The maximum temperature in the

vessel dropped to 307 K by the end of hold period. **Figure 5.5** shows the corresponding streamlines in water at the end of pressurization and end of hold period.

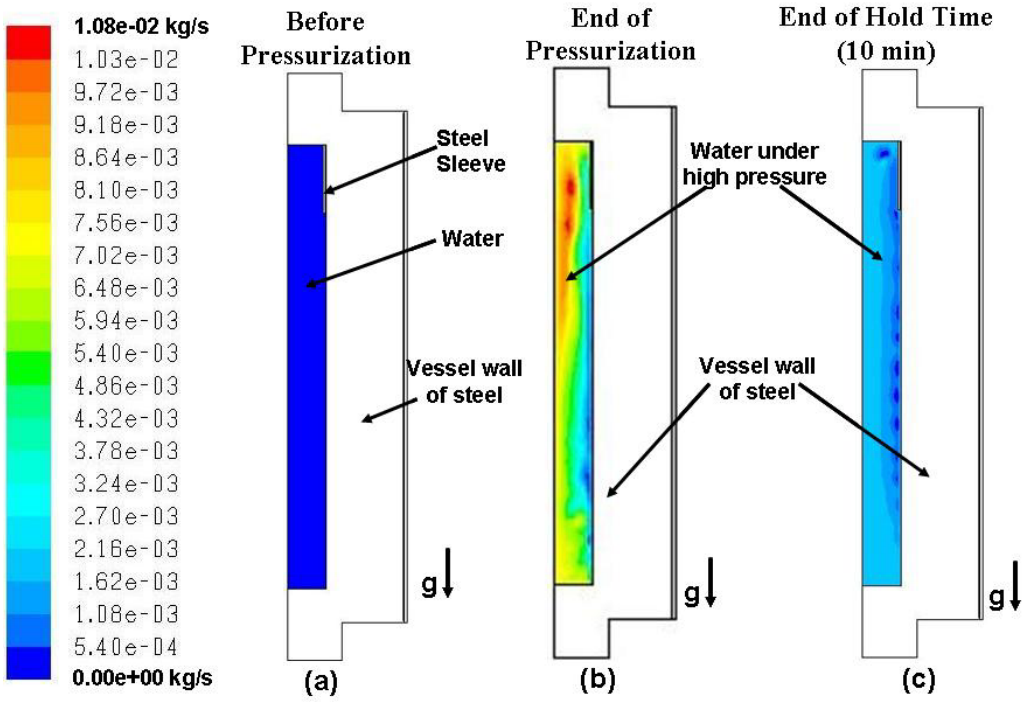

Figure 5.3 Streamlines in water T_i = 298.15 K, P = 586 MPa, (a) before pressurization, (b) end of pressurization (180 s), & (c) end of hold period (780 s) for conjugate heat transfer when the flow was simulated as laminar flow.

5.1.3. Conduction vs. conjugate heat transfer

The comparison between isotherms obtained from conduction only and conjugate heat transfer shows that though the maximum temperature achieved in both he cases at the end of pressurization was same, i.e., 315 K, in the conduction only case the temperature gradients were observed in the water near the wall of vessel whereas in convection case the temperature gradients from bottom arose along with heat loss at the wall. At the end of hold period it was observed that maximum temperature in the vessel for conduction only case was 315 K whereas in conjugate heat transfer case it dropped to 306 K. To compare the temperature variation for conduction only and conjugate cases,

dimensionless temperature $[(T-T_i)/T_{max}-T_i)]$ variation was plotted along axial and radial planes, as shown in **Figure 5.6.** T_{max} was the maximum temperature and was obtained from Fluent through the time-temperature history on the respective planes. It can be observed from **Figure 5.7** that including convection in the model made the temperature more uniform radially, whereas the axial temperature variation between top and bottom of the water column increased during the conjugate case as compared to the conduction, as shown in **Figure 5.8**.

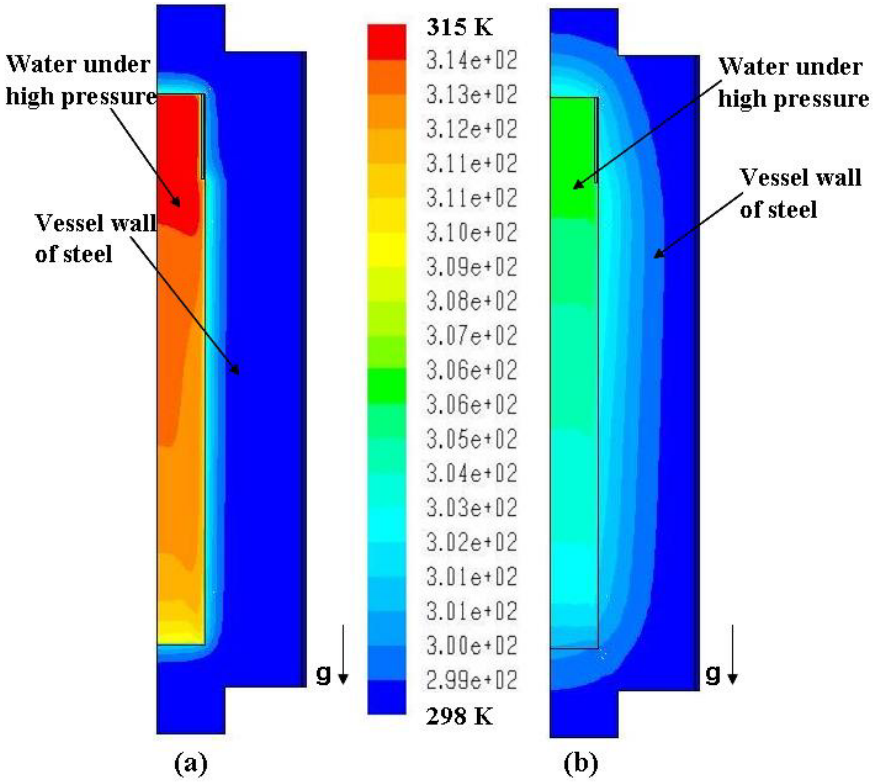

Figure 5.4 Isotherms in water and s.steel vessel at T_i = 298.15 K, P = 586 MPa, at the end of (a) pressurization (180 s), (b) hold period (780 s) for conjugate heat transfer when the flow was simulated as turbulent flow.

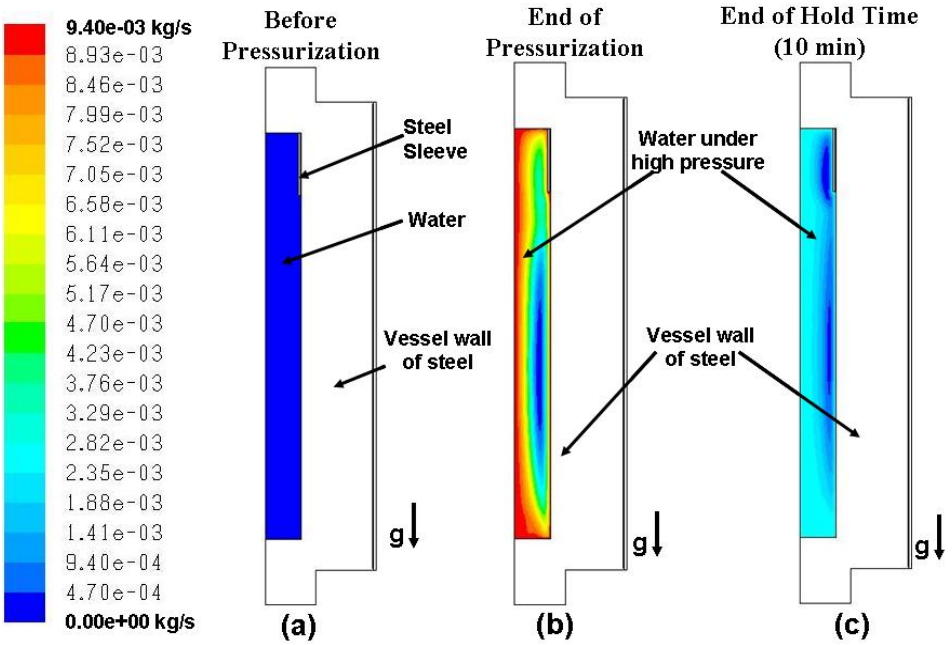

Figure 5.5 Streamlines in water at T_i = 298.15 K, P = 586 MPa, (a) before pressurization, (b) end of pressurization (180 s), & (c) end of hold period (780 s) for conjugate heat transfer when the flow was simulated as turbulent flow.

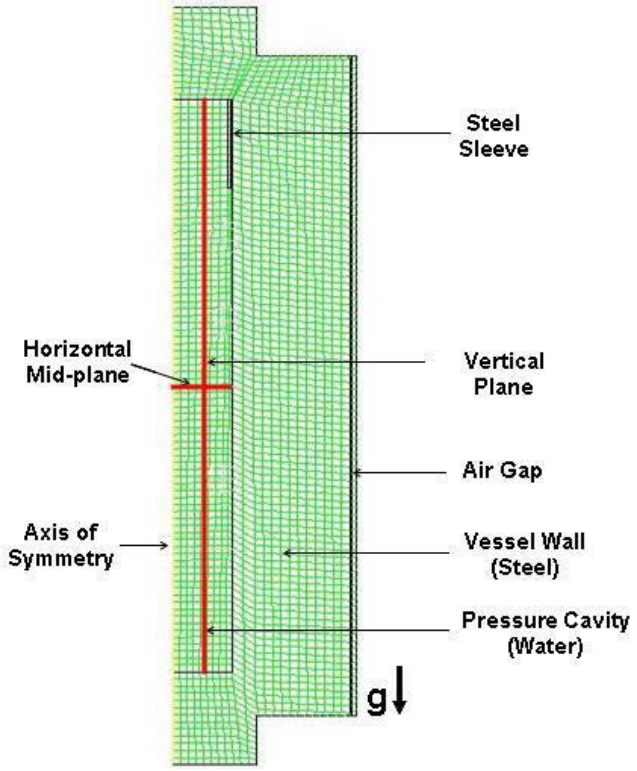

Figure 5.6 High pressure computational domain showing horizontal and vertical planes along which temperature variation was plotted.

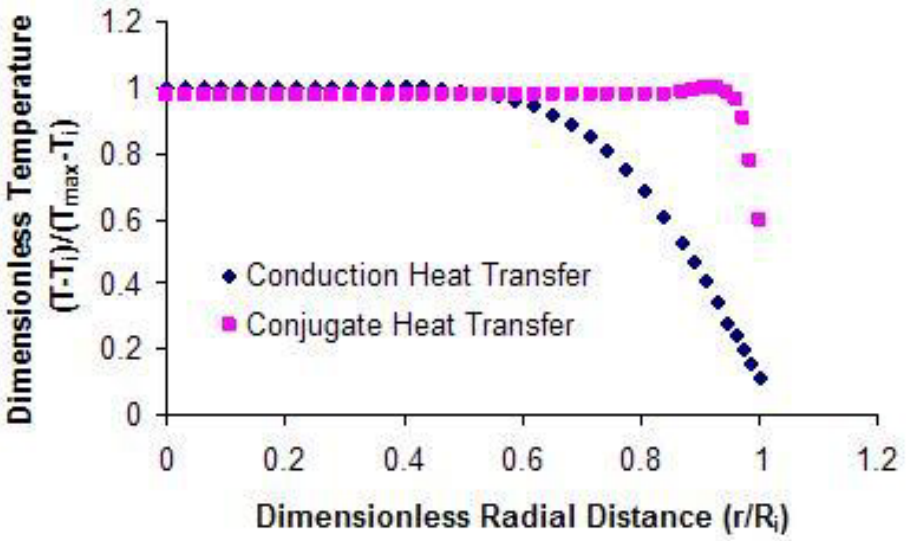

Figure 5.7 Numerically predicted dimensionless temperature variation along the horizontal mid-plane at the end of pressure hold period (780 s) for conduction and conjugate heat transfer.

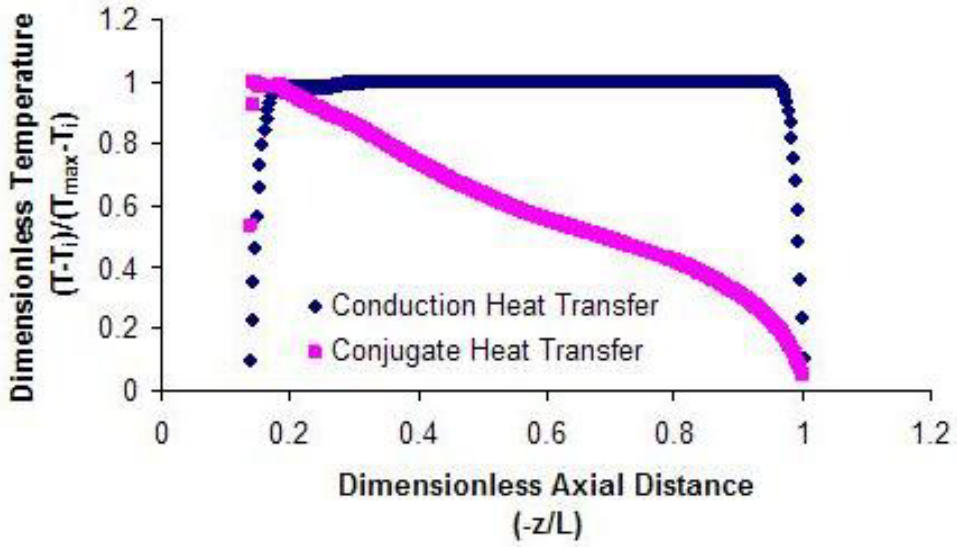

Figure 5.8 Numerically predicted dimensionless temperature variation along the vertical axis at the end of pressure hold period (780 s) for conduction and conjugate heat transfer.

5.1.4. Conjugate heat transfer (laminar vs. turbulent flow)

Isotherms and streamlines predicted numerically for conjugate heat transfer with laminar and turbulent flows respectively were found to be different. The temperature gradients

arising from the bottom in the simulation with laminar flow were found to be disordered as shown in **Figure 5.2** as compared to smooth in case of turbulent flow (**Figure 5.4**). The maximum temperature in the water at the end of hold period was 309 K for laminar flow whereas it was 306 K for turbulent flow. Also, to compare laminar and turbulent flow, the dimensionless temperature variation along the horizontal mid-plane and vertical plane were plotted, as shown in **Figure 5.9 and Figure 5.10** respectively. It was observed that although there was no difference between temperature variations along the horizontal mid-plane as shown by **Figure 5.9,** turbulence tends to make the temperature variation uniform as compared to laminar flow along the vertical plane as shown in **Figure 5.10**. Also, streamlines for turbulent flow show that the flow is more settled as compared to laminar flow as shown in **Figure 5.5**.

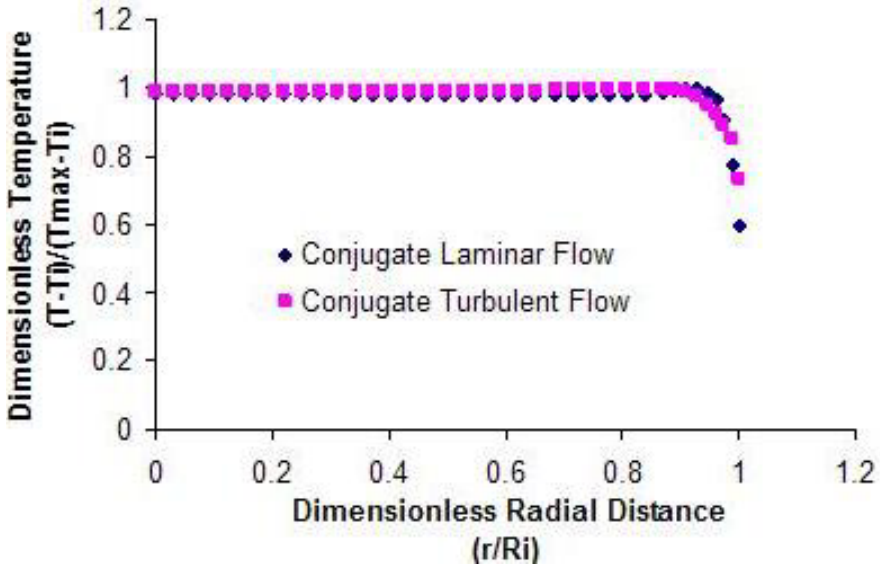

Figure 5.9 Numerically predicted dimensionless temperature variation along the horizontal plane at the end of pressure hold period (780 s) for conjugate heat transfer simulated with laminar and turbulent flow.

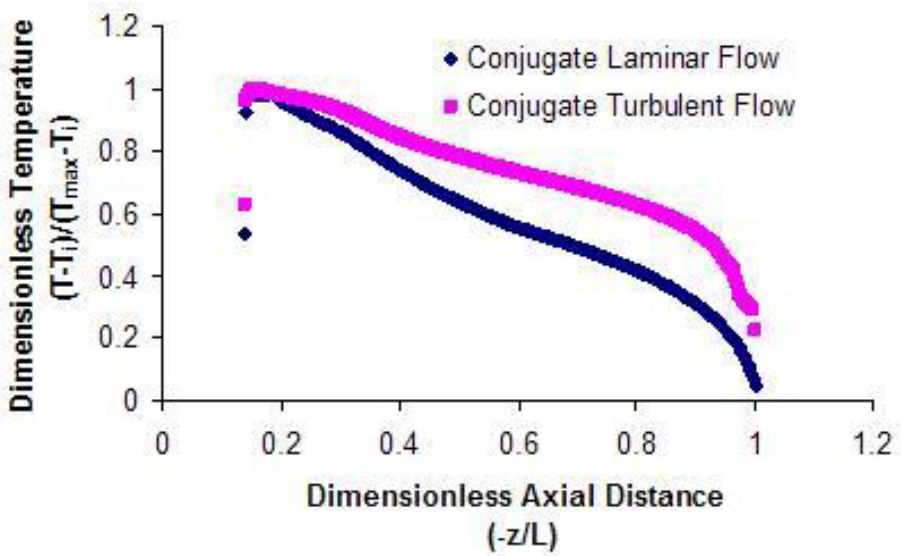

Figure 5.10 Numerically predicted dimensionless temperature variation along the vertical plane at the end of pressure hold period (780 s) for conjugate heat transfer simulated with laminar and turbulent flow.

Another numerical simulation was carried out at initial temperature of 288.15 K, because while carrying out experimental run the ambient temperature, temperature of steel mass, and that of water were at this temperature (during winter). **Figure 5.11** shows isotherms in water and s.steel vessel wall for an initial temperature of 288.15 K and 586 MPa pressure. We can observe the same pattern as in the case of initial temperature of 298.15 K. The velocity vectors shown in **Figure 5.11(c)** indicates that the resulting density differences within the pressurizing medium lead to a downward draft of fluid near the wall. Thus a circulation pattern sets up in the high pressure medium with fluid going down near the vessel side wall and rising in the middle.

5.1.5. Conjugate heat transfer for higher initial temperatures

Figure 5.12 shows isotherms when the initial temperature was 313.15 K. It can be seen that it follows the same trend as observed for the room temperature case, initially uniform

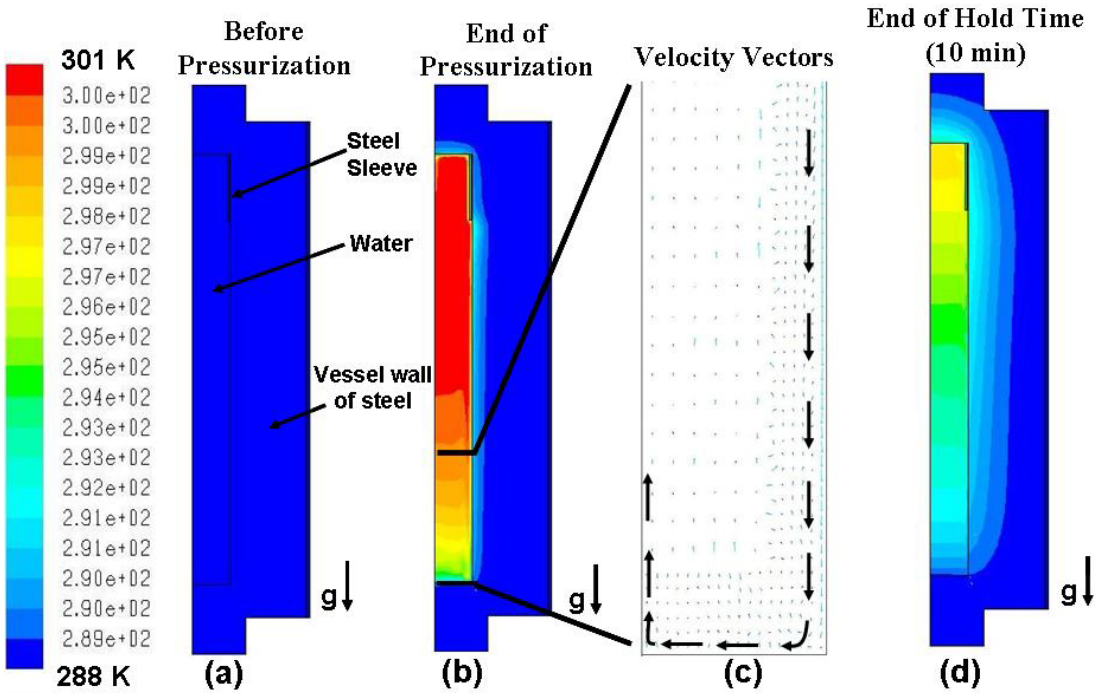

Figure 5.11 Isotherms in water and s.steel vessel at T_i = 288.15 K, P = 586 MPa, (a) before pressurization, (b) end of pressurization, (c) velocity vectors in water, & (d) end of hold period for conjugate heat transfer simulated for turbulent flow.

temperature became non-uniform at the end of the pressurization due to adiabatic heat generation in water and cooling at the walls. The maximum temperature in the vessel at the end of depressurization was 331 K whereas at the end of hold period the maximum temperature of water dropped to 323 K. Also, the temperature variation became worse during the hold period and remained so throughout the hold period. **Figure 5.13** shows streamlines in water at the end of pressurization and end of hold period.

Similarly, isotherms and streamlines were predicted for initial temperatures of 333.15 K and 353.15 K as shown in **Figure 5.14**, **Figure 5.15**, **Figure 5.16** and **Figure 5.17** respectively. It was observed that results obtained at initial higher temperatures also followed the same overall trend as room temperature.

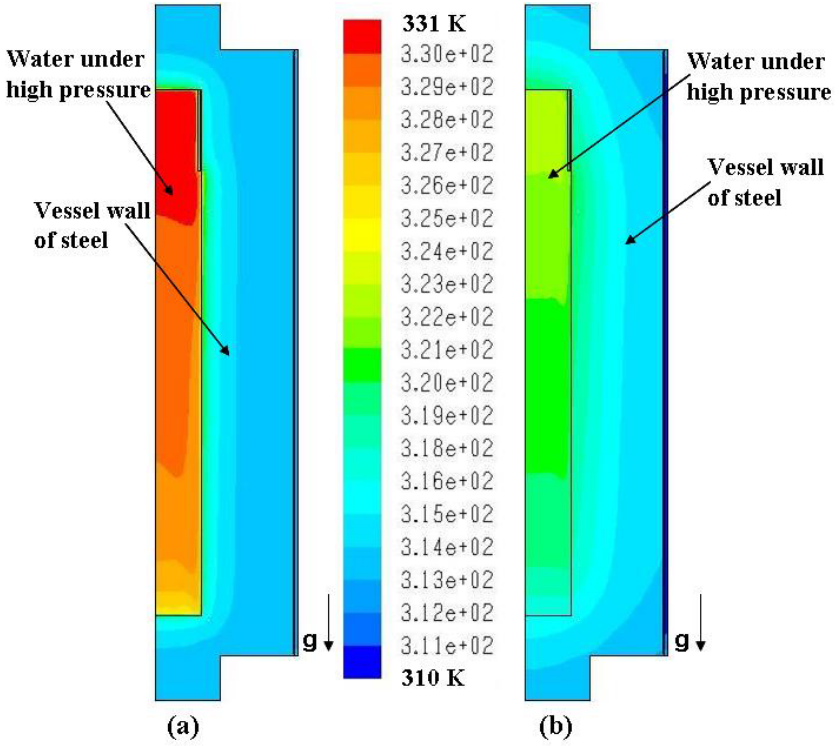

Figure 5.12 Isotherms in water and s.steel wall at T_i = 313.15 K, P = 586 MPa, at the end of (a) pressurization (172 s), (b) hold period (772 s) for conjugate heat transfer with turbulent flow.

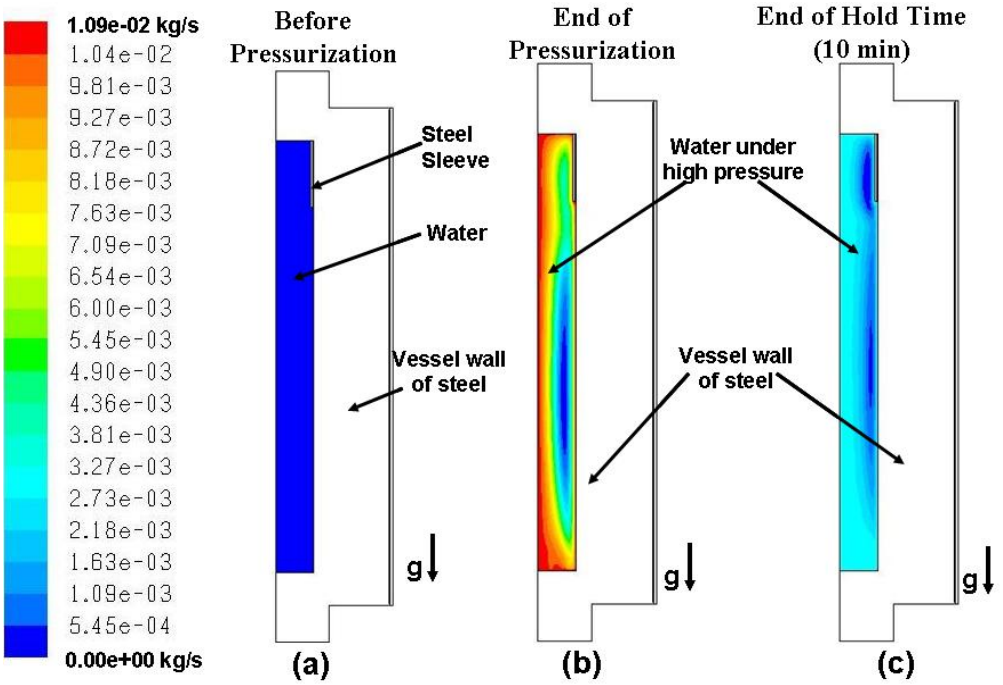

Figure 5.13 Streamlines in water at T_i = 313.15 K, P = 586 MPa, (a) before pressurization, (b) end of pressurization (172 s), & (c) end of hold period (772 s) for conjugate heat transfer with turbulent flow.

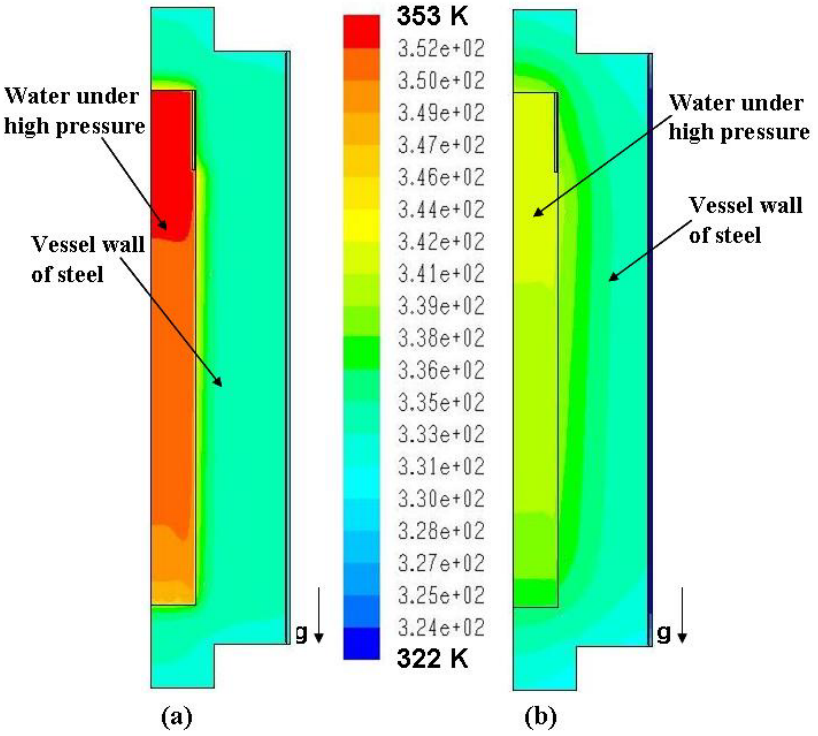

Figure 5.14 Isotherms in water and s.steel wall at T_i = 333.15 K, P = 586 MPa, at the end of (a) pressurization (180 s), (b) hold period (780 s) for conjugate heat transfer simulated for turbulent flow.

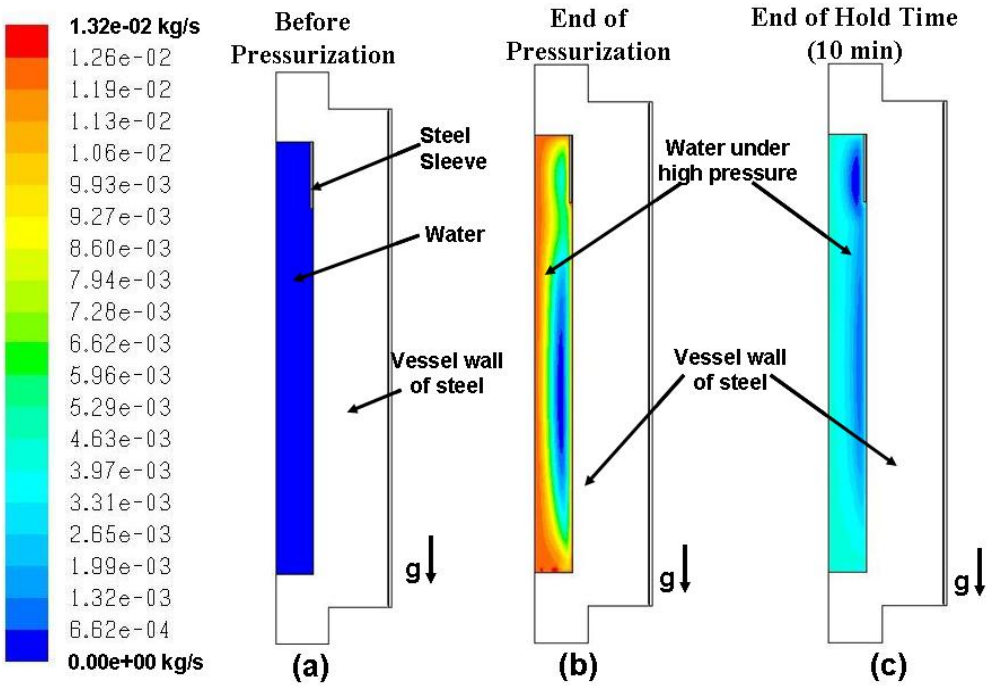

Figure 5.15 Streamlines in water at T_i = 333.15 K, P = 586 MPa, (a) before pressurization, (b) end of pressurization (180 s), & (c) end of hold period (780 s) for conjugate heat transfer with turbulent flow.

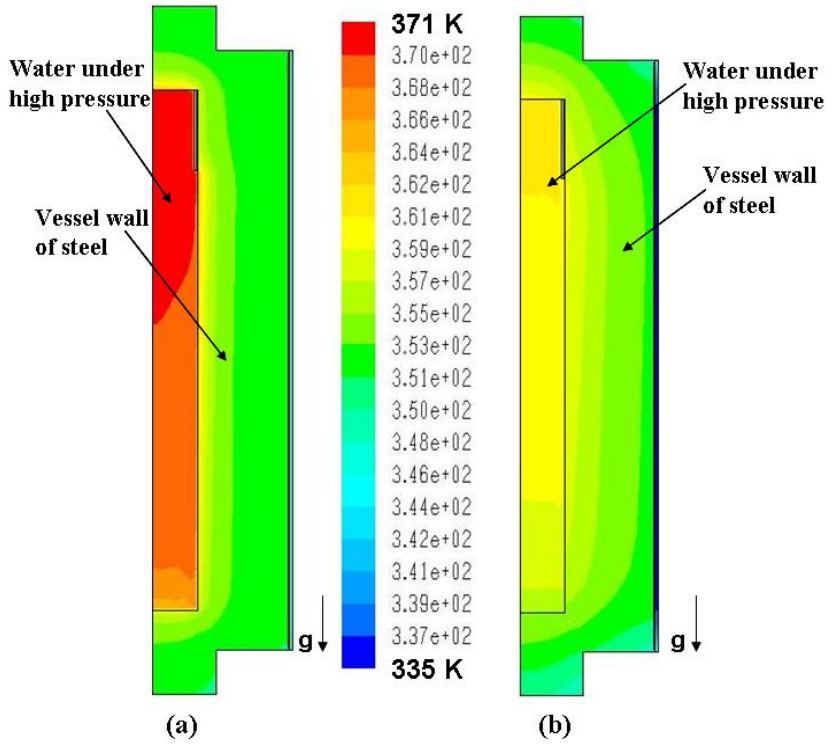

Figure 5.16 Isotherms in water and s.steel wall at T_i = 353.15 K, P = 586 MPa, at the end of (a) pressurization (180 s), (b) hold period (780 s) for conjugate heat transfer with turbulent flow.

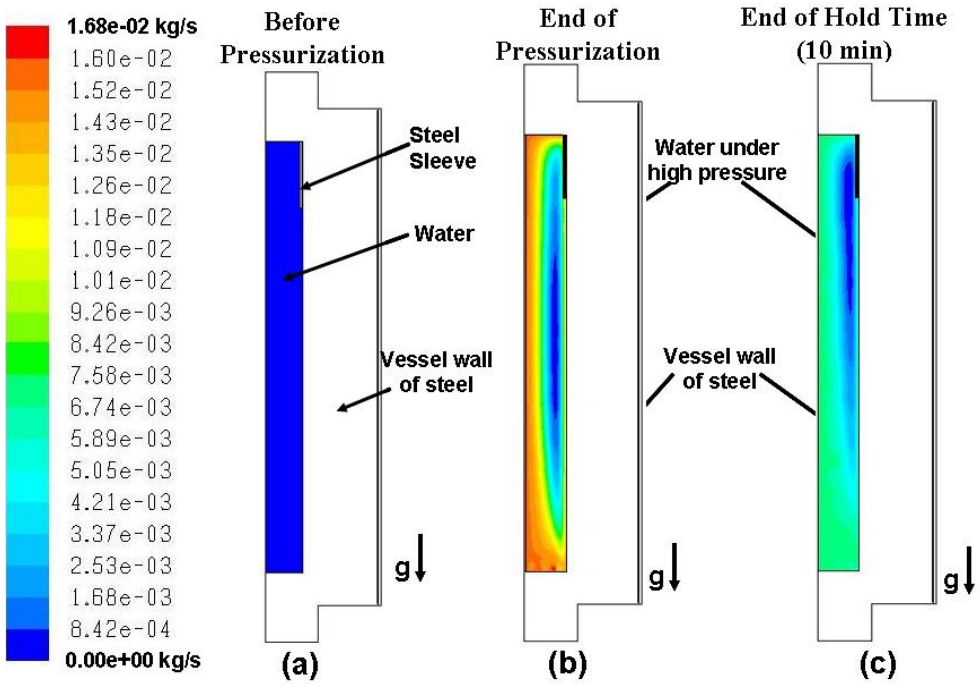

Figure 5.17 Streamlines in water at T_i = 353.15 K, P = 586 MPa, (a) before pressurization, (b) end of pressurization (180 s), & (c) end of hold period (780 s) for conjugate heat transfer with turbulent flow.

5.2. Results for Time Constant Experiments

From the experiments conducted to measure the response of thermocouples, the time constant (τ) for each thermocouple was found to be in the range of 5 to 7 s at extreme temperatures (ice point and boiling water) whereas at 50˚C (323.15 K) the values of time constant were found to be in the range of 10-14 s. By performing ANOVA (analysis of variance) on the time constant data it was found that thermocouple response time was more dependent on temperature than the length of the thermocouple tubing. The value of time constant of 10 s was included in the EXCEL program written to correct the experimental data for thermocouple lag.

5.3. Comparison of Numerically Predicted with Experimental Data

The time temperature history during the pressurization and hold time of high pressure process were recorded experimentally at three thermocouple points in the HHPP vessel and also predicted numerically at the same points as shown in **Figure 4.2**, for different initial temperatures in order to validate the numerical program. **Figure 5.18** and **Figure 5.19** shows the comparison between the corrected experimental (in which experimental data has been corrected for thermocouple response time using equations (3-72) and (3-77) and numerically predicted variation of temperature with time at T_i = 298.15 K and T_i = 288.15 K respectively. The maximum correction in temperature for thermocouple lag was found to be about 2 K. A very good agreement between the corrected experimental temperatures and numerically predicted temperatures were obtained with initial temperature of 298.15 K and 288.15 K.

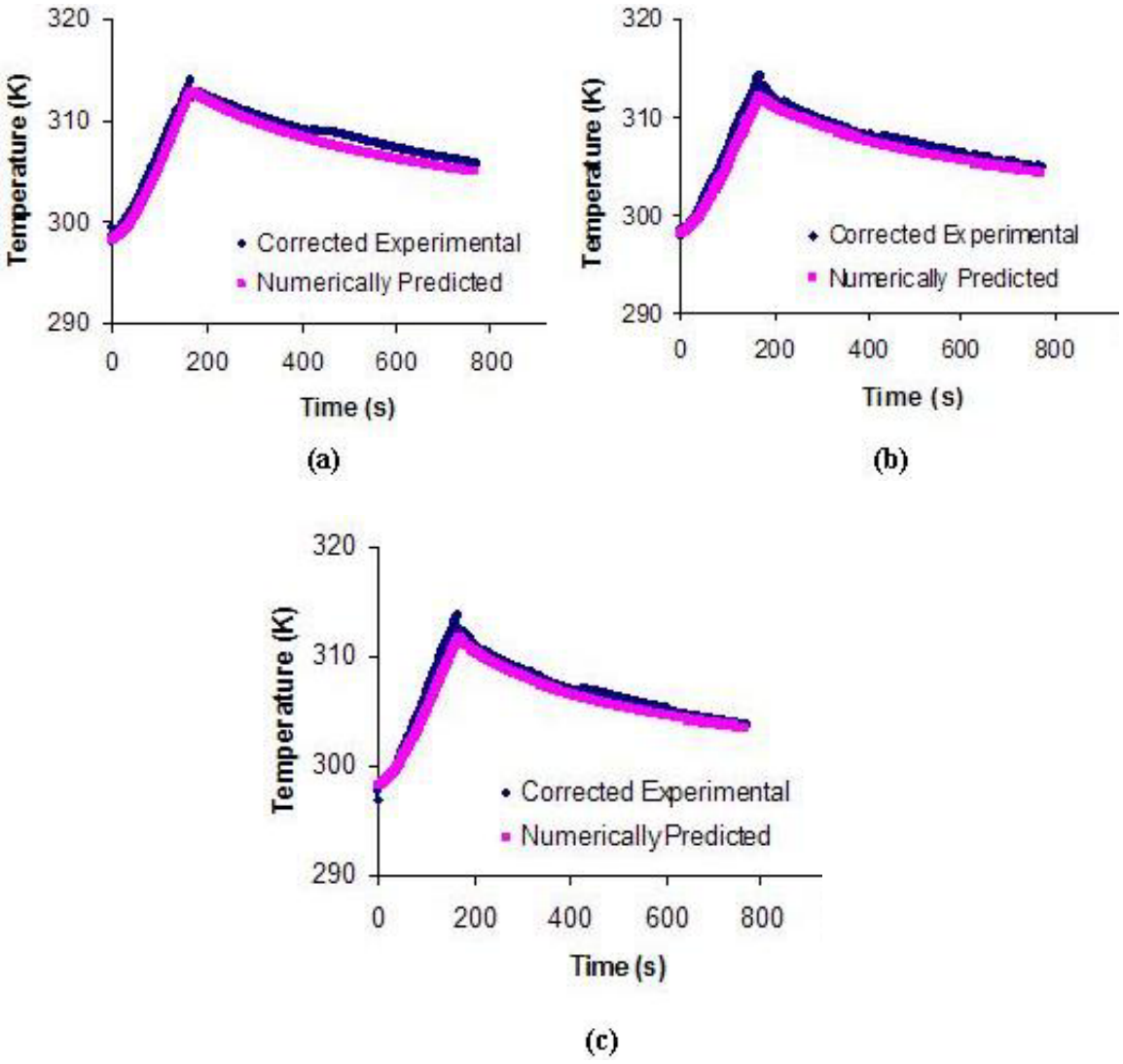

Figure 5.18 Comparison of corrected experimental and numerically predicted time-temperature variations at T_i = 298.15 K, P = 586 MPa, for the thermocouple located (a) near top of the vessel, (b) in between, & (c) near bottom of the vessel in water.

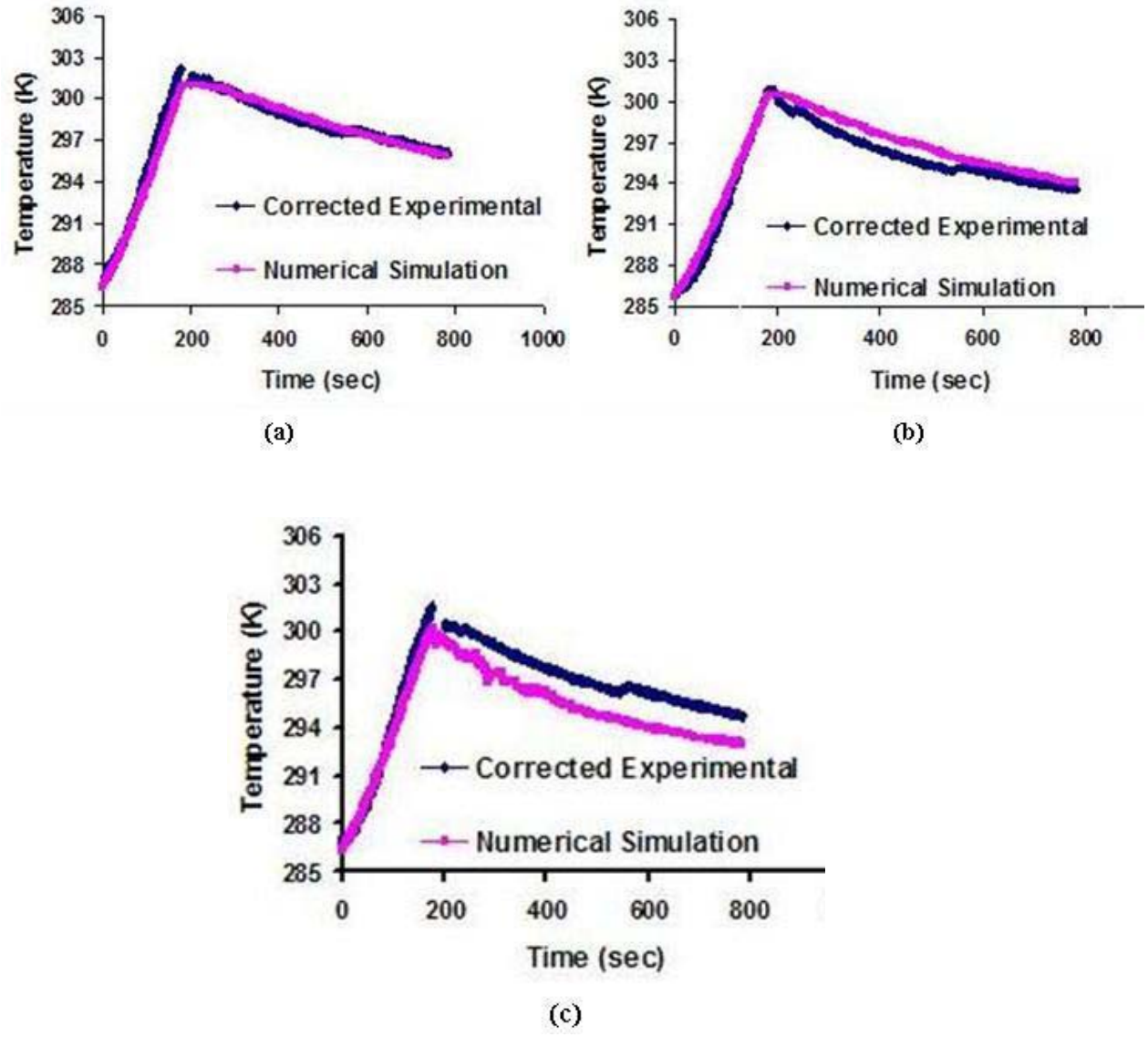

Figure 5.19 Comparison of corrected experimental and numerically predicted time-temperature variations at T_i = 288.15 K, P = 586 MPa, for the thermocouple located (a) near top of the vessel, (b) in between, and (c) near bottom of the vessel in water.

Similarly, **Figure 5.20 and Figure 5.21** show the comparison at higher initial temperatures, T_i = 313.15 K and T_i = 333.15 K, respectively. At initial temperatures of 313.15 K and 333.15 K the numerically predicted temperatures were found to be higher than experimental values at the end of pressurization and beyond. This could be because of the higher compression heating value (2.8 – 3.4 K) for 313.15 K and (3.8 – 4.2 K) for

333.15 K used in the simulation which were taken from NIST standard reference database (given in **Table 3.3**) as compared to compression heating values reported by other researchers at these temperatures. Another reason could be that in the numerically predicted data the effect of water addition to the vessel during pressurization was not taken into account. But the difference shows up only in case of higher initial temperatures and not at 298.15 K and 288.15 K because the temperature difference between the water added (which is at room temperature) and the temperature of water in the vessel is more in case of higher initial temperatures. Therefore, the more the difference more disagreement between the comparisons as can be seen in **Figure 5.21** for 333.15 K. Due to experimental limitation, it was not possible to carry out temperature measurement experiments at initial temperature higher than 60˚C (333.15 K). The seals in the top and bottom closure would start leaking as higher temperature would soften and expand them.

5.3.1. Temperature correction due to water addition from the top closure

Disagreement between numerically predicted and experimental data at higher initial temperature can be attributed to the fact that water added to the system to compensate for decrease in volume due to compression entered the system at a much lower temperature than water in the vessel. As discussed in section 3.5.2 a simple enthalpy balance correction was made to the numerically predicted temperature to take into account this water addition from top. **Figure 5.22** and **Figure 5.23** shows the comparison between corrected numerical prediction and corrected experimental at T_i = 313.15 K and T_i = 333.15 K. A better agreement was found between the experimental data and numerical prediction in both the cases.

Though a simplified approach was followed here to include the effect of water addition, but it gave good results. In future research, the actual flow coming in from the top of the vessel would be included in the model.

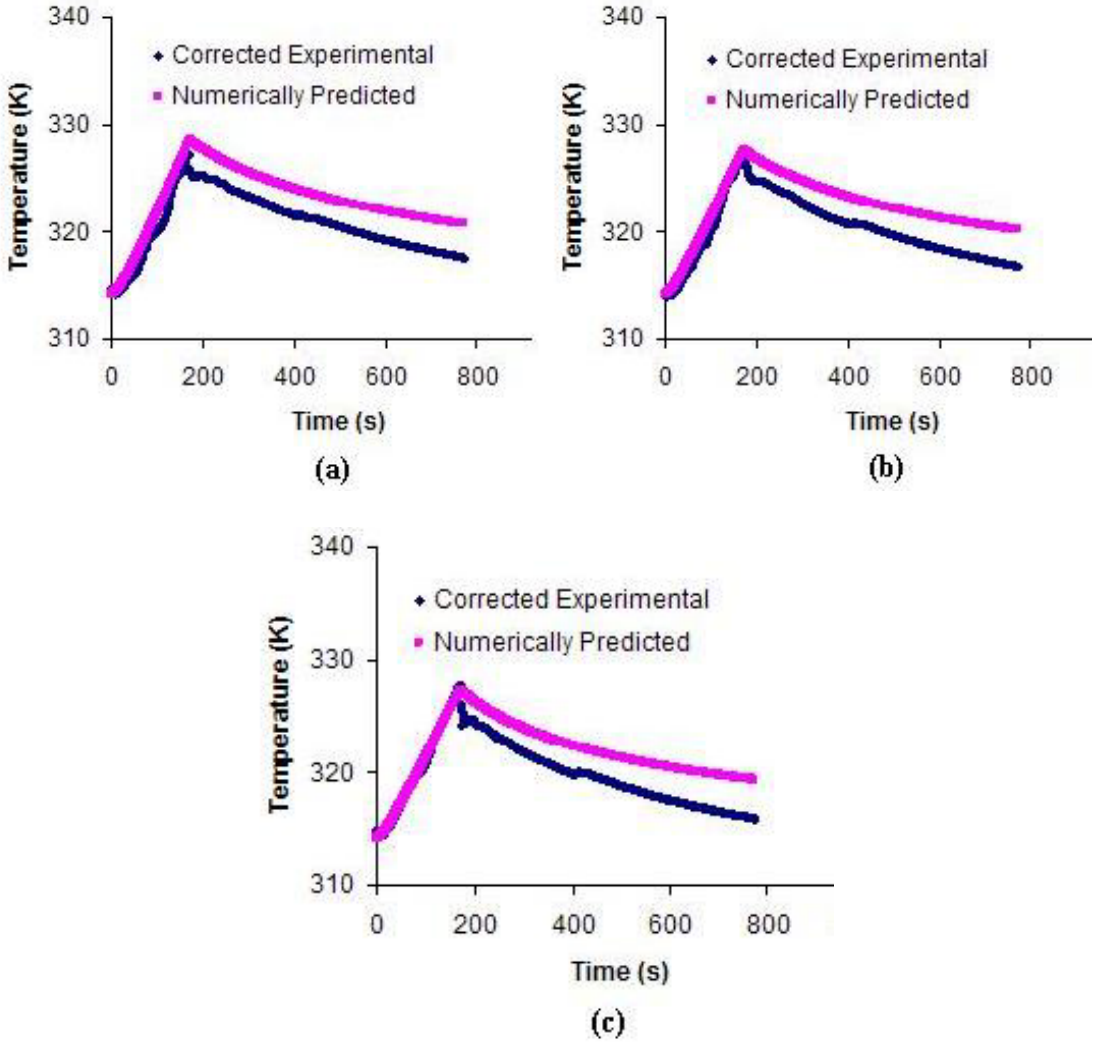

Figure 5.20 Comparison of corrected experimental and numerically predicted time-temperature variation at T_i = 313.15 K, P = 586 MPa, for the thermocouple located (a) near the top of the vessel, (b) in between, & (c) near bottom of the vessel in water.

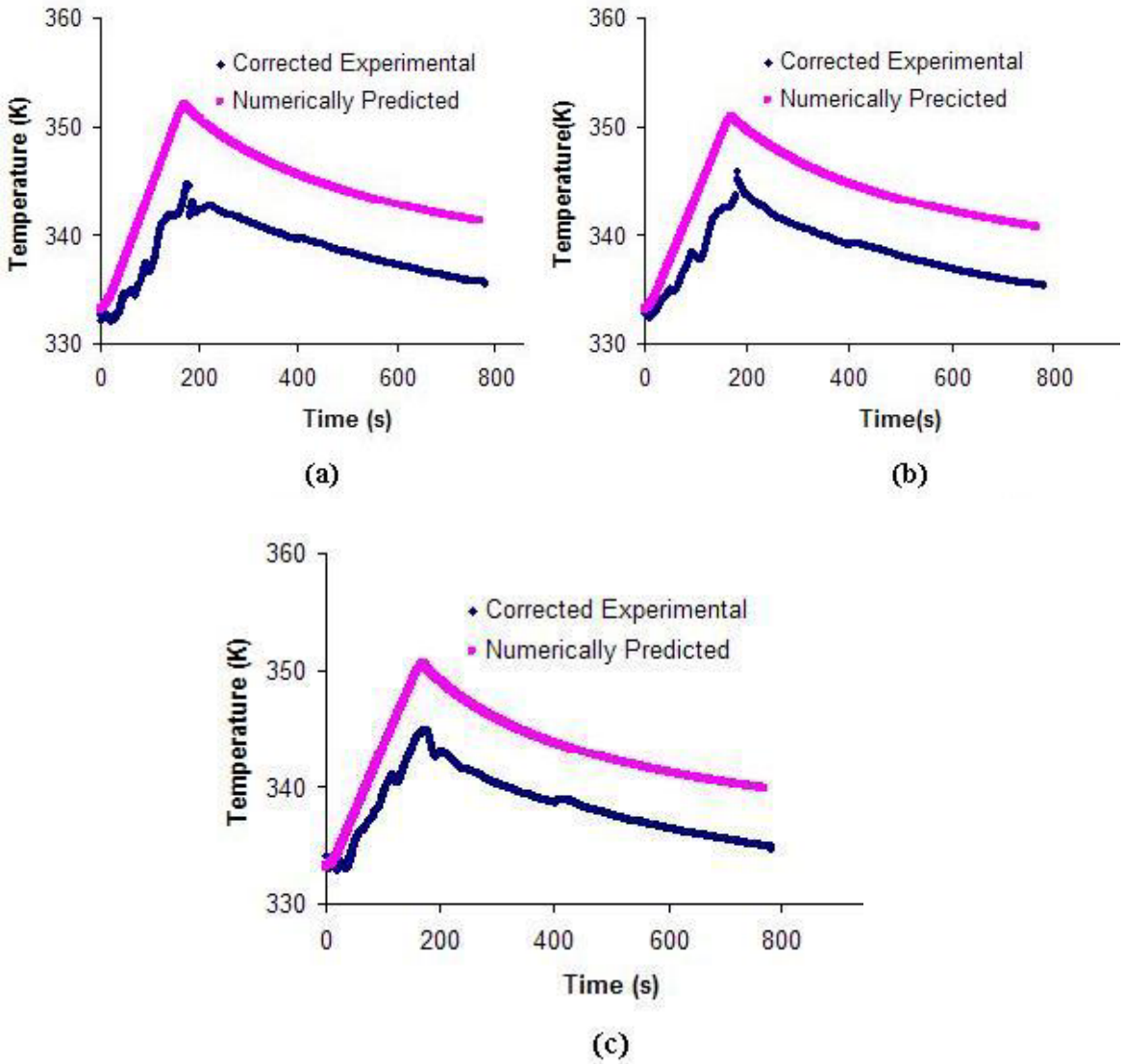

Figure 5.21 Comparison of corrected experimental and numerically predicted time-temperature variations at T_i = 333.15 K, P = 586 MPa, for the thermocouple located (a) near top of the vessel, (b) in between, & (c) near bottom of the vessel in water.

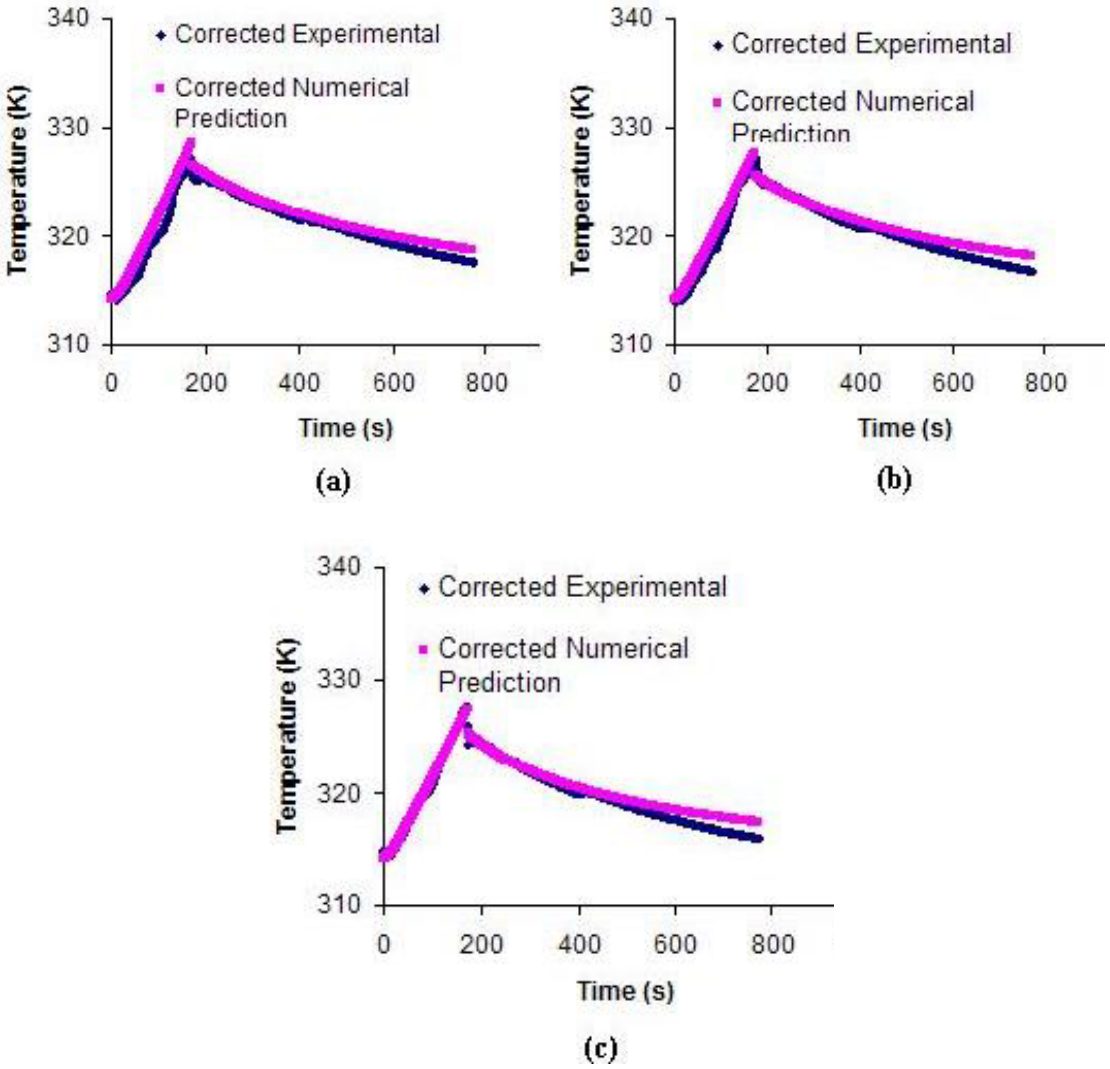

Figure 5.22 Comparison of corrected experimental and corrected numerical prediction time-temperature variation at T_i = 313.15 K, P = 586 MPa, for the thermocouple located (a) near top of the vessel, (b) in between, & (c) near bottom of the vessel in water.

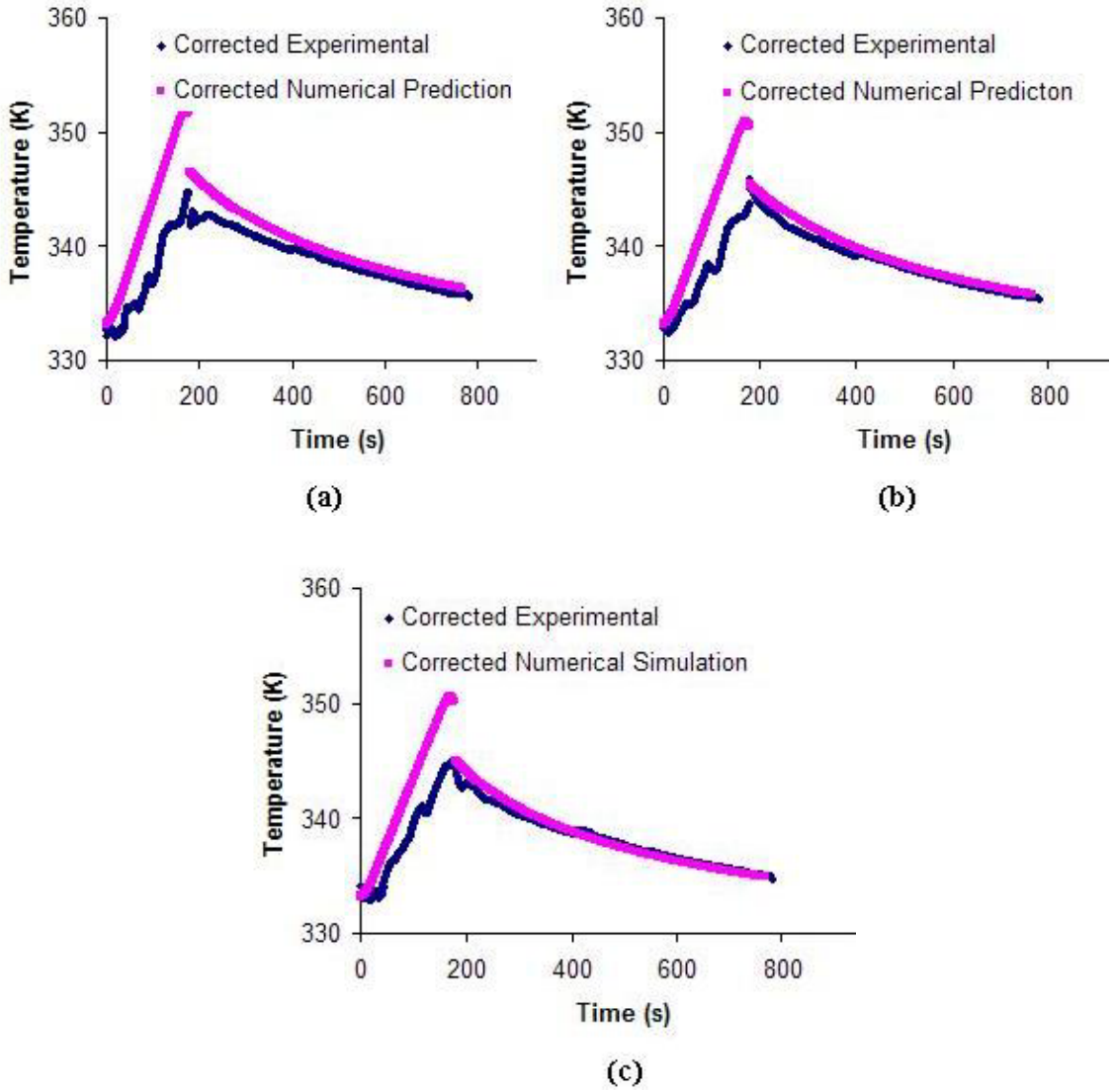

Figure 5.23 Comparison of corrected experimental and corrected numerical prediction time-temperature variation at T_i = 333.15 K, P = 586 MPa, for the thermocouple located (a) near top of the vessel, (b) in between, & (c) near bottom of the vessel in water.

5.4. Effect of High Initial Temperature on Axial & Transverse Temperature Distribution

The validated numerical simulation program was used to investigate the effect of higher initial temperature on the temperature distribution in the vessel. Simulations were carried out at four different initial temperatures with pressure come-up time of 180 s to reach 586

MPa and hold time of 600 s. The simulation results showed that as the initial temperature increased, the difference between the maximum and the minimum temperature within the water column increased and peaked around mid-hold as shown in **Table 5.1**. Within the water column the temperature was maximum at the top and minimum at the bottom as the hot fluid rises due to convection currents.

Table 5.1 Difference (in K) between the maximum (near the top) and the minimum (near the bottom) temperature in water.

Initial Temperature (K)	End of Pressurization(180 s)	At mid-hold (after 480 s)	End of hold time (after 780 s)
298.15	~ 5	~ 8	~ 6
313.15	~ 7	~ 8	~ 6
333.15	~ 7	~ 8	~ 7
353.15	~ 8	~ 11	~ 10

To compare the temperature profiles at different initial temperatures, non-dimensional temperature profiles were plotted as a function of non-dimensionaized distance at vertical and horizontal planes shown in **Figure 5.6**. The temperature was non-dimensionalized with respect to maximum temperature on the plane $[(T-T_i)/T_{max}-T_i)]$ and distance with the length of the water column (L) and radius (Ri) for vertical plane (-z/L) and horizontal mid-plane (r/R_i) respectively. It was also observed that the non-dimensional temperature profile along the axis of the vessel in the water column at different initial temperatures were similar, as shown in **Figure 5.24.** Similarly, **Figure 5.25** shows non-dimensional temperature profiles plotted along the radial distance at the horizontal mid-plane in water. It was observed that the radial temperature distribution was uniform over most of the region except near the walls and it was not affected by the initial temperature.

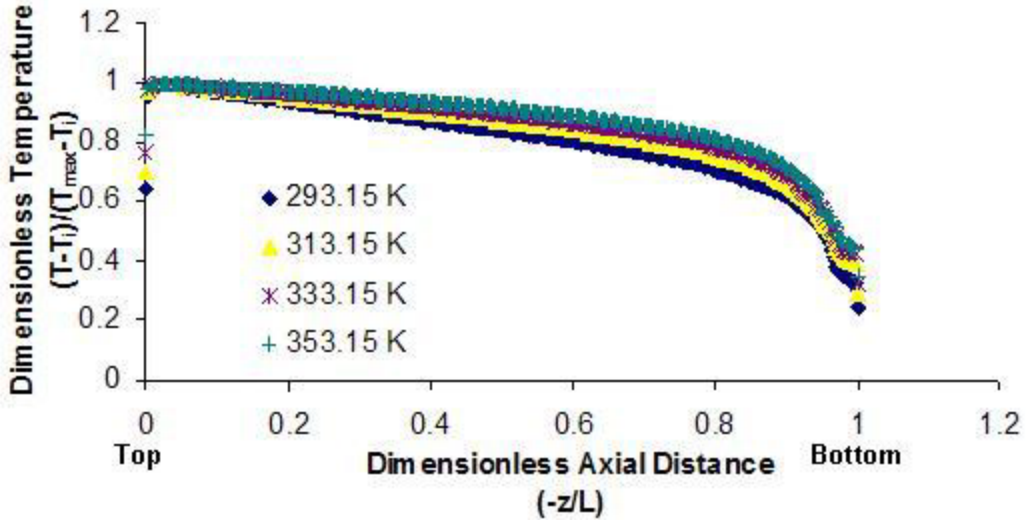

Figure 5.24 Numerically predicted dimensionless temperature profile along the vertical axis, at different values of T_i.

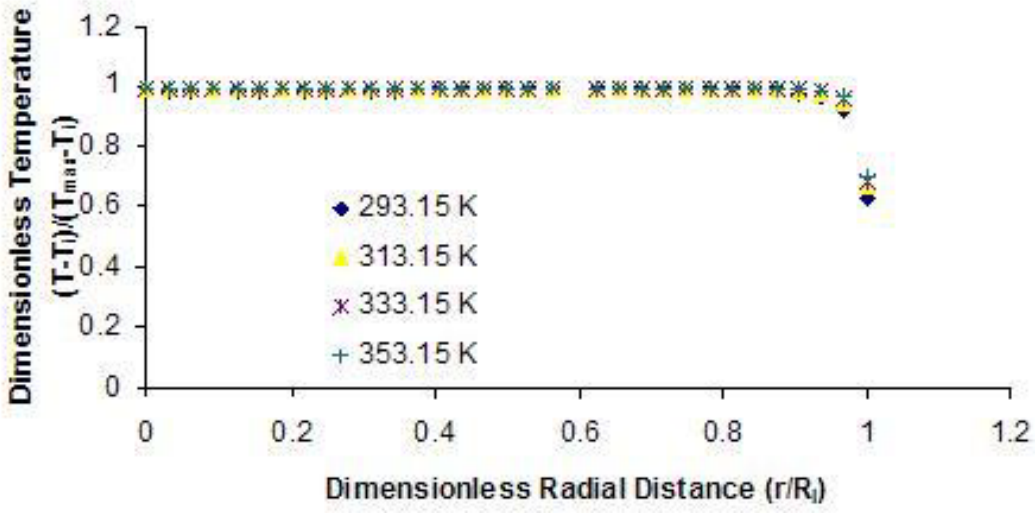

Figure 5.25 Numerically predicted dimensionless temperature profile along the radial distance in water at the horizontal mid-plane, at different values of T_i.

5.5. Effect of Vessel Size on Temperature Distribution

The numerical simulation program was further used to understand the effect of vessel size on temperature distribution in the water. In this case, a simpler axisymmetric geometry with straight top and bottom closures was used. Both conduction only (no gravity effects) and conjugate (conduction & convection) cases were compared. The

effect of vessel size on numerically predicted temperature profiles for conduction only and conjugate cases, along the horizontal mid plane of the vessel are shown in **Figure 5.26(a)** at the end of pressurization and in **Figure 5.26(b)** at the end of pressure hold time, for three different sizes of the vessel i.e, keeping the same height but varying inner radius (2Ri, Ri and Ri/2). For numerical simulation purposes only, the thickness of the s.steel vessel was kept constant. The radial distance was non-dimensionalized with respect to aRi where 'a' has the values 2, 1 and 0.5.

From **Figure 5.26(a)** and **Figure 5.26(b)** it can be seen that in the results for conduction cases the distribution of the dimensionless temperature $(T-T_i)/(T_{max}-T_i)$ becomes more uniform along dimensionless radial distance as the vessel size is increased. Similarly, during conjugate (conduction and convection) heat transfer cases it can be seen that vessel with 2Ri radius has the uniform distribution over a longer distance as compared to smaller radii vessels but the difference is not significant.

Between conduction only and conjugate heat transfer it was observed that the convection at the wall tends to make temperature distribution more uniform as compared to corresponding conduction case which is evident from **Figure 5.26(a)** and **Figure 5.26(b)**.

5.6. Effect of Insulating Sleeve on Temperature Distribution

From the results described in the previous section it is evident that one of the reasons for non-uniformity in temperature during high pressure process is due to heat loss to the thick metal wall of the vessel. One way to reduce the heat loss would be to add an insulating

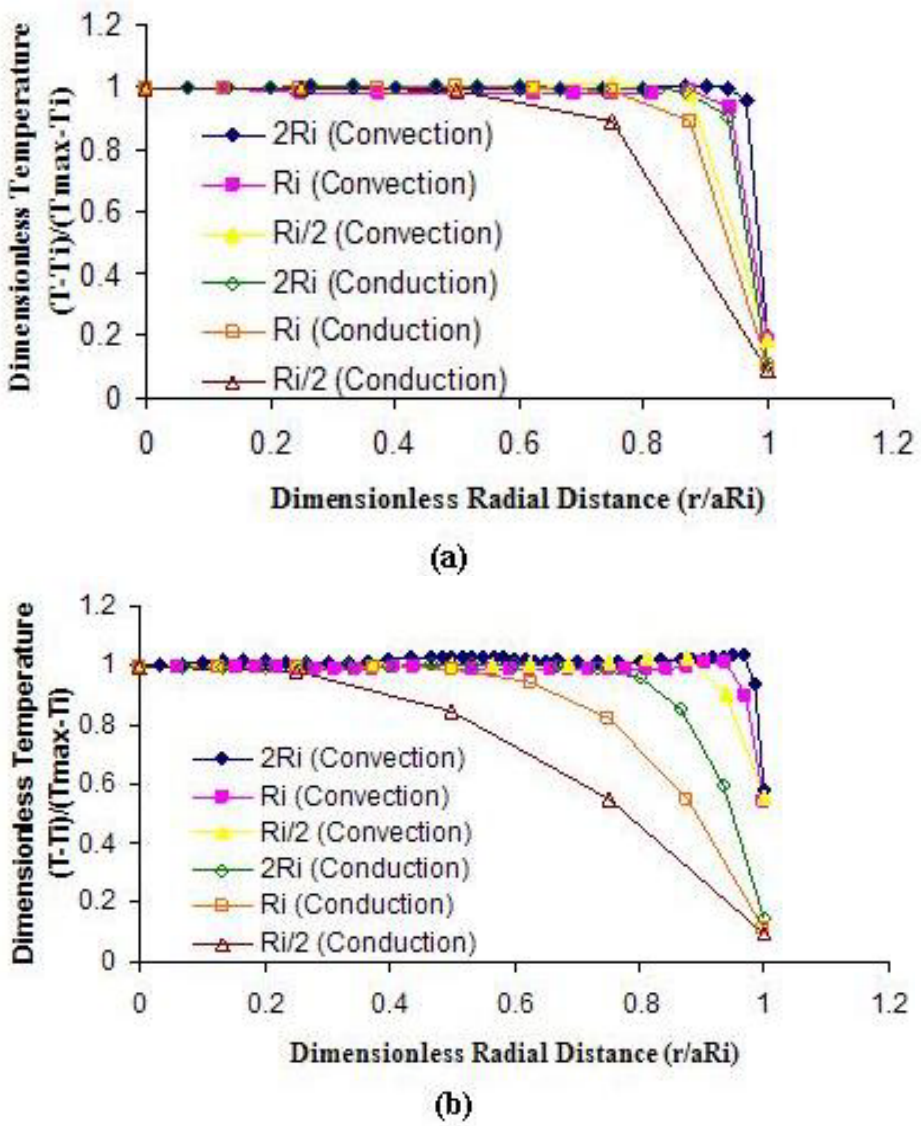

Figure 5.26 Numerically predicted dimensionless temperature variation along the horizontal mid-plane for vessels with different inner radii at the end of (a) pressurization (180 s), (b) hold period (780 s) for conduction only and conjugate heat transfers.

sleeve in the vessel. Therefore, the numerical simulation program was used to predict the temperature distribution in water with an insulating sleeve of certain thickness inserted in the vessel. Properties of Teflon® (k = 0.2 W/m-K) (Tummala and Rymaszewski, 1997) as insulating material were used in the model.

5.6.1. Numerically predicted results for room temperature (293.15 K)

A grid was regenerated with the 0.635 cm thick insulation sleeve in place. The outer diameter of the sleeve was same as the inner diameter of the vessel. A crude mesh was created and based on the velocity gradients arising during the process, the mesh was refined approximately 8 times in Fluent.

The numerically predicted isotherms in water were found to be more uniform as compared to the case without the sleeve, after pressurization and hold period, as shown in **Figure 5.27** and **Figure 5.28**, respectively. Also, the maximum temperature in vessel with insulation at the end of hold period was found to be 308 K as opposed to 299 K when the sleeve was not included, as shown in **Figure 5.28**. Therefore, we can say that addition of an insulation sleeve to the vessel leads to less heat loss at the wall as shown in **Figure 5.28** and hence less temperature variation within the fluid (water).

As mentioned earlier, the temperature in the water is of more concern when a combination of initial high temperature and high pressure is used particularly for spore inactivation. Therefore, the numerical simulation program was used to predict the temperature distribution in the vessel with an insulating sleeve at higher initial temperature, i.e., at $T_i = 60^{\circ}C$ (333.15 K).

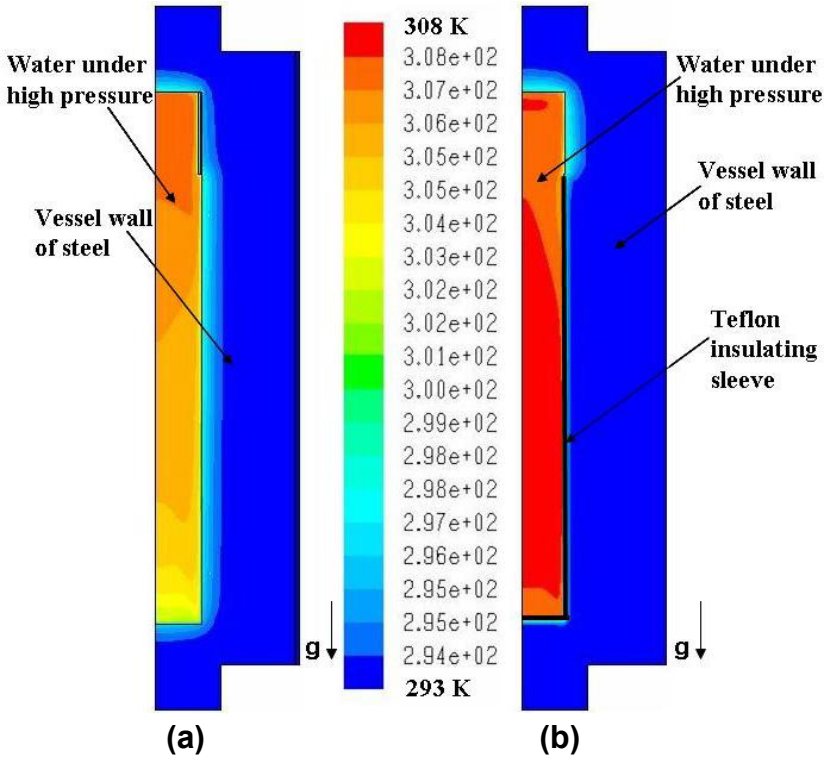

Figure 5.27 Isotherms in water and s.steel wall at T_i = 293.15 K, P = 586 MPa, at the end of pressurization (180 s) (a) without Teflon® sleeve, (b) with Teflon® sleeve 0.635 cm thick.

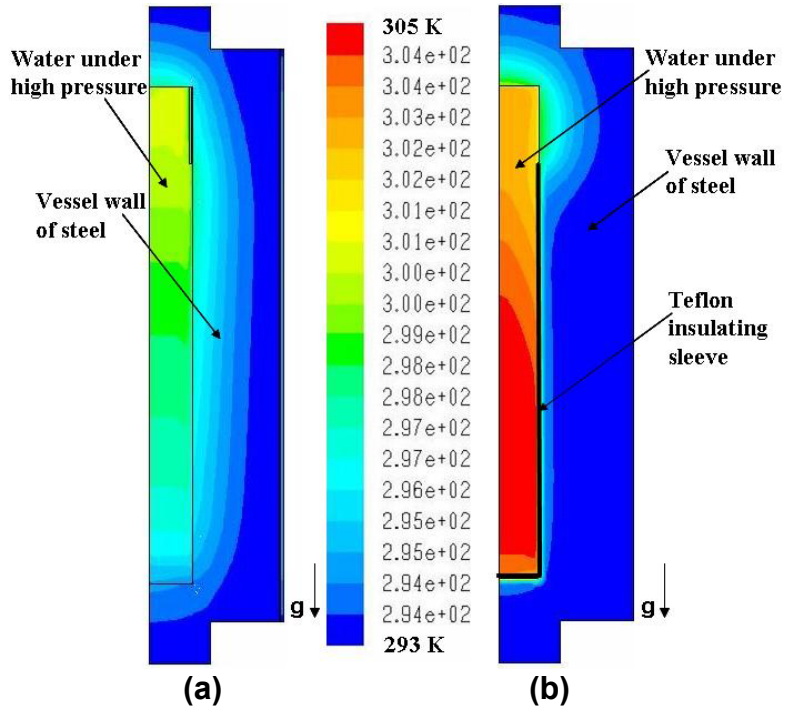

Figure 5.28 Isotherms in water and s.steel wall at T_i = 293.15 K, P = 586 MPa, at the end of hold period (780 s) (a) without Teflon® sleeve, (b) with Teflon® sleeve 0.635 cm thick.

5.6.2. Numerically predicted results for high initial temperature (333.15 K), with Teflon® insulation

Numerical simulation was carried out when the initial temperature was 60˚C (333.15 K) and vessel was pressurized to 586 MPa. The original vessel geometry was modified to include Teflon® insulation of different thickness (0.3175 cm and 1.2 cm). The predicted results were then compared with the without insulation case at 60˚C (333.15 K). **Figure 5.29** and **Figure 5.30** show isotherms at the end of pressurization (180 s) and end of hold (780 s) respectively. It can be seen from **Figure 5.29** that the maximum temperature of water in the vessel was 355 K for the vessel with 1.2 cm as well as 0.3175 cm thick insulation as opposed to without insulation in which the maximum temperature was 350 K at the end of pressurization. Similarly, it can be seen from **Figure 5.30** that at the end of the hold period the maximum temperature was retained for longer vertical distance in the vessel with 1.2 cm thick insulation. The streamlines at the end of hold for the cases with and without insulation are shown in **Figure 5.31**. Also, results show that increase in thickness of the insulation leads to decreased temperature variation in water. To define what will be a good enough thickness, optimization of the insulation thickness with respect to the process requirements is needed.

To get a better insight on the temperature distribution with an insulating sleeve in the vessel, dimensionless temperature profiles were plotted along the radial and axial planes shown in **Figure 5.6**. The temperature was non-dimensionalised with respect to maximum temperature on the respective planes. The radial and axial distances were non-dimensionalised with respect to Rmax and L, respectively. **Figure 5.32** and **Figure 5.33** show the dimensionless temperature profiles on radial and axial planes, respectively. It

can be seen that addition of an insulating sleeve does not have a significant effect on radial temperature distribution as shown in **Figure 5.32** whereas it makes the axial temperature distribution more uniform as compared to the case when their is no insulation as shown in **Figure 5.33**.

5.7. Effect of Changing Properties of Water

Thermophysical properties such as density, heat capacity, thermal conductivity, viscosity, and coefficient of thermal expansion of water are functions of both temperature and pressure. In the results presented in the previous sections, the properties used were only a function of temperature, i.e., dependence of properties on pressure was not included. In this section, the results are given for simulations carried out at 60˚C when the effect of

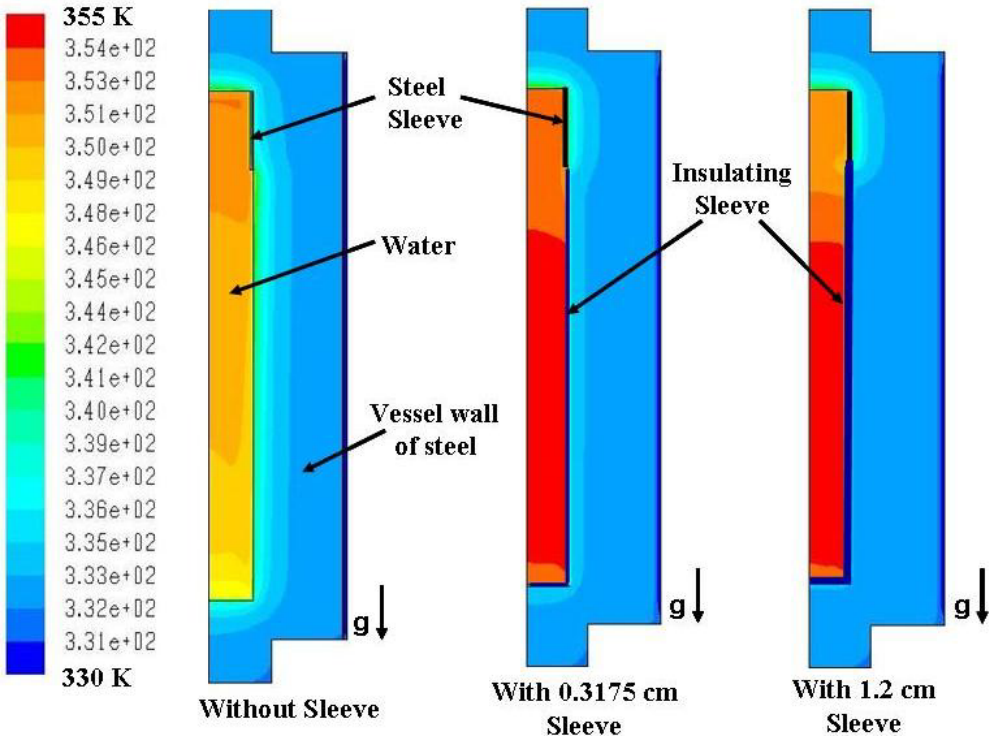

Figure 5.29 Isotherms in water and s.steel wall at T_i = 333.15 K, P = 586 MPa, for Teflon insulating sleeve of different thickness at the end of pressurization.

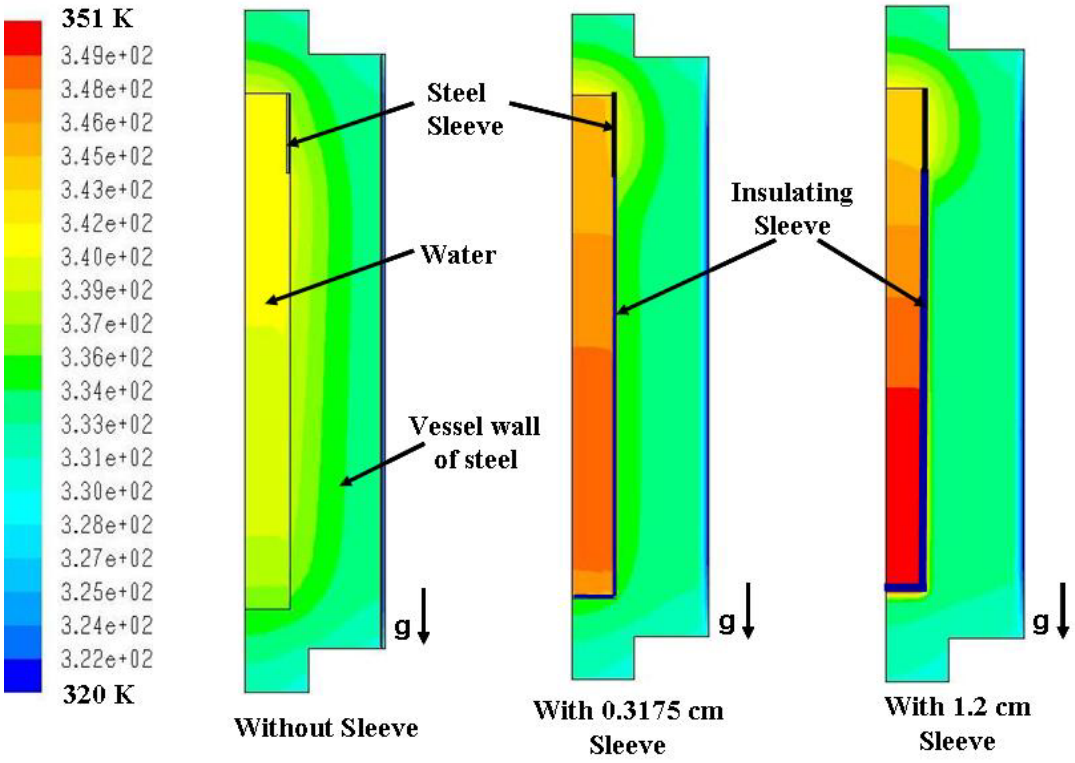

Figure 5.30 Isotherms in water and s.steel wall at T_i = 333.15 K, P = 586 MPa for Teflon insulating sleeve of different thickness at the end of hold period (780 s).

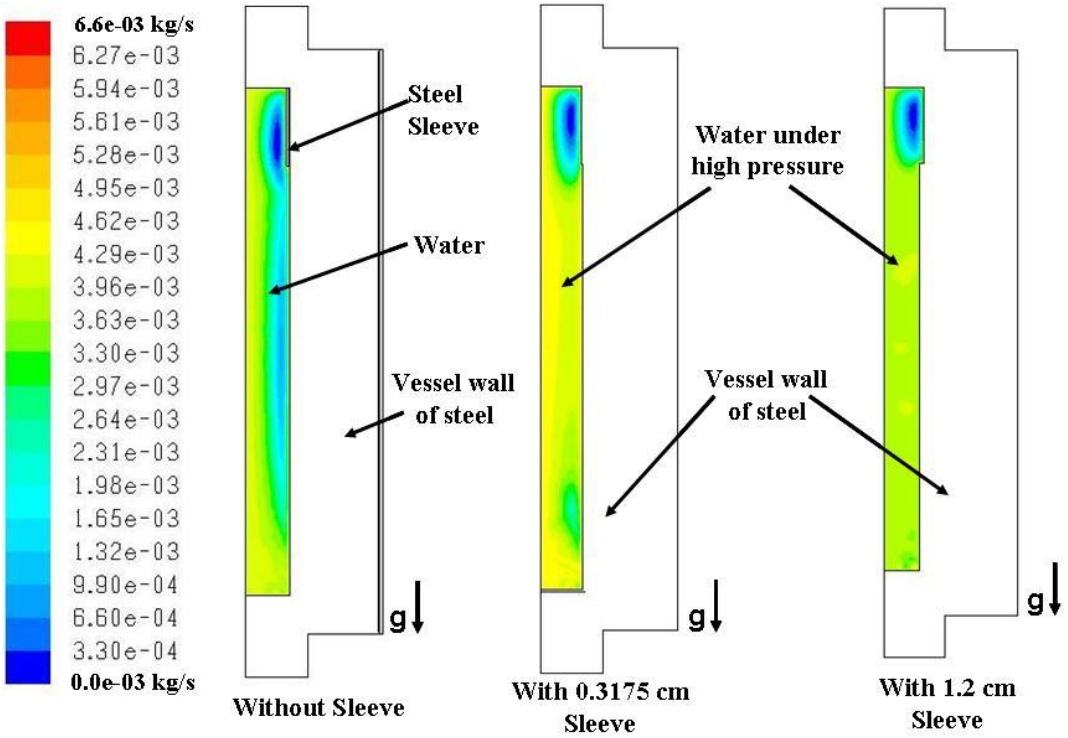

Figure 5.31 Streamlines in water at T_i = 333.15 K, P = 586 MPa, for Teflon insulation of different thickness at the end of hold period (780 s).

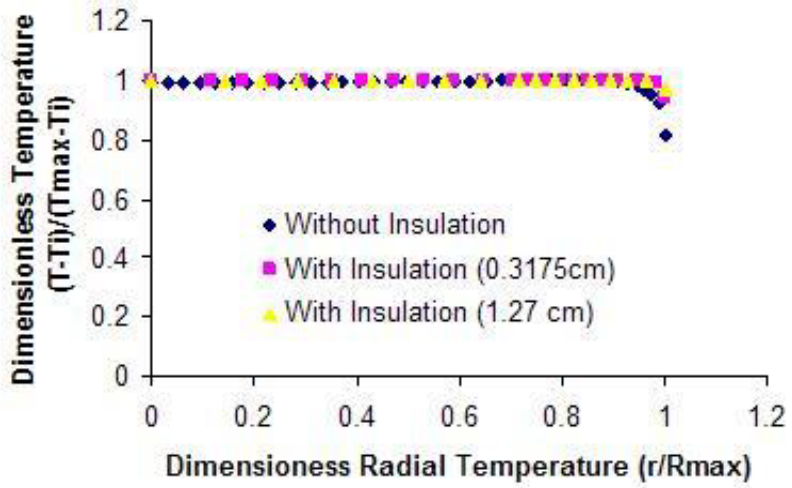

Figure 5.32 Numerically predicted dimensionless temperature profile for with and without insulation along the radial distance in water at the horizontal mid-plane at the end of hold time (780 s).

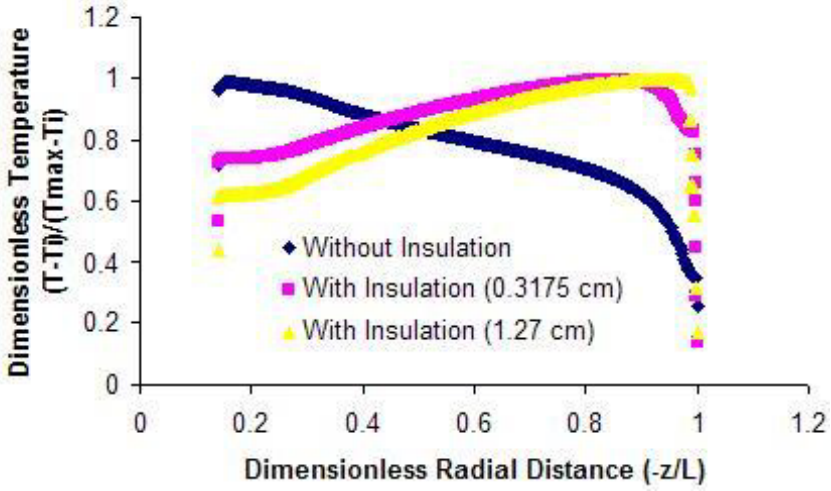

Figure 5.33 Numerically predicted dimensionless temperature profile for with and without insulation along the axial distance in water at the vertical plane at the end of hold time (780 s).

pressure on physical properties was included. The results are presented only for a two cases to illustrate whether changes in physical properties with pressure are important. The two cases are (i) when the effect of pressure and temperature was included only for the thermal conductivity of water, and (ii) when the effect of pressure and temperature was

included for density, heat capacity, and thermal conductivity of water. The values of viscosity and the coefficient of thermal expansion at 60˚C remained unchanged when the pressure was increased from 0.1 MPa to 586 MPa.

5.7.1. Effect of changing only the thermal conductivity of water

At higher pressures, the thermal conductivity of water is higher than its thermal conductivity value at atmospheric pressure. Also, the thermal conductivity of water increases with increasing temperatures. Thus, to evaluate the effect of the change in thermal conductivity of water on the predicted temperature distribution, the numerical simulation was carried out with initial temperature of 60˚C (333.15 K) and hold pressure of 586 MPa. Due to the combined effect of pressure and temperature, the thermal conductivity value used in the simulation was 0.85 W/(mK) as opposed to 0.66 W/(mK) using the previously described case at 60˚C. The value the thermal conductivity of water at high pressure and temperature was obtained from Barbosa-Canovas et al. (2005) at 586 MPa and 60˚C. The values of density, specific heat, viscosity, and the coefficient for thermal expansion of water were obtained from Singh and Heldman (2003) at 60˚C and the dependence of these properties on pressure was not included.

Figure (5.34) and **Figure (5.35)** show the isotherms in water and s.steel wall when thermal conductivity of water was 0.85 W/(mK) and 0.66 W/(mK), respectively. **Figure (5.36)** and **Figure (5.37)** show the corresponding streamlines in water. No significant change was observed between the cases when thermal conductivity was pressure and temperature dependent, and only temperature dependent. The increase in temperature at the end of pressurization and temperature variation at the end of hold period were found

to be very close in both the cases. Also, the mass flow rate values for by streamlines were not significantly different.

5.7.2. Effect of changing thermal conductivity, density, and heat capacity

As discussed in the previous section, increase in pressure and temperatures results in increase in the thermal conductivity of water. Similarly, as pressure increases the density of water increases whereas the heat capacity of water decreases. Thus, to evaluate the effect of simultaneous change in thermal conductivity, density, and heat capacity of water on the predicted temperature distribution, the numerical simulation was carried out with initial temperature of 60˚C (333.15 K) and hold pressure of 586 MPa. The properties used for this simulation were: the thermal conductivity of 0.85 W/(mK) instead of 0.66 W/(mK), density of 1150 kg/m^3 instead of 983.2 kg/m^3 and heat capacity of 3750 J/(kgK) instead of 4181 J/(kgK) used in the previously described cases at 60˚C. The values for the thermal conductivity, density, and heat capacity of water at high pressure were obtained from Barbosa-Canovas et al. (2005) at 586 MPa and 60˚C.

Figure (5.38) and **Figure (5.39)** show the isotherms in water and s.steel wall with and without, respectively, the effect of pressure on thermal conductivity, density, and heat capacity of water. **Figure (5.40)** and **Figure (5.41)** show the corresponding streamlines in water. A difference in temperature for the two cases was about 1 K. Also, the maximum mass flow rate given by streamlines was found to be slightly greater in case of pressure-temperature dependent properties.

Therefore, at the pressure and temperature conditions examined no significant change in the temperature distribution of water due to changes in properties was observed. The effect of continuous change in properties will be included in future research.

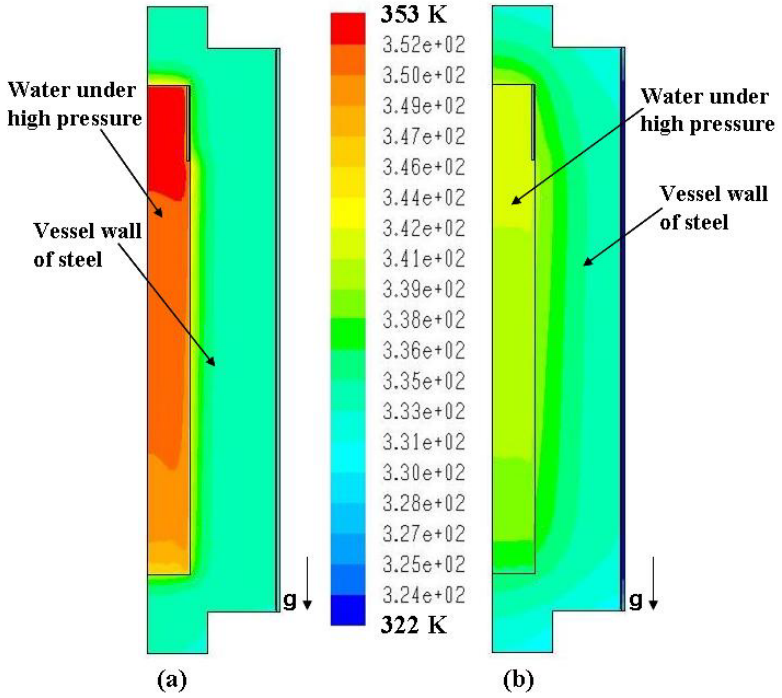

Figure 5.34 Isotherms in water and s.steel wall at T_i = 333.15 K, P = 586 MPa, at the end of (a) pressurization (180 s), (b) hold period (780 s) when thermal conductivity was pressure and temperature dependent.

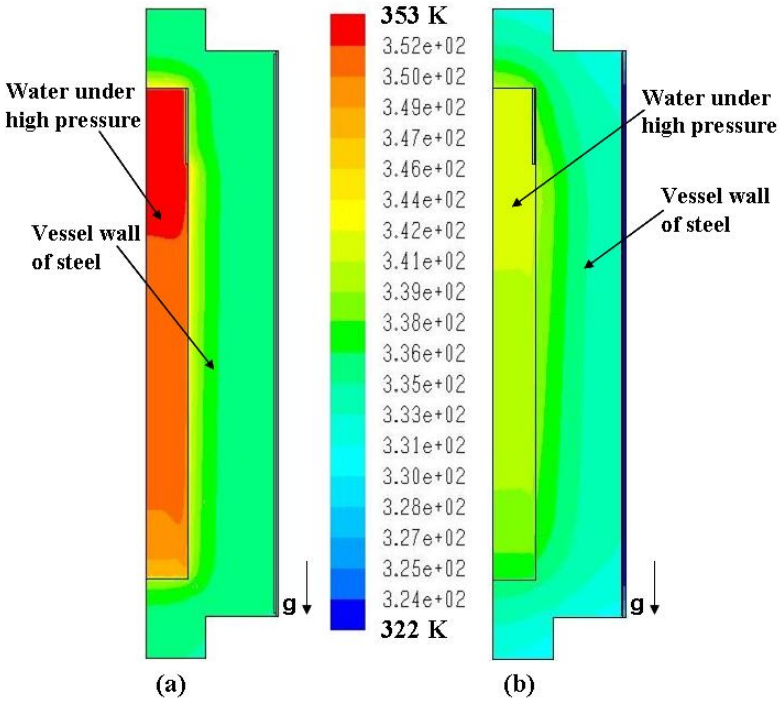

Figure 5.35 Isotherms in water and s.steel wall at T_i = 333.15 K, P = 586 MPa, at the end of (a) pressurization (180 s), (b) hold period (780 s) when thermal conductivity was only temperature dependent.

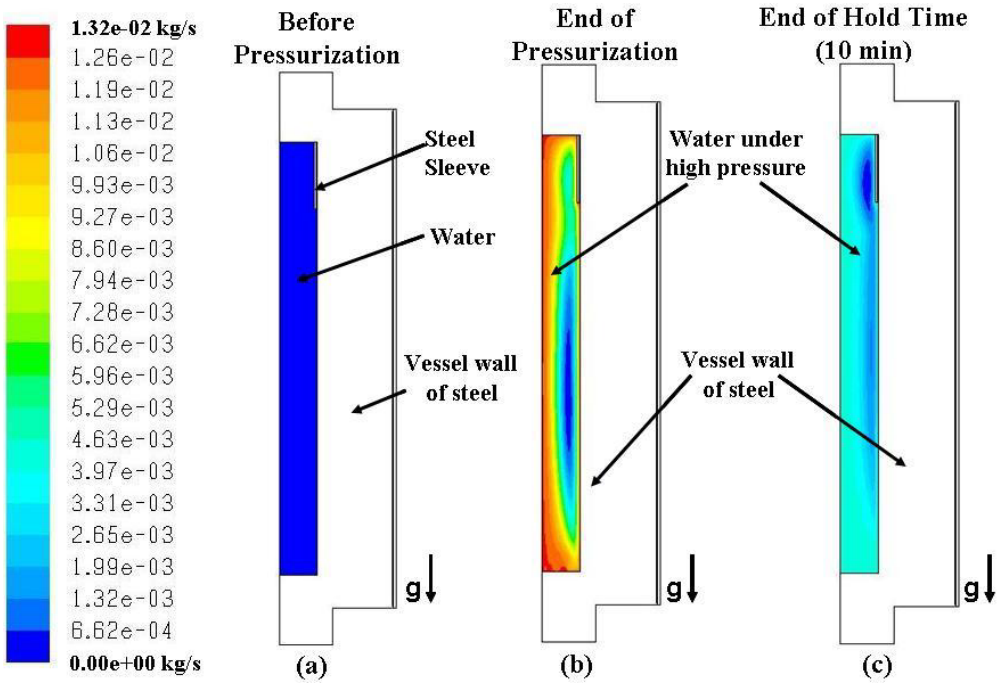

Figure 5.36 Streamlines in water at T_i = 333.15 K, P = 586 MPa, (a) before pressurization, (b) end of pressurization (180 s), & (c) end of hold period (780 s) when thermal conductivity was pressure and temperature dependent.

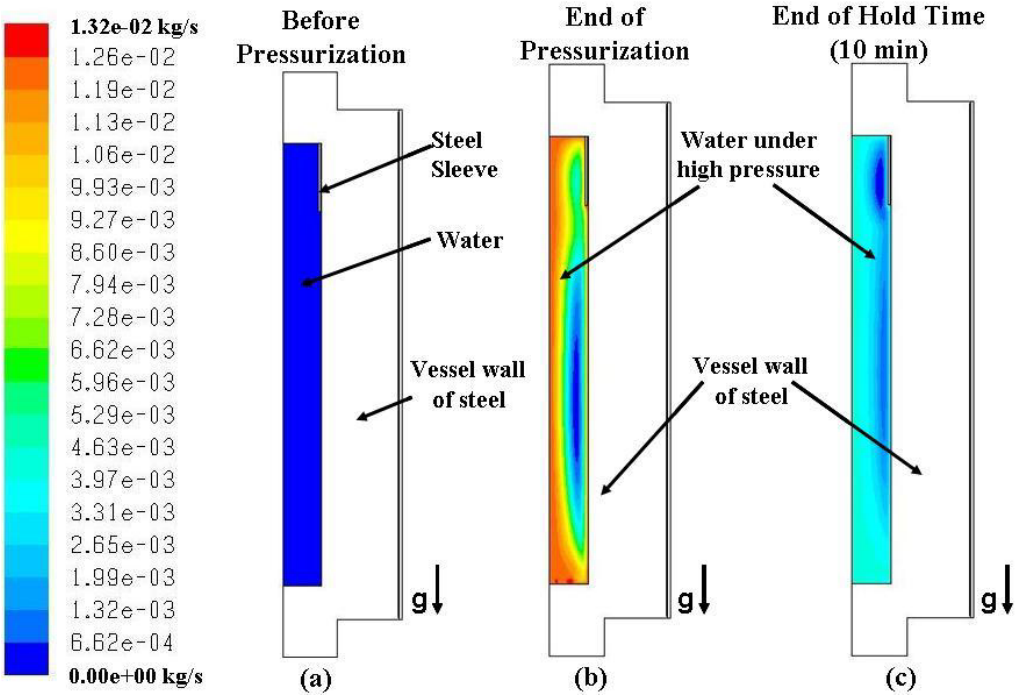

Figure 5.37 Streamlines in water at T_i = 333.15 K, P = 586 MPa, (a) before pressurization, (b) end of pressurization (180 s), & (c) end of hold period (780 s) when thermal conductivity was only temperature dependent.

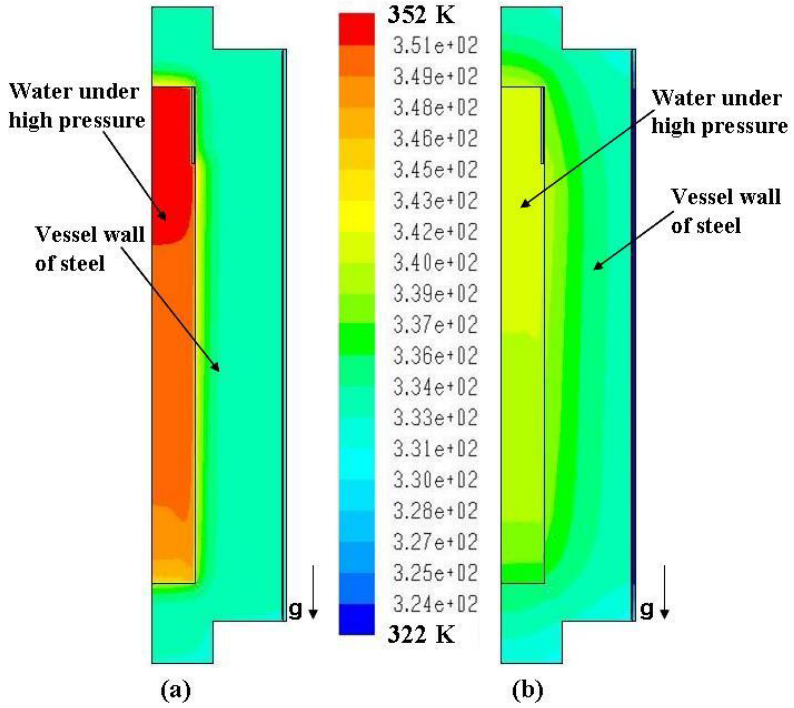

Figure 5.38 Isotherms in water and s.steel wall at T_i = 333.15 K, P = 586 MPa, at the end of (a) pressurization (180 s), (b) hold period (780 s) when pressure-temperature dependent thermophysical properties were used.

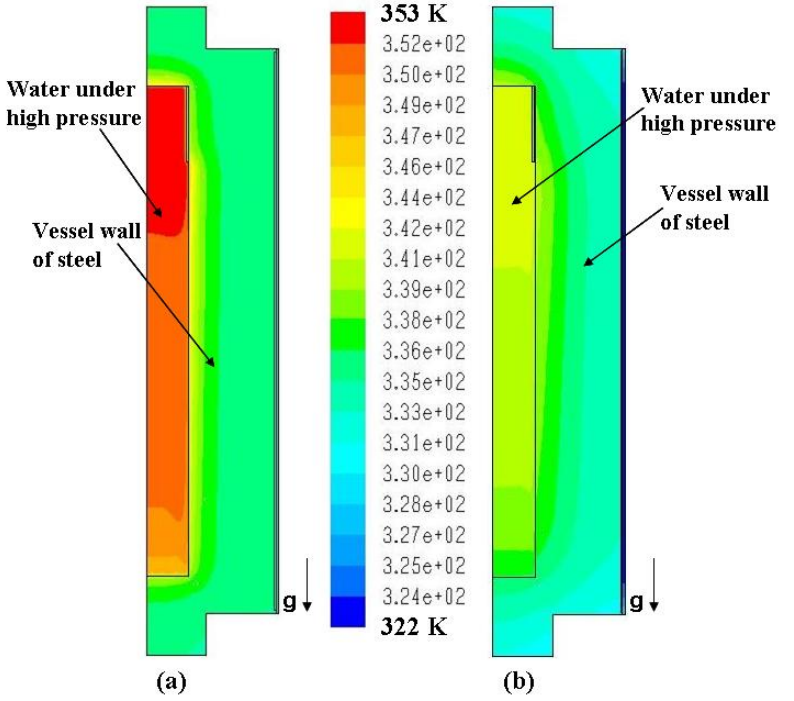

Figure 5.39 Isotherms in water and s.steel wall at T_i = 333.15 K, P = 586 MPa, at the end of (a) pressurization (180 s), (b) hold period (780 s) when thermophysical properties were only temperature dependent.

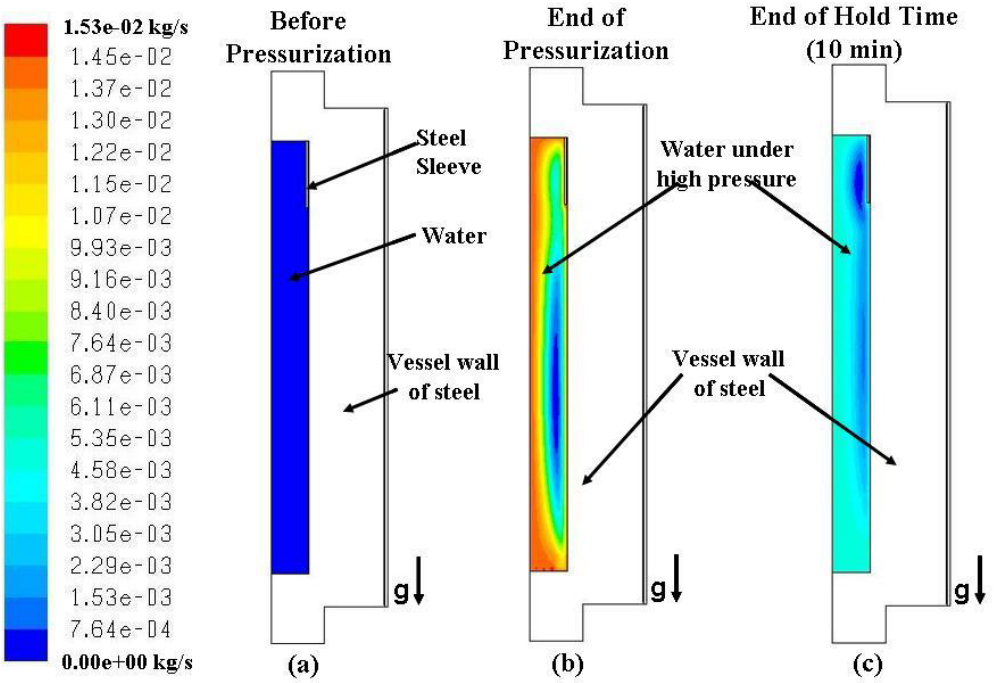

Figure 5.40 Streamlines in water at T_i = 333.15 K, P = 586 MPa, (a) before pressurization, (b) end of pressurization (180 s), & (c) end of hold period (780 s) when pressure-temperature dependent thermophysical properties were used.

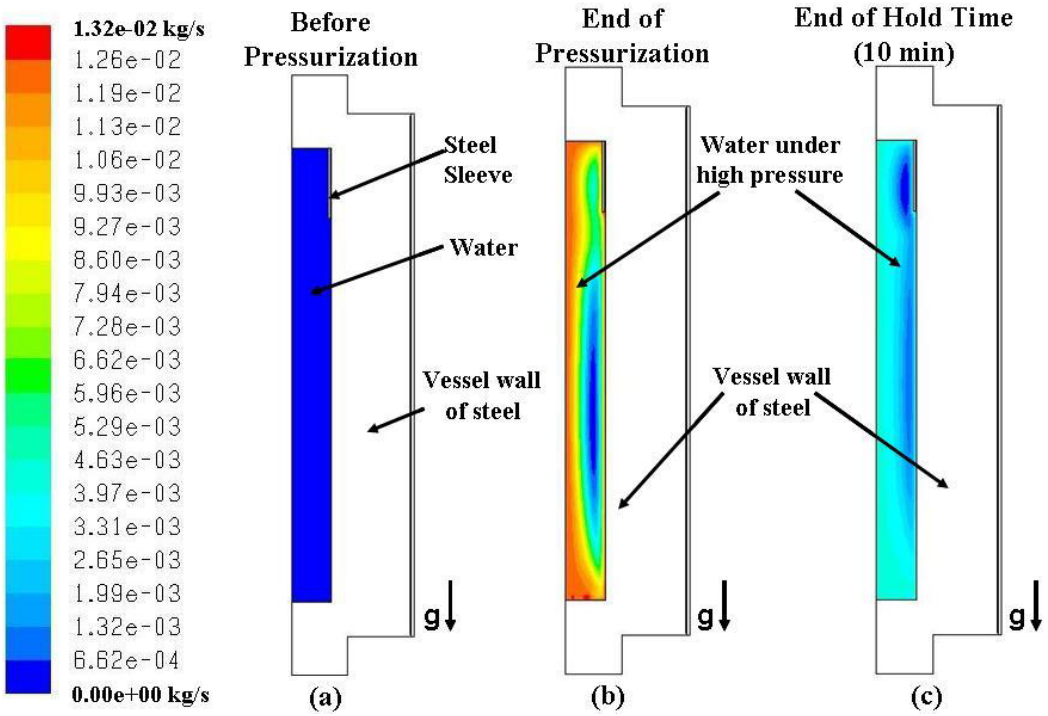

Figure 5.41 Streamlines in water at T_i = 333.15 K, P = 586 MPa, (a) before pressurization, (b) end of pressurization (180 s), & (c) end of hold period (780 s) when thermophysical properties used were only temperature dependent.

6. CONCLUSIONS

Numerical simulation of temperature distribution inside a high hydrostatic pressure food processing vessel was carried out. The results obtained from the numerical simulation were validated with experimental data in terms of temperature vs. time at selected locations. It was observed that the temperature non-uniformity arises in the pressurizing medium (water) during high pressure processing due to adiabatic compression heating and heat loss at the vessel walls. The non-uniformity is aggravated during the hold time because of natural convection cooling at the vessel walls.

Simulation results showed that due to conjugate heat transfer occurring in the high pressure vessel, temperature variation of 6 K arose when initial temperature was 298.15 K and hold pressure was 586 MPa. Also, starting the process at higher initial temperature made temperature distribution more non-uniform at the end of pressurization and pressure hold. At initial temperature of 353.15 K and hold pressure of 586 MPa temperature variation of 10 K was obtained at the end of pressure hold period, from the numerical simulations.

The dynamic response of the high pressure thermocouple assembly was found to be dependent on temperature. Therefore, it must be taken into account to obtain accurate temperature history. The response time of the thermocouples used in our experiments was about 10s. It was used to correct the experimentally measured temperature values and temperature lag was found to be ~ 2˚C. The comparison of corrected experimental data and numerical predictions at thermocouple locations showed a very good agreement at room temperatures whereas at higher initial temperatures the discrepancy increased.

A simplified enthalpy balance model was used to take into account the effect of water addition to the vessel. The temperature correction was found to be a function of initial water temperature and was about 2-5˚C. This simple correction made the agreement between the numerical predictions and experimental data much better, especially at higher initial temperatures.

Validated numerical simulation model confirmed that increasing the vessel size and inserting an insulating sleeve would decrease the non-uniformity of temperature in the pressurizing medium. Also, it was observed that the coldest region in the vessel was located near the wall or near vessel bottom closure (when water addition from the top of the vessel is not taken into account), the phenomenon reversed with the addition of an insulating sleeve to the vessel, i.e., coldest region was located near the top closure.

7. FUTURE WORK

In future research, the entire high pressure process including the variation of the thermophysical properties of water with pressure and temperature, and the effect of water addition to the vessel will be considered. Further, numerical simulation will be used to study temperature distribution within a packaged food sample in the pressurizing medium during HHPP. The fluid-package interaction will be taken into account. Also, the effect of the orientation of the vessel, i.e., horizontal or vertical, on the temperature distribution in the vessel will be studied. The numerical simulation program will be enhanced by incorporating the pressure and temperature inactivation kinetics data for enzymes and spores. We will also include the effect of pressure cycling on the temperature non-uniformity and inactivation of enzymes and spores.

8. REFERENCES

ABBOTT, M.M. AND VAN NESS, H.C. 1972. Theory and problems of thermodynamics. McGraw-Hill, NY-USA.

BALASUBRAMANIAN, S. AND BALASUBRAMANIAM, V.M. 2003. Compression heating influence of pressure transmitting fluids on bacteria inactivation during high pressure processing. Food Research International, 36: 661-668.

BARBOSA-CANOVAS, G.V., & RODRIGUEZ, J.J. 2005. Thermodynamic aspects of high hydrostatic pressure food processing. Novel Food Processing Technologies. CRC Press Florida, USA.

BECKWITH, T.G.; BUCK, N.L. & MARANGONI, R.D. 1982. Temperature measurements. Mechanical Measurements, Addison-Wesley Publishing, MA-USA. pp 519-574.

BRODKEY, R.S.; HERSHEY, H.C. 2003. Transport Phenomena. A unified approach, Broadkey publishing, OH-USA.

BROWN, P.; MEYER, R.; CARDONE, F.; AND POCCHIARI, M. 2003. Ultra-high pressure inactivation of prion infectivity in processed meat: A practical method to prevent human infection. Proceedings of National Academy of Sciences of the United States of America, 100: 6093-6097.

BUTZ, P.; EDENHARDER, R.; FERNANDEZ GARCIA, A.; FISTER, H.; MERKEL, C.; AND TAUSCHER, B. 2002a. Changes in functional properties of vegetables induced by high pressure treatment. Food Research International, 35: 295-300.

BUTZ, P.; FERNANDEZ, A.; FISTER, H.; AND TAUSCHER, B. 1997. Influence of high hydrostatic pressure on aspartame: Instability at neutral pH. J. Agric. Food. Chem., 45: 302-303.

BUTZ, P.; FERNANDEZ, A.; TAUSCHER, B. 2002b. Influence of high pressure treatment on sensorial and nutritional quality of fruit and vegetables. Trends in High Pressure Bioscience and Biotechnology. Progress in Biotechnology. Edited by Rikimaru Hayashi. Elsevier Science B.V. Amsterdam, Netherlands.

BUTZ, P. AND TAUSCHER, B. 2002. Emerging technologies: Chemical aspects. Food Research International, 35: 279-284.

CHEFTEL, J.C.; LEVY, J.; AND DUMAY, E. 2000. Pressure-assisted freezing and thawing: Principles and Potential and Potential Applications. Food. Rev. Int., 16(4), 453-483.

CHEVALIER, D.; LE BAIL, A.; SEQUEIRA-MUNOZ, A.; SIMPSON, B.K.; AND GHOUL, M. 2002. Pressure shift freezing of turbot (Scophtlalmus maximus) and carp (Cyprinus carpio): effect on ice crystals and drip volumes. Trends in High Pressure Bioscience and Biotechnology. Progress in Biotechnology. Edited by Rikimaru Hayashi. Elsevier Science B.V. Amsterdam, Netherlands.

CHOUROT, J-M.; BOILLEREAUX, L.; HAVET, M.; AND LE BAIL, A. 1997. Numerical modeling of high pressure thawing: Application to water thawing. Journal of Food Engineering 34: 63-75.

DENYS, S.; LUDIKHUYZE, L.R.; VAN LOEY, A.M.; AND HENDRICKX, M.E. 2000. Modeling conductive heat transfer and process uniformity during batch high pressure processing of foods. Biotechnol. Prog., 16: 92-101.

DENYS, S.; VAN-LOEY, A.M.; HENDRICKX, M.E.; AND TOBBACK, P. 1997. Modeling heat transfer during high-pressure freezing and thawing. Bitechnol. Prog., 13: 416-423.

FARKAS, D.F. 2005. Internet site http://www.elmhurstresearch.com/hpp_history.htm

FRYER, D.M. AND HARVEY, J.F. 1997. High pressure vessels. pp 140-142, Springer, NY-USA.

GAO, Z.; MEI, V.C.; & CHEN, F.C. 2003. CFD solution and experimental testing of buoyancy-driven convection caused by condensers immersed in a water tank of HPWH, pp 33-38. American Society of Mechanical Engineers.

GEBHART, B.; JALURIA, Y.; MAHAJAN, R.L. AND SAMMAKIA, B. 1988. Buoyancy induced flows and transport. Hemisphere Publishing Corporation, NY-USA.

GHANI, A.G.A. & FARID, M.M. 2007. Modeling of high pressure food processing using CFD, Computational Fluid Dynamics in Food Processing, pp 537-553. D.-W.Sun, ed., CRC Press, Florida-USA.

GREWAL, B.S. 1996. Higher engineering mathematics. Khanna publishers, Delhi-India.

HARTMANN, C. 2002. Numerical Simulation of Thermodynamic and Fluid-dynamic processes during the high pressure treatment of fluid food systems. Innovative Food Science and Emerging Technologies, 3: 11-18.

HARTMANN, C. AND DELGADO, A. 2002a. Numerical simulation of thermo fluid dynamics and enzyme inactivation in a fluid food system under high hydrostatic pressure. Trends in High Pressure Bioscience and Biotechnology. Progress in Biotechnology. Edited by Rikimaru Hayashi. Elsevier Science B.V. Amsterdam, Netherlands.

HARTMANN, C. AND DELGADO, A. 2002b. Numerical simulation of convective and diffusive transport effects on a high pressure induced inactivation process. Biotechnology and Bioengineering, Vol. 79, No. 1, July 5:94-104.

HARTMANN, C. AND DELGADO, A. 2003. the influence of transport phenomena during high-pressure processing of packed food on the uniformity of enzyme inactivation. Biotechnology and Bioengineering, Vol. 82, No. 6, June 20: 725-735.

HARTMANN C. AND DELGADO A. 2004. Numerical simulation of the mechanics of a yeast cell under high hydrostatic pressure. Journal of Biomechanics, 37: 977-987.

HARTMANN, C.; DELGADO, A.; AND SZYCZYK, J. 2003. Convective and diffusive transport effects in a high pressure induced inactivation process of packed food. Journal of Food Engineering, 59: 33-44.

HAYAKAWA, I.; LINKO, Y.; AND LINKO, P. 1996. Novel mechanical treatments of biomaterials. Lebensm-Wiss. U.-Technol., 29: 395-403.

HAYASHI, R. 2002. High pressure in bioscience and biotechnology: pure science encompassed in pursuit of value, Biochimica et Biophysica Acta 1595, 397-399.

HENDRICKX, M. E.G., & KNORR, D., 2001. Ultra high pressure treatments of foods. Plenum Publishers, New York- USA.

HENRY, C.J.K., CHAPMAN, C. 2002. Nutrition handbook of food processors. pp 435, Woodhead publishing, Cambridge-UK.

HOGAN, E., KELLY, A.L., SUN, D.-W. 2005. High pressure processing of foods: An overview. Emerging Technologies for Food Processing. pp 23-27.

HOLMAN, J.P. 1981. Heat Transfer. McGraw-Hill Book Company New York-USA.

HOOVER, D.G.; METRICK, C.; PAPINEAU, A.M.; FARKAS, D.; AND KNORR, D. 1989. Biological effects of high hydrostatic pressure on food microorganisms. Food Technology. March: 99-107.

JALURIA, Y., TORRANCE, K. 1986. Computational heat transfer. Hemisphere Publishing, Washington D.C.-USA.

KINGSLEY, D.H.; HOOVER, D.G.; PAPAFRAGKOU, E.; AND RICHARDS, G. 2002. Inactivation of Hepatitis A virus and a calcivirus by high hydrostatic pressure. Journal of Food Protection, 65(10), 1605-1609.

KNORR, D. 1999. Novel approaches in food processing technology: new technologies for preserving foods and modifying function. Current Opinion in Biotechnology, Vol. 10, Iss 5: 485-491.

KNORR, D.; ADE-OMAWAYE, B.I.O.; AND HEINZ, V. 2002. Nutritional improvements of plant foods by non-thermal processing. Proceedings of the Nutrition Society, 61:311-318.

KNORR, D. 2003. Impact of non-thermal processing on plant metabolites. Journal of Food Engineering, 56: 131-134.

KOIZUMI, M. AND NISHIHARA, M. 1991. Isostatic pressing: technology and applications, pp 2, Springer, New York-USA.

LE BAIL, A.; CHEVALIER, D.; MUSSA, D.M.; AND GHOUL, M. 2002a. High pressure freezing and thawing of foods: A Review. International Journal of Refrigeration, 25: 504-513.

LE BAIL, A.; MUSSA, D.; ROUILLE, J.; RAMASWAMY, H.S.; CHAPLEAU, N.; ANTON, M.; HAYERT, M.; BOILLEREAUX, L.; AND CHEVALIER, D. 2002b. High pressure thawing. application to selected sea-foods. Trends in High Pressure Bioscience and Biotechnology. Progress in Biotechnology. Edited by Rikimaru Hayashi. Elsevier Science B.V. Amsterdam, Netherlands.

LOPEZ-MALO, A.; PALOU, E.; BARBOSA-CANOVAS, G.V.; SWANSON, B.G.; & WELTI-CHANES, J. 2000. Minimally processed foods with high hydrostatic pressure. Trends in Food Engineering. pp 271.

MAKITA, T. 1992. Application of High pressure and thermo physical properties of water to biotechnology. Fluid Phase Equilibria, 76: 87-95.

MESSENS, W.; CAMP, J.V.; AND HUYGHEBAERT, A. 1997. The use of high pressure to modify the functionality of food proteins. Trends in Food Science and Technology, 8: 107-112.

MOLINA, E. AND LEDWARD, D.A. 2003. Effects of combined high pressure and heat treatment on the textural properties of soya gels. Food Chemistry, 80: 367-370.

OTERO, L.; MOLINA-GARCIA, A.D.; RAMOS, A.M.; AND SANZ, P.D. 2002a. A model for real thermal control in high pressure treatment of foods. Biotechnol. Prog., 18: 904-908.

OTERO, L.; MOLINA, A.D.; AND SANZ, P.D. 2002b. Thermal control simulation in high pressure treatment of foods. High Pressure Research, Vol. 22: 627-631.

OTERO, L.; MOLINA-GARCIA, A.D.; AND SANZ, P.D. 2002c. Some interrelated thermo physical properties of liquid water and ice. I. A user-friendly modeling review for food high-pressure processing. Critical Reviews in Food Science and Nutrition, 42 (4): 339-352.

PEHL, M.; WERNER, F.; AND DELGADO, A. 2000. First visualization of temperature fields in liquids at high pressure using thermochromic liquid crystals. Experiments in Fluids, 29: 302-304.

PEHL, M.; WERNER, F.; AND DELGADO, A. 2002. Experimental investigation on thermofluiddynamical processes in pressurized substances. trends in high pressure bioscience and biotechnology. Progress in Biotechnology. Edited by Rikimaru Hayashi. Elsevier Science B.V. Amsterdam, Netherlands.

PONCE, E.; BELTRAN, E.; SENDRA, E.; MOR-MUR, M.; GUAMIS, B.; AND PLA, R. 1998. Development of a cream caramel by high hydrostatic pressure at low temperature. Advances in High Pressure Bioscience and Biotechnology. Edited by Horst Ludwig. Springer-Verlag Berlin Heidelberg, Germany.

RASANAYAGAM, V.; BALASUBRAMANIAM, V.M.; TING, E.; SIEZER, C.E.; BUSH, C.; AND ANDERSON, C. 2003. Compression heating of selected fatty food materials during high pressure processing. Journal of Food Science, Vol. 68, No.1: 254-259.

RASTOGI, N.K., AND RAGHAVARAO, K.S.M.S., BALASUBRAMANIAM, V.M., NIRANJAN, K. AND KNORR, D. 2007. Opportunities and challenges in high pressure processing of foods, Critical Reviews in Food Science and Nutrition, 47:69-112.

SANCHEZ-MORENO, C.; PLAZA, L.; DE ANCOS, B.; AND CANO, M.P. 2003B. Vitamin C, provitamin A, carotenoids and other carotenoids in high-pressurized orange juice during refrigerated storage. J. Agric. Food Chem., 51: 647-653.

SCHAUWECKER, A. 2004. New technologies: Under pressure. Food Product Design. July 2004.

SINGH, R.P. AND HELDMAN, D.R. 2003. Introduction to food engineering. Academic Press, London-UK.

SOLT, M. AND AUTIO, K. 1998. Microscopic and rheological characterization of high pressure treated starch dispersions. Advances in High Pressure Bioscience and Biotechnology. Edited by Horst Ludwig. Springer-Verlag Berlin Heidelberg, Germany.

SUZUKI, A. 2002. High pressure-processed foods in Japan and the world. Trends in High Pressure Bioscience and Biotechnology. Progress in Biotechnology. Edited by Rikimaru Hayashi. Elsevier Science B.V. Amsterdam, Netherlands.

TING, E.; BALASUBRAMANIAM, V. M.; & RAGHUBEER, E. 2002. Determining thermal effects in high pressure processing. Food Technology 56(2): 31-35.

TRUJILLO, A.J.; CAPELLAS, M.; BUFFA, M.; ROYO, C.; GERVILLA, R.; FELIPE, X.; SENDRA, E.; SALDO, J.; FERRAGUT, V.; AND GUAMIS, B. 2000. Application of high pressure treatment for cheese production. Food Research International, 33: 311-316.

TUMMALA, R.R. AND RYMASZEWSKI, E.J. 1997. Microelectronics packaging handbook - subsystem packaging. Springer, pp III-85.

VENUGOPAL, V. 2006. Seafood processing: adding value through quick freezing, retortable packaging, and cook-chilling, pp 335, CRC press, Florida-USA.